HOTSPOTS OF SOIL WATER MOVEMENT

INDUCED BY VEGETATION CANOPIES

Dissertation

zur Erlangung des akademischen Grades doctor rerum naturalium (Dr. rer. nat.)

vorgelegt dem Rat der Chemisch-Geowissenschaftlichen Fakultät

der Friedrich-Schiller-Universität Jena

von Master of Science Geowissenschaften Johanna Clara Metzger

geboren am 30.10.1985 in Gießen, Deutschland

Gutachter:

1. Prof. Dr. Anke Kleidon-Hildebrandt, Friedrich-Schiller-Universität Jena (DE)
2. Dr.ir. Miriam Coenders-Gerrits, Technische Universiteit Delft (NL)

Tag der Verteidigung: 17.02.2021

Zusammenfassung

Vegetation und Boden bilden ein hochgradig interaktives System. Wasser ist darin ein wichtiger Faktor. Beim Eintrag in das System durch Niederschlag wird Wasser von der Vegetation abgefangen (Interzeption) und umverteilt. Es erreicht den Boden schließlich in Form von Kronendurchlass und Stammabfluss (Bestandsniederschlag) in einer starken kleinräumigen Heterogenität. Diese könnte sich auf nachfolgende bodenhydrologische Prozesse und letztlich auf das größerskalige unterirdische Abflussverhalten auswirken. Kenntnis über den Einfluss von Ökosystemen auf Wasserflüsse ist von großer Bedeutung, insbesondere in Zeiten globalen Wandels, durch den Ökosysteme und Wasserressourcen gleichermaßen gefährdet sind.

Aktuell gibt es bei Auswirkungen des heterogenen Niederschlagseintrags in Wäldern auf unterirdische Prozesse noch viele Unbekannte. Es wurde gezeigt, dass Bestandsniederschlagsmuster, neben Wettereinflüssen, von der Baumart und -morphologie abhängen. Die räumliche Variabilität des Kronendurchlasses ist zeitlich stabil, die durch die Baumkronen erzeugten Muster sind folglich systematisch. Stammabfluss stellt oft Hotspots des Wassereintrags in den Boden dar, seine Variabilität und zeitliche Stabilität ist jedoch kaum untersucht. Eine Analyse von Stammabflussfaktoren anhand von Einzelbäumen kann diverse Wälder nur unvollständig abbilden, doch Nachbarschafts- und Bestandseigenschaften wurden bisher wenig berücksichtigt. Häufig wurden durch Stammabfluss verursachte präferentielle Bodenwasserflüsse beobachtet. Auswirkungen der Bestandsniederschlagsmuster auf den Bodenwassergehalt konnten dagegen noch nicht abschließend nachgewiesen werden. Ebenso ist das Infiltrationsverhalten von Stammabfluss ungeklärt. Wenige frühe Studien fanden einen Gradienten der Bodeneigenschaften abhängig von der Baumdistanz in Wäldern. Wechselseitige Einflüsse von Stammabfluss-induziertem Bodenwasserflüssen und Bodeneigenschaften wurden bisher nicht untersucht.

In dieser Dissertation bearbeite ich folgende übergreifende Forschungsfragen: (1) Durch welche Faktoren erzeugt die Vegetationsgemeinschaft systematisch Hotspots des

Bestandsniederschlags? (2) Wie wirkt sich die hohe Heterogenität des Bestandsniederschlags auf Boden und Bodenwasser aus?

Zu Beantwortung dieser Fragen wurde ein hochaufgelöst und statistisch angelegtes experimentelles Design zur Erfassung raumzeitlicher Muster von Bestandsniederschlag und Bodenwasser entwickelt. Auf einer 1 ha großen Waldfläche im Hainich (Thüringen) wurde 2013-2016 eine umfangreiche Feldstudie durchgeführt. Der Standort ist ein unbewirtschafteter temperater Buchenmischwald auf flachen Cambisolen und Luvisolen aus Muschelkalk mit geringmächtiger Lössauflage. Die Bestandseigenschaften wurden kartiert. Stammabfluss (n = 65) wurde flächendeckend auf 11 Subplots (je 100 m^2) gemessen. Kronentraufe (n = 350) sowie Bodeneigenschaften und -wassergehalt (n = 210, jeweils in 7,5 und 27,5 cm Bodentiefe) wurden in unabhängigen stratifizierten Zufallsdesigns erhoben. Der Bestandsniederschlag wurde ereignisbezogen während der Sommer, der Bodenwassergehalt kontinuierlich erfasst. Der Einfluss von Baum-, Nachbarschafts- und Bestandseigenschaften auf den Stammfluss wurde mit linearen gemischten Modellen untersucht. Die Muster von Bestandsniederschlag und Bodenwassergehalt wurden anhand ihrer statistischen Eigenschaften und ihres raumzeitlichen Verhaltens miteinander verglichen. Aus Bestandsniederschlags-, Niederschlagsintensitäts- und bodenhydraulischen Leitfähigkeitsdaten wurden Stammabfluss-Infiltrationsflächen und die Infiltrationsverteilung des gesamten Bestandniederschlags berechnet. Durch den Vergleich von baumnahen und baumfernen Bodenmesspunkten untersuchte ich die Auswirkungen von Wassereintrags-Hotspots auf Bodenwassergehalt und -eigenschaften.

Während der Kampagnen wurden ca. 600 mm Freilandniederschlag erfasst, wovon der Stammabfluss ca. 3 % und die Kronentraufe ca. 65 % betrugen. Die beobachteten Muster des Bestandsniederschlags (in Bezug auf Kronentraufe als auch Stammabfluss) und des Bodenwassergehalts waren zeitlich stabil.

Meine Ergebnisse zeigen, dass Nachbarschafts- und Bestandseigenschaften einen wichtigen Einfluss auf die Bildung von Stammabfluss-Hotspots haben. Der Stammabfluss variierte beträchtlich von Baum zu Baum, und überdies ebenso auf der Skala kleinerer Baumgruppen. Dies unterstützt das Modellergebnis, dass Beschattungseffekte innerhalb des Kronendachs auf den Stammabfluss von geringer Bedeutung sind. Im Gegensatz dazu erhöhte die Baumdichte den Stammfluss auf beiden Skalen erheblich. Sie vergrößert die Holzoberfläche, die eine

Auffangfläche für Regentropfen und Fließwege bietet, und verändert die Baummorphologie vorteilhaft für die Stammabflussbildung. Die Artenvielfalt verstärkte diesen Effekt, da sie eine effizientere Kronenraumnutzung durch unterschiedliche Wuchsformen ermöglicht.

Stammabfluss-Infiltrationsgebiete sind meiner Berechnung zufolge deutlich kleiner als bisher angenommen, und somit die Hotspot-Stärke des Stammabflusses deutlich größer. Die Infiltration des Stammabflusses erreichte regelmäßig die Infiltrationskapazität des Bodens und war Größenordnungen höher als die Infiltrationshöhe der Kronentraufe. Das bedeutet auch, dass Niederschlags-Hotspots sich auf einen sehr kleinen Flächenanteil beziehen: 3,6 % des Niederschlagsvolumens infiltrieren auf 0,036 % des Untersuchungsgebiets.

Unerwarteterweise wirkte sich die Heterogenität des Bestandniederschlags kaum auf die Muster des Bodenwassergehalts aus. Zunächst erzeugten Bestandsniederschlagseinträge zusätzliche Variabilität, diese war jedoch sehr kurzlebig. Der Haupteinflussfaktor des Bodenwassergehalts waren die Retentionseigenschaften des Bodens. Daraus resultiert, dass lokal erhöhte Wassereinträge nicht im Boden verbleiben, sondern in den tieferen Untergrund abfließen.

Die Bodeneigenschaften in Stammnähe zeigten signifikante Unterschiede zu stammfernen Messpunkten. Stammnahe Punkte waren durch erhöhte Makroporosität, Tonauswaschung und Kohlenstoffakkumulation charakterisiert. Daraus folgten eine veränderte Bodenwasserretention und -leitfähigkeit sowie geringere Wassergehalte. Insgesamt signalisieren die Ergebnisse eine ausgeprägtere Bodenstruktur und beschleunigte Bodenbildung in Baumnähe, die durch Stammabfluss-induzierte Hotspots des Bodenwasserflusses angetrieben werden.

Zusammengefasst erzeugte die heterogene Bestandsstruktur am Untersuchungsstandort eine hohe Variabilität des Bestandsniederschlags mit starken Stammabfluss-Hotspot. Die Eintragsmuster wirkten sich weniger auf den Bodenwassergehalt als auf die -flüsse aus. Stammabfluss-Hotspots setzten sich im Untergrund fort und erzeugten durch beschleunigte Bodenbildung Boden-Mikrostandorte. Durch erhöhte Makroporosität wirkten Input-induzierten Hotspots des Bodenwasserflusses selbstverstärkend. Auf diese Weise erzeugt die Vegetation Kurzschlüsse der abwärts gerichteten Wasserflüsse zwischen Baumkrone und tieferem Untergrund. Dies könnte die Trennung der Niederschlagseinträge in bodengebundenes, pflanzenverfügbares Wasser einerseits, oder Tiefenversickerung und Grundwasserneubildung andererseits, beeinflussen.

Summary

Vegetation and soil form a highly interactive system, within which water is one of the most important factors. By the redistribution of precipitation and its separation into interception, throughfall and stemflow, vegetation canopies introduce a strong small-scale heterogeneity to downwards-directed water fluxes in forests and shrublands. This heterogeneity could affect subsequent hydrological processes in the soil, with a potential to ultimately alter storm response, plant water availability and groundwater recharge. Understanding an ecosystem's water management is important especially in times of global change, where sustainability of both ecosystems and water resources are at risk.

Yet, to date, the fate of below-canopy ("net") precipitation heterogeneity in the soil still is largely in the dark. Throughfall and stemflow amounts are found to depend on tree or shrub species and traits, and throughfall spatial variability has shown to be stable in time. Thus, variability and patterns produced by the canopy are systematic. Stemflow often constitutes a hotspot of water input to the soil. However, stemflow variability and its temporal stability have rarely been addressed. Especially in diverse forests, the single-tree approach on drivers of stemflow generation is insufficient, but tree neighborhood and stand diversity have hardly been considered. Stemflow has been shown to produce preferential flow in near-stem soils. Impacts of net precipitation on soil water content, meanwhile, are subject mainly to assumptions and contradicting results of modeling studies and limited field data. Likewise, the discussion about stemflow infiltration areas is ongoing. Early studies have sporadically reported a gradient in soil properties depending on the tree distance in forests. The potential impact of soil microsites around trees on the fate of stemflow, and, vice versa, a potential impact of stemflow inputs on near-tree soils, has not been taken into consideration yet.

In this thesis, I address the overarching research questions, of (1) By which factors does the vegetation community systematically generate hotspots of net precipitation? (2) How does the high heterogeneity of net precipitation translate to soil water conditions and processes?

In a comprehensive experimental approach, I chose a high-resolution statistical design to capture overall patterns, and I used hotspot locations – trees – to pin down systematic patterns and define extreme impacts of canopy-induced water flow heterogeneity on soil water and properties. To this end, an extensive field study was conducted (2013-2016), surveying stand and soil properties as well as measuring net precipitation and soil water content collectively on a 1 ha forest plot in central Germany. The stand was an unmanaged temperate mixed beech forest on shallow cambisols and luvisols developed from limestone with a thin loess cover. Stemflow (n = 65) was measured on 11 subplots (100 m^2) within the plot. Throughfall (n = 350) and soil properties (n = 210) were measured in independent stratified random designs. Soil was addressed in two depths (7.5 and 27.5 cm). Stand and soil properties were surveyed once, net precipitation was measured on an event basis during the summers, and soil water content was recorded continuously. I approached the impact of tree, neighborhood and stand properties on stemflow with linear mixed effects models. To link patterning of net precipitation and soil water content, I compared their statistical properties and spatiotemporal behavior. I used net precipitation, gross precipitation intensity and soil hydraulic conductivity data to calculate stemflow infiltration areas and the overall distribution of net precipitation infiltration. By statistically comparing soil areas near tree stems to the bulk soil, I assessed the impact of net precipitation hotspots on soil water and soil properties.

Of about 600 mm of gross precipitation measured during the campaigns, stemflow amounted ca. 3 %, throughfall ca. 65 %. Observed patterns of net precipitation (throughfall as well as stemflow) and soil water content, were stable in time, and therefore systematic.

I found, that stand and tree neighborhood properties importantly affect stemflow hotspot generation. Stemflow varied considerably between trees, and what is more, the variation persisted on the forest patch scale in the same order of magnitude. Variability translating to a larger scale also confirmed the result that shading within the canopy, which was the most frequently assumed neighborhood effect, plays a minor role for stemflow patterns. To the contrary, tree density importantly increased stemflow on both scales. Tree density is associated with woody surface area, providing catch area for raindrops and flow pathways. Tree density also changes tree morphology towards more steeply inclined branches, enhancing channeling of intercepted water to stemflow. Additionally, species diversity had a positive impact on stemflow

generation. Species diversity allows a more efficient space occupation due to different growth strategies, increasing tree density and woody surface area.

Calculation of stemflow infiltration areas showed, that they are much smaller, and therefore the hotspot character of stemflow is much stronger, than previously assumed. Stemflow infiltration typically reached soil infiltration capacity, and was orders of magnitude higher than throughfall infiltration. Thus, extreme input hotspots apply to an extremely small fraction of the area: 3.6 % of precipitation volume infiltrated on 0.036 % of the plot.

Unexpectedly, heterogeneity of inputs induced by the canopy did not imprint on soil water content patterns. Additional variation introduced by net precipitation patterns quickly dissipated after rain events. The major driver for soil water content were soil hydraulic properties, namely field capacity. This means that large water inputs are not retained in the soil, but mostly bypass it and drain to the deeper subsurface.

Near tree stems, soil properties were significantly altered, forming tree-induced soil microsites. There was a higher macroporosity, resulting in a lower water retention and higher hydraulic conductivity close to tree stems. This led to increased drainage and lower water contents at the microsites. Additionally, clay dislocation and carbon accumulation were increased. Overall, results signal a more pronounced soil structure and an accelerated soil formation close to trees, which are driven by stemflow-induced hotspot fluxes.

In summary, the heterogenous and diverse canopy on my investigated site established a high variability of net precipitation and strong stemflow hotspots. Net precipitation patterns did not imprint on soil water content, but did imprint on soil water fluxes. Stemflow hotspots persisted in the soil, and created soil microsites by accelerated soil formation. Due to increased macroporosity, stemflow-induced soil water flux hotspots were self-reinforcing. Thus, vegetation induces water bypass flow from the canopy to below the rooting zone. This is likely to influence hydrological precipitation response and the separation of rainfall to soil-bound, plant-available water on one hand or deep percolation and groundwater recharge on the other.

"Rather than concentrate exclusively on specific domains, we need to explore the neglected boundaries along which contiguous domains interact and interconnect within their larger context. Our science will progress by devoting ever greater attention to details while simultaneously striving to expand our sphere of inclusion in order to achieve a more encompassing view of the soil's role in terrestrial ecosystems."

Daniel Hillel, 1998: Environmental soil physics.

Acknowledgements

First of all, I owe my thanks to my advisor. Anke, it was a pleasure to get to know you, work with you and learn from you. I feel that I developed so much during this time (while I was still able to keep my stubbornness, sorry…), very much thanks to you. We shared some eventful times, and you kept supporting me throughout. I couldn't have wished for better.

I thank my second reviewer, Miriam, for giving me the honors of dealing with this thesis.

I also thank my colleagues, Christine, Nicolas, Marcus, Marcel, Janett, Gökben, Sven and Martin, for their companionship, the talks and the coffee breaks we shared. Christine, when I arrived in Jena, without knowing me, you invited me to your home and into your circle of friends, that was so incredibly kind. Janett, your hands-on and good-humored attitude is admirable and made my life so much easier. A special thanks also to Joe (the "Smutje"), Christoph (Master of the trash movies) and Danny (the pinch of serenity), the students who had the questionable opportunity of living with me in the Hainich for months during the soil sampling and installation. I really want to thank all of the many helpers during field work. I also thank everyone who gave feedback on this dissertation, thereby helping me a lot to improve it: Annette, Christine, Gökben, Magdalena, Peter, Simon, Sven and Vincent.

This great research opportunity was made possible thanks to the DFG-funded AquaDiva collaborative research center. I want to thank the speakers, the field site organizers, and the series of charming coordinators within AquaDiva for all their support. I especially want to thank AquaDiva, Anke, and Christian Messier and François Lorenzetti from ISFORT for making my research stay in Québec, Canada, possible. It was such a great experience. I also thank all the project's researchers for their interest, thought and inspiration. Special thanks to Beate for being part of my Ph.D. Advisory Committee and supporting me.

I want to thank my advisors and colleagues in Braunschweig and Hamburg, who set me on this path. And I would like to thank those friends who advised me to quit the doctorate, because you reminded me that this is my choice.

The people I lived with during the last years were my friends and family, my counselors and therapists. Elly, Chris, Milly and Chanti, there is so much wisdom and beauty in you! I thrived in your company, you never let me down.

Peter, you are such a special person. You have calm and drive, good-naturedness and opinion, patience and passion, and you are the least pretentious person I know. You never question what I do, never confine me, and support me whenever I ask you to. We know this thesis has not been the biggest task we had to manage lately. But know that I never took your presence for granted. I hope that I will share so much more with you.

Lastly, I want to thank my family. Oma Marianne, du bist mein größtes Vorbild! My parents Annette and Guido: you enabled me to become the person I am, and my siblings Magdalena and Simon: you were and are my companions on that way. I guess, the Metzger gene has had its share in me writing this thesis. But it is all the other things I share with you all that give me confidence. I’m proud of what wonderful people you are.

Content

Figures

Tables

Abbreviations and Symbols

#	Number of	-
θ	Soil water content (volumetric)	vol-%
θ_{FC}	Soil water content at field capacity (– 60 hPa)	vol-%
ρ	Spearman's rank correlation coefficient	-
ρ_b	Soil bulk density	g cm^{-3}
ρ_m	Density of the soil mineral component	g cm^{-3}
$\rho_{TF\ can}$	Spearman's ρ for the correlation between canopy cover and throughfall	-
$A_{i\ SF}$	Stemflow infiltration area	m^2
A_{plot}	Plot area	m^2
A_{tree}	Tree basal area (at breast height)	m^2
AIC	Akaike Information Criterion	
$C_{i\ SF}$	Stemflow infiltration capacity	mm h^{-1}
C_{org}	Organic carbon content	mass-%
CQV	Coefficient of quartile variation	
d_{tree}	Tree diameter at breast height	m
D	Simpson index of biodiversity (Simpson, 1949)	-
DBH	Tree diameter at breast height	
E_I	Interception loss of gross precipitation	%
$h_{n\ rel}$	Relative height of the neighborhood (area within r)	-
h_{tree}	Tree height	m
$h_{tree,j}$	Height of the reference tree j	m
$h_{tree\ max}$	Height of the highest tree in the neighborhood (area within r)	m
H	Size heterogeneity index (Krämer and Hölscher, 2009)	-
I_{SF}	Stemflow input rate	L h^{-1}
ID	Identification number	
K_s	Soil saturated hydraulic conductivity	mm h^{-1}

m-CQV	Median of the coefficient of quartile variation	
$m_{s\,dry}$	Soil sample dry weight	g
n	Number of elements in a statistical sample	-
n_i	Number of individuals of species i per unit area	-
$n_{s\,app}$	Soil porosity estimated from bulk density	vol-%
$n_{trees\,plot}$	Number of trees on the plot	-
p	Probability value of statistical significance	-
P_g	Gross precipitation	mm
P_{TF}	Throughfall net precipitation	mm
P_{SF}	Stemflow net precipitation	mm
Q_1	First sample quartile	
Q_3	Third sample quartile	
r	Radius of the neighborhood area, mean tree distance	4.7 m
R_F	Stemflow funneling ratio (Herwitz, 1986)	-
V_s	Soil sample volume	cm^3
V_{SF}	Stemflow volume	L
$V_{SF\,j,e}$	Stemflow volume per tree j and event e	L
$V_{SF\,n}$	Normalized tree/subplot stemflow (Vachaud et al., 1985)	-
w	Width of an assumed annular stemflow infiltration area around a tree	m

1 General introduction

Plants are the basis of our existence. As autotrophs, they create life from inorganic matter, an ability which humans – as heterotrophs – completely depend on. What is more, they produce oxygen in such quantities that it is freely available in the atmosphere, allowing us to gain our energy most efficiently from respiration (Hillel, 1998). Apart from these vital services, plants provide us with a set of benefits, as fiber, fuel, medicine, air and water filtration, flood protection, carbon sequestration, and cooling of the earth's surface (Lyons et al., 2014; Trumbore et al., 2015). We share our living space with plants. For the appearance and the organizational structure of this living space, plants play a dominant role. Vegetation communities strongly depend on environmental conditions. At the same time, vegetation shapes the environment it is settled in and establishes ecosystems (Perugini et al., 2017; Bruelheide et al., 2018; Freschet et al., 2018). Especially at times of strong environmental changes, it is key for us to understand the feedbacks between vegetation and environmental factors to sustain the sources of our livelihood (Sheil, 2014; Trumbore et al., 2015).

One environmental factor which interacts highly dynamically with vegetation is water. Vegetation effects on water cycling create relevant feedbacks on all scales (Pielke et al., 1998). Most prominently, vegetation removes large amounts of water from the soil and feeds it to the atmosphere by transpiration. Transpired water forms rain clouds, and forests in particular are often sources of abundant rainfall (van der Ent et al., 2012; Sheil, 2014; Watson et al., 2018) – a self-sustaining system at the larger landscape scale (Syktus and McAlpine, 2016). Plants need large amounts of water. They need it as an ingredient for photosynthesis, but the major part of water taken up by plants is just a by-product of this process. The moment they open their stomata to take up CO_2 by diffusion, diffusion also causes them lose water. Just like that, incidentally, plants power the water cycle and weather patterns as well as cool down themselves and their surroundings (Hillel, 1998; Syktus and McAlpine, 2016; Aubrey, 2020). Plants extract the vast amounts of water needed in this process from the soil water storage, which is replenished by rainfall. A less well-known interaction of vegetation with the water cycle, compared to

transpiration, is the alteration of rainwater inputs to the soil: By its physical existence, the canopy acts like a porous buffer zone for rainfall before it reaches the earth's surface. Water is retained, delayed, and spatially redistributed in the canopy. It is enriched with airborne deposits and plant surface-associated biological material, and plants can extract water and nutrients from intercepted droplets (Aubrey, 2020). After passing through the canopy, small-scale heterogeneity has been introduced to the spatial distribution of rainfall. While overall, water input is reduced, and therefore, the major part of the vegetated area receives less than above-canopy rainfall, some hotspots evolve, where water input is highly concentrated (Li et al., 2012). With water redistribution, also concentrations and inputs of nutrients and pollutants become heterogeneous (Aubrey, 2020).

Heterogeneity is a principle prevalent in nature on all scales. The importance of large-scale heterogeneities of environmental variables is evident: They create the gradients that drive exchanges and processes leading to all environmental phenomena. Gradients force the ocean currents, the climate and the weather, and global matter cycles (Schönwiese, 2013). Gradients decide the stability of ecosystems and drive population dynamics (Legendre and Fortin, 1989). But how relevant are small scale heterogeneity gradients and processes? In general, small-scale processes can have an effect on larger-scale functioning. This is because of the non-linearity of relationships between driving and dependent variables, which applies to many environmental processes. Local extremes due to high variance might be most important for effects that are visible on a larger scale. For example, plant water uptake from the soil depends on soil water content non-linearly, with an efficiency optimum for medium soil water content (Hillel, 1998). A heterogeneous distribution of soil water, in space or time, changes plant water uptake compared to a more homogeneous distribution. A mean value of soil water content does not consider this effect, and therefore gives incomplete information (Famiglietti et al., 2008). Feedbacks and thresholds are additional aspects of non-linear behavior in which heterogeneity becomes important (Lenton, 2013). We therefore can consent to the famous statement: "The whole is more than the sum of its parts" (Smuts, 1926). To evaluate the relevance of small-scale heterogeneities, we need to know them, characterize their organizing elements and point out couplings, feedbacks and thresholds that impact larger scale functioning.

The retention and redistribution of precipitation in the canopy is likely to affect subsurface processes. Interception is the “first process in the chain of interlinked rainfall-runoff processes”, hence affecting all subsequent hydrological and connected ecological processes (Savenije, 2004). The introduced small-scale heterogeneity has the potential to, by non-linear coupling, change the hydrological behavior of the vegetation-soil system at larger scales (Guswa and Spence, 2011). A series of studies has therefore focused on subsurface effects of below-canopy precipitation within the last decades (details will be given in Section 1.1). Increased and preferential soil water fluxes due to stemflow have been observed in the vicinity of trees. Yet, due to the difficulty of implementing a representative and comprehensive approach, other evidence is fragmented and contradictive. This includes findings on quantitative fluxes, their spatiotemporal distribution, and their destination – the question, which hydrological compartments ultimately benefit from the flow hotspots, arises. Such, soil water storage could also be affected by net precipitation patterns. The impact of net precipitation on the spatiotemporal behavior of soil water content has not yet been experimentally substantiated. Changed dynamics of soil water could also impact on flow processes and pathways, shaping the permeated soil over time. The field of potential impacts of net precipitation patterns on soil properties has hitherto received little attention. In addition to a broad data basis, an interdisciplinary understanding is necessary to resolve whether and in which ways variability of inputs translates into subsurface water storage and flow processes. Water input heterogeneity underneath canopies opens up a vast field of scientific inquiry. By precipitation redistribution and coupled soil water processes, the properties of the ecosystem could impact on hillslope and landscape-scale hydrological functioning, like storm response, plant water availability and groundwater recharge. This, in turn, carries implications, from the small-scale distribution of microbial communities (Baldrian, 2017), up to the role of the soil-atmosphere interface for hydrological catchment as well as climate functioning (Pielke et al., 1998; Gedney and Cox, 2003), nutrient cycling (Parker, 1983; Levia and Frost, 2003), the health of ecosystems (Van Stan II and Friesen, 2020) and related vital ecosystem functions.

In this thesis, I seek out small-scale heterogeneities of below-canopy rainfall and trace their fate in the soil. I approached statistical patterns and hotspots of precipitation inputs experimentally in a near-natural forest in central Germany. In the following, I will give a brief introduction to the state of the research and identify the knowledge gaps which my work sets out from.

Subsequently, I will present the aim of my study and the research questions and hypotheses I developed to that end. I will then give an overview on my approach and a short outline of the thesis's chapters.

1.1 State of the art and research gap

Precipitation constitutes the incoming side of the soil water balance (neglecting lateral water fluxes and capillary rise), while the outgoing fluxes are runoff, drainage, evaporation (from various sources) and transpiration (Hillel, 1998; Savenije, 2004). In vegetated systems, a fraction of precipitation is intercepted by the plant surfaces and evaporates directly back to the atmosphere, such that the incoming water to the soil is the precipitation minus the interception, called net precipitation. The incident precipitation above the vegetation canopy is named gross precipitation. Net precipitation has two components, distinguished by their pathway through the canopy: Throughfall drips through or from the canopy, while stemflow stays attached to plant surfaces and flows down to the soil along plant stems. The process of the differentiation of precipitation into interception, throughfall and stemflow in the canopy is called precipitation partitioning (Crockford and Richardson, 2000).

While precipitation partitioning occurs in all vegetation, it is mostly studied in forests. Trees are the giants of the plant world, holding the records for most plant processes, such as transpiration or primary production (Sheil, 2014; Trumbore et al., 2015; Baldrian, 2017; Watson et al., 2018). This makes forests the climax vegetation wherever resources allow so, and in spite of human interference, forests still cover ca. 25 % of Earth's terrestrial surface (Watson et al., 2018). What is more, trees open up habitats for other organisms that live in, on and under their canopies, making them hosts of productivity, diversity, and a whole subset of related ecosystem services and functions (Trumbore et al., 2015; Baldrian, 2017; Watson et al., 2018). While the global importance of forest ecosystems is undisputed, their scale additionally makes net precipitation easier to determine and created patterns likely more influential.

The effect of forest canopies on precipitation inputs has been researched since the 19th century, and then already have researchers noticed its spatial heterogeneity and looked for its drivers (Van Stan II and Friesen, 2020). Net precipitation has been investigated throughout the following

century, but gained momentum in recent decades. First, the reduction in precipitation depth caused by the canopy due to interception was inquired, and examined how best to determine representative values of interception from throughfall and stemflow measurements (Leonard, 1961; Helvey, 1967; Reynolds and Henderson, 1967; Rutter et al., 1971; Gash, 1979). In this context, the spatial variance of throughfall was approached (Lloyd and de O. Marques F., 1988; Durocher, 1990; Loustau et al., 1992). Stemflow was found to funnel precipitation to the stem base, therefore concentrating water inputs, and stemflow studies focused on stemflow yield and funneling (Herwitz, 1986; Crockford and Richardson, 1990; Hanchi and Rapp, 1997). With the knowledge about heterogeneity of net precipitation inputs in forests, researchers looked for the drivers of net precipitation patterns (Návar, 1993; Aboal et al., 1999) and the potential impacts the patterns might have belowground (Pressland, 1976; Durocher, 1990; Taniguchi et al., 1996). These topics are still investigated and discussed today, which I will go into more detail about below.

Canopy interception usually constitutes 10 % to 30 % of gross precipitation, though values can be much higher depending on the ecosystem and the climate (Savenije, 2004; Llorens and Domingo, 2007; Miralles et al., 2010). Interception behavior of leaves and bark directly impact stemflow and throughfall generation. Interception, throughfall and stemflow all depend on climate and vegetation, though vegetation seems to have a stronger impact (Sadeghi et al., 2020). In their review, Sadeghi et al. (2020) found global ranges for throughfall and stemflow relative to gross precipitation of 65.5–83.2 % and 0.8–6.2 %. Abiotic factors of throughfall and stemflow amounts and variability are precipitation event size and meteorological conditions during precipitation (Levia and Frost, 2003; Levia Jr and Frost, 2006). Identified biotic factors comprise canopy structure and plant traits, including plant surface properties as well as plant architecture (Levia and Frost, 2003; Levia Jr and Frost, 2006; Levia and Germer, 2015; Sadeghi et al., 2020; Van Stan et al., 2020). Many of these traits are species-specific (Levia and Frost, 2003; Levia and Germer, 2015). Due to both climate and leaf phenology, there are significant seasonal differences in throughfall and stemflow, including different types of precipitation (Levia and Frost, 2003; Levia Jr and Frost, 2006).

1.1.1 Drivers of stemflow variation

The heterogeneity of net precipitation is well-recognized and -researched. This applies especially to throughfall variation and stemflow funneling. Yet, the tree-to-tree variation of stemflow has been reported in only a few studies (Loustau et al., 1992; Holwerda et al., 2006; Terra et al., 2018). The sample of trees for stemflow measurement does often not allow for an investigation of stemflow variation, because it is too small and/or not random. Nevertheless, stemflow spatial variability has been approached in identifying stemflow drivers. Hereby, a main focus lay on the individual tree (or shrub) stemflow yields. Tree size has been found to be the main driver of stemflow variation (Reynolds and Henderson, 1967; Takahashi et al., 2011). Additionally, many morphological traits were identified as drivers of stemflow production, as number and angle of branches, bark roughness and leaf hydrophobicity (Iida et al., 2005b; André et al., 2008; Krämer and Hölscher, 2009; Van Stan and Levia, 2010; Takahashi et al., 2011; Molina and del Campo, 2012; Levia et al., 2015; McKee and Carlyle-Moses, 2017). Few studies researched the effect of stand properties on stemflow. While tree size increases individual stemflow yield, small trees and understory increase stemflow per area (Murakami, 2009; Takahashi et al., 2011; González-Martínez et al., 2017). Stand density was observed to increase tree stemflow in a thinning experiment (Molina and del Campo, 2012), and Krämer and Hölscher (2009) found a temporary (negative) impact of other species intermixing with European beech on stand stemflow. Stand properties and tree heterogeneities within a stand, e.g., concerning species or size, are likely to affect stemflow production on the tree and the stand level. Additionally, single tree architectural traits are also influenced by their neighboring trees (Frech et al., 2003; Schröter et al., 2012; Juchheim et al., 2017), which applies also to those traits identified as stemflow drivers. Yet, rarely have potential influences of neighboring trees on stemflow been included in studies (Aboal et al., 1999; Terra et al., 2018). Proposed neighborhood effects are typically related to shading or competition (André et al., 2008; Takahashi et al., 2011). No wider-spread study, encompassing various possible neighborhood effects, exists. Thus, there is a knowledge gap concerning tree neighborhood, stand property and stand heterogeneity effects on stemflow generation.

Stemflow often constitutes hotspots of net precipitation. It shows a strong variation, which cannot be explained by tree size alone. Individual tree, neighborhood and stand properties could affect stemflow hotspot formation on the tree and on the tree community scale.

1.1.2 Infiltration patterns of net precipitation

While stemflow and throughfall shares of above-canopy precipitation are well researched, it remains unclear how precipitation variability looks at the point of infiltration, where stemflow and throughfall reunite. To understand the actual hotspot strength of stemflow as it reaches the soil, and such becomes relevant for plant support and groundwater recharge, we have to know the soil surface area where stemflow inputs infiltrate (Pressland, 1976; Herwitz, 1986; Tanaka et al., 1996; Liang et al., 2011; Buttle et al., 2014; Carlyle-Moses et al., 2018; Van Stan II and Allen, 2020). Different methods to map or estimate stemflow infiltration areas have been established (Reynolds and Henderson, 1967; Tanaka et al., 1990; Tanaka et al., 1996; Schwärzel et al., 2012), but have been applied to few (rather large) events and trees. Altogether, estimated stemflow infiltration areas would imply lateral spreading of stemflow on the soil surface, effectively reducing stemflow concentration. Recent studies argue that stemflow funneling could be smaller (Van Stan and Gordon, 2018; Van Stan II and Allen, 2020) or larger (Carlyle-Moses et al., 2018) than generally discussed based on stemflow infiltration areas.

Knowing the stemflow infiltration area is the prerequisite to a meaningful evaluation of the hotspot strength of stemflow. Infiltration of net precipitation patterns is the first step of their belowground fate, where heterogeneity could be destroyed or persist.

1.1.3 Impact of net precipitation on soil water content patterns

Especially the rainfall-concentrating effect of stemflow has inspired research to find out the subsurface fate of those fluxes. Patterns of soil water drainage could affect groundwater recharge and the fate of nutrients and pollutants (Taniguchi et al., 1996; Guswa and Spence, 2011; Levia and Frost, 2003; Levia Jr and Frost, 2006). It has been established by numerous observations that stemflow causes preferential flow in soils (Johnson and Lehmann, 2006; Li et al., 2013). The impact of stemflow as well as throughfall on soil water content is less clear. Soil water content

provides plant-available water and is an important driver for biogeochemical processes and microbiological habitats (Chang and Matzner, 2000; Drenovsky et al., 2004). An increase in soil water content near stems after precipitation events was found repeatedly (Pressland, 1976; Li et al., 2008; Wang et al., 2011; Jian et al., 2014), but also lower water contents were observed near stems (Rutter, 1964; Liang et al., 2007; Buttle et al., 2014). A number of studies expected throughfall patterns to imprint on soil water content patterns (Pressland, 1976; Bouten et al., 1992; Alva et al., 1999; Schume et al., 2003; Jost et al., 2004; Teuling and Troch, 2005; Zehe et al., 2010; Bachmair et al., 2012; Guswa, 2012; Rosenbaum et al., 2012; Coenders-Gerrits et al., 2013; Fatichi et al., 2015; Traff et al., 2015). Yet, few studies focused on resolving the problem. Testing this hypothesis requires an extensive data set from a useful sampling design, measuring canopy and soil water content at the same location, and achieving spatial and temporal representativity. To date, these data requirements, which have been repeatedly called for (Teuling and Troch, 2005; Bachmair et al., 2012; Zucco et al., 2014), could not be fully met. Several field studies on soil water content distributions found hints of an impact of throughfall (Zehe et al., 2010; Rosenbaum et al., 2012; Traff et al., 2015), but field studies explicitly researching the topic could not find a relationship between throughfall and soil water content patterns (Pressland, 1976; Raat et al., 2002). Additionally, modeling approaches found local drivers of soil water content to be dominant compared to throughfall effects (Bouten et al., 1992; Coenders-Gerrits et al., 2013). In summary, despite scientific consideration, results on the impact of small-scale variability of inputs on soil water content in forests are scarce and the topic remains unresolved.

The increased heterogeneity of rainfall introduced by the canopy could have consequences for soil water. The assumption of an effect of net precipitation patterns on soil water content is common. However, experimental evidence for this assumption is still missing.

1.1.4 Vegetation and single tree effects on soil properties

Vegetation has been observed to impact soil properties in forests and grasslands (Eviner and Chapin, 2003; Zuo et al., 2009; Thompson et al., 2010; Zucco et al., 2014; Fischer et al., 2015; Freschet et al., 2018). Focusing on litter and net precipitation chemistry, few early studies found a single-tree impact on soil chemistry (Gersper and Holowaychuk, 1971; Lodhi, 1977;

Falkengren-Grerup, 1989; Boettcher and Kalisz, 1990), and acidic rain has been repeatedly found to have decreased soil pH next to tree stems due to concentrated stemflow inputs (Neite and Runge, 1986; Falkengren-Grerup, 1989; Rampazzo and Blum, 1992; Koch and Matzner, 1993). Vegetation and water are factors of soil formation (Blume et al., 2010). Because of chemical signals and large introduced water fluxes, stemflow could impact soil formation processes around tree stems. There is decisive evidence that stemflow triggers preferential flow (Taniguchi et al., 1996; Liang et al., 2007; Li et al., 2008; Sansoulet et al., 2008; Li et al., 2009; Bialkowski and Buttle, 2015). It stands to reason that stemflow could be changing physical properties in the subsurface, and shape the conditions for its own subsurface fate. The only study to my knowledge which has touched this subject is Rashid et al. (2015), who recently reported changed soil hydraulic properties (van Genuchten parameters derived from measurements) near stems. Overall, possible soil microsites at tree stems, their formation mechanisms and their potential impact on stemflow-induced water fluxes have been hardly addressed.

Stemflow is known to trigger preferential soil water flow. Subsurface flow mechanisms of stemflow could be impacted by the evolution of soil microsites around tree stems. As soil chemistry can be influenced by stemflow, a mechanistic development of discrete microsites with changed hydraulic properties is possible, but has not been reported yet.

1.2 Contribution

Forest ecohydrology has advanced rapidly in recent decades. It has been established, that canopies create a spatially variable precipitation pattern, which is systematic. Canopy structure and tree morphology shape this pattern. While overall, precipitation input is decreased due to interception evaporation, stemflow can concentrate rainfall, such that water input at the tree base is a multiple of gross precipitation. Stemflow at many sites triggers soil preferential flow below trees and likely increases soil- and groundwater recharge. These results prove, that the effect of the canopy on precipitation inputs is important for the water balance and for water cycling. The type of ecosystem or forest has an impact not only on transpiration and evaporation, but also on downwards-directed water fluxes (the two of which are, of course, in a constant exchange). Knowing this, a lot of the mechanisms which systematically create, and are created by, net

precipitation variability, are not identified yet. Carving out systematic mechanisms requires taking a broader perspective. I want to take this broader perspective in a statistical and interdisciplinary approach. A statistical approach means, taking a step back and evaluating processes that take place by their relative frequency and strength. An interdisciplinary approach means, looking at the whole system to identify and understand interactions between vegetation, water and soil.

With this work, I aimed to further close the gaps in our understanding and evaluation of small-scale patterning, and resulting hotspots, in downwards-directed water fluxes in the vegetation-soil system. I focused on advancing our knowledge of below-canopy water heterogeneity into the soil. The present study was made possible by a comprehensive and elaborate survey, sampling, and monitoring scheme of net precipitation and soil water content as well as stand and soil properties in a 1 ha forest plot. For analysis, a set of statistical tools were used to approach structures and dependencies from different directions. By this strategy, I intended to test popular assumptions from the research area and integrate the results into a new conceptual framework of the ecohydrological fate of rainfall, which I developed by the interpretation of the observed data.

1.2.1 Research questions and hypotheses

In the previous subsection, I described the state of knowledge in the field of forest ecohydrology and addressed research gaps relevant for my thesis. Based on the aforementioned research gaps, I here derive the overarching research questions and further specify the hypotheses as follows:

Research question 1: By which factors does the vegetation community systematically generate hotspots of net precipitation?

Tree morphology has been found to impact its stemflow yields. Stand and neighborhood properties impact a tree's growth. I therefore pose the hypothesis:

H1.1: Neighborhood and stand properties impact tree individual stemflow generation (Chapter 3).

Large trees have been found to produce most stemflow, yet, small trees show the strongest rainfall funneling. Beech trees are known to be stemflow-prolific, yet, in mixed stands, trees can

make better use of canopy space, and increased tree density has been found to increase stemflow. On a tree community scale, either cumulating or shading effects on stemflow could predominate. I hypothesize:

H1.2: In a natural, diverse forest, different forest patches can strongly vary in stemflow production depending on their community traits. Diverse stands and forest patches increase stemflow variation and therefore hotspot generation (Chapter 3).

Research question 2: How does the high heterogeneity of net precipitation translate to soil water conditions and processes?

The strength of stemflow funneling depends on stemflow infiltration areas. By overland flow of stemflow, and the overlap of stemflow and throughfall, stemflow hotspots could be mitigated.

H2.1: Stemflow infiltrates into the soil in direct proximity to the trunk, and has a distinct hotspot character compared to throughfall and throughfall dripping points (Chapter 4).

Throughfall and stemflow have been repeatedly assumed to be mirrored in forest soil water content patterns. Water content patterns affect plant water availability, microbial activity and biogeochemical soil processes.

H2.2: Net precipitation patterns imprint on soil water content patterns, and points of high inputs, especially stemflow hotspots, create areas of increased soil water recharge (Chapter 2).

If stemflow creates distinct hotspots of water infiltration to the soil, the soil must be channeling high water fluxes at the base of trees. Additionally, stemflow waters are chemically enriched. Vegetation and water fluxes and chemistry are known to impact soil physical and chemical properties.

H2.3: Soil properties in the vicinity of tree stems differ distinctly from tree-distant areas, forming microsites, which impact the fate of stemflow fluxes (Chapters 2 and 4).

1.2.2 Approach

Addressing the research questions posed above calls for an experimental approach. Observing and analyzing small-scale heterogeneity and short-term response processes in the canopy and the

soil offers a lot of challenges. Both domains are three-dimensional and structured. We realize structure visually, but we have little means to characterize or even quantify it (Hillel, 1998). The challenge of experimentally tackling ecohydrological interactions are threefold: (1) Access: Measurement of fluxes in different layers (i.e., the canopy, different soil horizons, and the deeper subsurface) disturbs the fluxes in all layers further down, making measurements at the same locations in different layers and, thus, a direct linking of processes there, impossible. Soil is non-transparent and rigid, hiding its inner structure from us. Getting direct information about this structure is always associated with its destruction. Therefore, installing a soil moisture sensor makes it impossible to determine soil properties at the exact location of the sensor. Similarly, extracting a soil sample makes resampling of the same exact location impossible, and, thereby, recording its temporal evolution. (2) Observation: Measurements in high spatial and temporal resolution are necessary to address the questions. This means, that a large investment of equipment and time is required. (3) Analysis: A complex, four-dimensional data set measured at different locations and in different time intervals makes it challenging to extract information from it. Every analysis can only reveal one fragment of the system. The measured data often does not meet the preconditions for the application of geostatistical tools: it is not normally distributed, skewed, and the data which would statistically be considered outliers are representing focal points of the processes of interest. Thus, there are no well-worn paths of analysis to follow, instead, new paths must be explored.

To overcome these obstacles, the first objective of my study was to create a design and thereby a dataset, which allows for a representative measurement of small-scale patterns of throughfall, stemflow, soil water content and soil properties in the same plot without disturbing each other, and which at the same time enables the comparison and linking of all different variables. I addressed this problem by establishing independent statistical designs for net precipitation and soil water content/properties measurements. The statistical designs were realized in stratified random sampling, which has been well-researched for throughfall sampling (Zimmermann et al., 2010; Zimmermann et al., 2016). To allow for autocorrelation analyses, additional transects were added to cover small distances, resulting in altogether 350 throughfall measurement points. For stratified random sampling, the plot is subdivided into subplots, within which a regular number of random sampling locations is determined. Therefore, I subdivided the plot into 100 subplots

(10 m × 10 m each). I used the subplot-structure to achieve random and representative sampling of stemflow by dedicating 11 subplots to stemflow measurement in a regular pattern, yielding 65 trees. The area-based stemflow measurement allowed for an exact determination of stemflow depth as well as a community stemflow analysis for small forest patches. To not measure soil water content disturbed by the retention of stemflow in the stemflow measurement process, I excluded stemflow subplots and three adjacent, downslope-directed subplots for each stemflow subplot from soil water content measurement. In the remaining subplots, organized in a checkerboard-like design, I established the stratified random sampling design for soil water content. To this design, as in the throughfall sampling design, I added transects for autocorrelation analysis. By virtual sampling, I tested different distances to use for the transects, such that the frequency of all distance classes would be as evenly distributed as possible in spite of the larger gaps in the design due to the stemflow measurement subplots. For soil water content measurement, a sensor network was installed. I decided to invest half of the available sensors to measure in two soil depths in order to cover the soil profile. Additional measurement profiles were located in tree transects (three profiles, in 0.3 m-1.5 m from the trunk) for analyzing the potential tree (and stemflow) impact on soil properties and soil water content. For these transects, trees that randomly already had more than one measurement profile within these distances were chosen, in addition to randomly selected trees with one measurement profile within the radius. In this manner, 22 tree transects could be realized by adding 30 measurement profiles. Altogether, 420 soil water content sensors were installed, grouped into 210 profiles of two sensors in 7.5 cm and 27.5 cm. In the course of sensor installation, one undisturbed soil sample was taken as close as possible to each sensor position in downslope direction of the sensor. Additionally, soil profiles were surveyed. From every third soil profile, undisturbed samples were taken in four depths. Net precipitation was sampled in campaigns on an event bases, soil water content time series were recorded continuously in 6-min intervals.

Because variables cannot be measured in the same location for the different layers (canopy-soil), statistical characteristic instead provide a comparison between the layers. A statistical design also yields the distribution (proportion, frequency) of high and low points, offering a representative characterization of the whole area instead of unconnected point sites. For the analysis, a combination of simple statistical methods was used: Rank correlations were applied

for the comparison of spatial fields to examine temporal stability and similarity of patterns. Statistical properties of spatial distributions and their temporal developments served to compare characteristics of different variables or location groups. Additionally, linear mixed effects models were used to investigate controlling factors, their relative strength, and their share on the variation of a target variable. As there is no method to process the multi-dimensional, interdependent data all together, standard geostatistical tools cannot be applied to the data, and part of the information of interest can only be quantified by proxies or not at all, I could not follow a fixed procedure. Yet, I based my analysis on some principles: (1) To considerately select temporal and spatial data chunks representative of certain conditions or processes, to approach these conditions or processes, (2) to develop (and test) informed hypotheses, such that significant correlations and differences are meaningful (Nuzzo, 2014), and (3) to carefully and thoughtfully interpret the results based on the methodical powers and constraints. I did my best to follow these rules to disentangle the bulk data volume, shift it to figurative angles where detecting patterns was possible and consider the cause of these patterns. In this manner, I sought to work my way from what we know to obtaining novel insights into the hydrological functioning of the researched site.

1.2.3 Study site

The experimental site was established as part of the Hainich Critical Zone Exploratory in the framework of the AquaDiva collaborative research center of the Deutsche Forschungsgemeinschaft (German Research Foundation) (Küsel et al., 2016). The Hainich forested low mountain ridge is situated in Thuringia, central Germany. It constitutes the largest coherent woodland in Germany, and almost half of it has been declared a National Park in 1997 and left unmanaged since then. The Hainich National Park is part of the Unesco World Natural Heritage (Hainich National Park Authority, 2020). The Hainich is situated in the transition zone between oceanic and continental climate (Hainich National Park Authority, 2020), the Köppen-Geiger climate class is Dfb (cold, without dry season, warm summer) (Köppen and Geiger, 1930; Peel et al., 2007).

The study plot lies inside the borders of the Hainich National Park at a north-eastern facing gentle slope. The bedrock is formed from interlayered shallow Triassic marl- and limestones

(Kohlhepp et al., 2017) with a thin Pleistocene loess cover. The stand is a mixed beech forest, comprising 70 % of European beech (*Fagus sylvatica*) and, in order of declining fractions, Sycamore maple (*Acer pseudoplatanus*), European ash (*Fraxinus excelsior*), European hornbeam (*Carpinus betulus*), Large-leafed linden (*Tilia platyphyllos*), Norway maple (*Acer platanoides*) and Scots elm (*Ulmus glabra*). The age structure is very heterogeneous with old-growth trees (about 200 a, estimated from diameter at breast height) and of a lot of juvenescence. Tree density was 581 ha^{-1} with a basal area of 38 m^2 ha^{-1}.

1.3 Outline

In this thesis, I follow spatial patterns of rainfall water fluxes from the forest canopy into the rooting zone to understand their relationships and discover pattern and process couplings between the different spheres. Especially, I want to highlight systematic flow hotspots due to stemflow, determine the factors of their evolution in the canopy and track them down into the soil. This is to evaluate the potential of hotspots due to increased heterogeneity for impacting the system's hydrological functioning.

The thesis consists of five chapters, of which this introduction is the first. Chapters 2-4 present self-contained studies focusing on different aspects of the overarching topic (details below). I present these chapters in chronological order, first approaching the overall impact of net precipitation patterns on soil water content, and in the following going into more detail on origins and impacts of stemflow hotspots. Chapters 2 and 3 have been published as scientific journal articles in Metzger et al. (2017) and Metzger et al. (2019) (further information in the appendix, p. 183). I begin by examining the effect of net precipitation on soil water content spatiotemporal patterns in **Chapter 2**. It shows that net precipitation has a minor impact, in contrast to soil properties, which are the main controlling factor for soil water content heterogeneity. Yet, soil properties show a systematic pattern due to vegetation: I discovered soil microsites at the base of trees, where increased drainage capacity leads to lower average soil water contents despite high stemflow inputs. **Chapter 3** is concerned with stemflow hotspot formation and variability, and the impact of neighborhood and stand trait heterogeneity. Stemflow was highly variable on the individual tree as well as on the forest patch scale. Stand

density and diversity showed to foster the creation of stemflow on both scales, outweighing shading and interception effects. **Chapter 4** traces stemflow hotspots in the soil. From throughfall and stemflow amounts and soil properties, the spatial distribution of infiltration into the forest soil is derived. Stemflow infiltration areas showed to be extremely small, such that stemflow introduces soil water fluxes that are several orders of magnitude larger than maximum throughfall fluxes. These high soil water fluxes showed to accelerate soil formation underneath trees. Interestingly, tree-induced soil microsites were larger in extent than (temporally averaged) stemflow infiltration areas. Finally, **Chapter 5** presents the synthesis of all achieved findings. Here, I critically evaluate my results, develop a conceptual understanding from them, and give an outlook into future research opportunities.

2 Vegetation impacts soil water content patterns by shaping canopy water fluxes and soil properties: High resolution measurements in a mixed beech forest plot

2.1 Introduction

Soil water content exhibits enormous spatial heterogeneity, also at small scales (Vanderlinden et al., 2012). Especially in forests, water input varies considerably on the small scale due to the redistribution of water in the canopy. This creates niches for microbial activity (Bundt et al., 2001; Brockett et al., 2012) and nutrient dynamics (Chang and Matzner, 2000; Bischoff et al., 2015) and affects transpiration dynamics, the formation of hotspots of soil bypass flow (Klos et al., 2014; Levia and Germer, 2015), expected deep percolation and its spatial variation (Guswa, 2012), and potentially subsurface runoff (Bouten et al., 1992; Zehe et al., 2010; Guswa, 2012).

Ecohydrological and hydrological studies have repeatedly proposed that the heterogeneity of soil water content in forests may be strongly driven by heterogeneous precipitation input caused by the interception and redistribution of precipitation in tree canopies (Alva et al., 1999; Schume et al., 2003; Keim et al., 2006; Liang et al., 2007; Blume et al., 2009; Zimmermann et al., 2009; Návar, 2011; Bachmair et al., 2012; Guswa, 2012; Rosenbaum et al., 2012). Yet, there is very limited experimental data to support this proposition, which is partly caused by the fact that both variables (precipitation input and resulting soil water content) can hardly be measured at the same place and time. Thus, although soil water content and net precipitation (below canopy precipitation, consisting of stemflow and throughfall) patterns have frequently been assessed, there are few cases where they have been studied on the same plot (Raat et al., 2002). However, observations at larger scales and under a variety of land covers found that both meteorological

forcing (e.g. precipitation gradients) and other factors such as seasonality, topography, soil texture, and vegetation characteristics/shading affect spatial soil water content variability (Famiglietti et al., 1999; Kim and Barros, 2002; Bachmair et al., 2012; Peng et al., 2013; Brocca et al., 2014; Renner et al., 2016).

Because field data at the plot scale are scarce, models were often used to identify potential drivers of the observed soil water content patterns (Teuling and Troch, 2005; Lawrence and Hornberger, 2007; Vivoni et al., 2010; Zehe et al., 2010; Coenders-Gerrits et al., 2013; Martinez et al., 2013; Bertoldi et al., 2014; Martínez García et al., 2014; Qu et al., 2015). These models' results point towards a strong impact of soil hydraulic properties as a driver for soil water content patterns. However, model applications are limited by the type of the equations applied and by underlying assumptions regarding, for example, the soil water flow and retention curve, and often lack representation of preferential flow.

To overcome this, several researchers notify a need for comprehensive experimental approaches, that include observation of temporal evolution of soil water content dynamics and measurement of soil hydraulic properties and precipitation in concert (Keim et al., 2006; Zimmermann et al., 2009; Bachmair et al., 2012; Coenders-Gerrits et al., 2013; Klos et al., 2014). Our study provides such a comprehensive approach. We conducted measurements of soil water content at high temporal and spatial resolution during the year 2015 on a 1 ha forest plot and analyzed them together with event-based net precipitation (sampled April-July) as well as soil porosity and field capacity (sampled once) measured on the same plot. We analyzed temporal stability of and relationship among these spatial patterns, with the objective of elucidating how spatial variation in soil water is affected by heterogeneous net precipitation, versus local and more temporally stable factors, like soil hydraulic properties.

2.2 Material and Methods

2.2.1 Site description

The research area is located on the upper lee side of a forested northeastern facing slope of the Hainich low mountain range in central Germany. The investigated site is part of the Hainich

Critical Zone Exploratory, which comprises forest, cropland and grassland sites within a hillslope monitoring transect (Küsel et al., 2016). Mean annual temperature ranges from 7.5 C° to 9.5 C° and total annual precipitation from 900 mm to less than 600 mm between the top of the ridge and the valley (Küsel et al., 2016). We established a 1 ha monitoring plot in the forested upper hill area with an altitude varying between 362 m and 368 m a.s.l.. The parent rock consists of thin-bedded alternations of lime- and marlstones of the Middle Triassic, overlain by shallow Pleistocene loess loam. Soils of the area are predominantly cambisols and luvisols (Schrumpf et al., 2014; Kohlhepp et al., 2017), with a median depth to the weathered bedrock surface on our plot of 37 cm, varying between a minimum of 15 cm and a maximum of 87 cm. The deciduous forest has been unmanaged since the founding of Hainich National Park in 1997 (Kohlhepp et al., 2017). The forest within the plot has a basal area of 38 m^2 ha^{-1}. The tree community has a heterogenous age structure and consists of 581 individuals (diameter breast height ≥ 5 cm), composed of 70 % European beech trees (*Fagus sylvatica*) accompanied by Sycamore maple (*Acer pseudoplatanus*), European ash (*Fraxinus excelsior*), European hornbeam (*Carpinus betulus*), Large-leafed linden (*Tilia platyphyllos*), Norway maple (*Acer platanoides*) and Scots elm (*Ulmus glabra*).

2.2.2 Precipitation measurements and processing

Both gross (above canopy) and net (below canopy) precipitation were manually sampled using gauges on a per-event basis for 16 precipitation events from May 7 to July 30, 2015. After each event, the collected volume of all sampling containers was measured using graduated cylinders. Sampling started two hours after the end of an event and lasted approximately 8 h. Thus, rain events are separated by a rain-free period of at least 10 h; shorter interruptions lead to cumulative events of longer duration and size.

Manual precipitation measurements were collected using circular funnels (diameter = 12 cm), with the orifice located about 37 cm above the ground surface. They were fabricated from two polyethylene bottles connected at the necks, with the bottom of the upper bottle removed to form a funnel and the lower bottle serving as storage container. A table tennis ball was placed into the opening to prevent evaporation. Throughfall sampling locations were chosen according to a stratified random design (Zimmermann et al., 2010; Zimmermann et al., 2016). For this, the 1 ha

plot was subdivided into 100 subplots (size 10 m by 10 m, Figure 1), each equipped with two randomly located throughfall samplers (kernel points). Additional transect points were implemented at random kernel points in random directions: 25 short transects, consisting of one sampler 0.1 m from the kernel, and 25 long transects, consisting of five samplers placed 0.1 m, 0.5 m, 1 m, 2 m and 3 m from the kernel. In total, 450 throughfall sampling points were established. For the calculation of average plot throughfall, only measurements at kernel points were used. Canopy cover above the throughfall samplers was estimated by counting the number of branch layers overcasting it, based on visual assessment by the same person at all samplers.

Stemflow was measured on every tree of 11 selected subplots (size 10 m × 10 m), which yielded a total of 65 measurement points (constituting 11 % of both the plot's area and number of trees). The selected subplots for stemflow sampling were regularly spaced across the plot. Stemflow was measured using collars made of lay-flat hose that was cut open, wrapped around the tree and sealed with silicone. A plastic tube connected the collar to a storage container. The mean

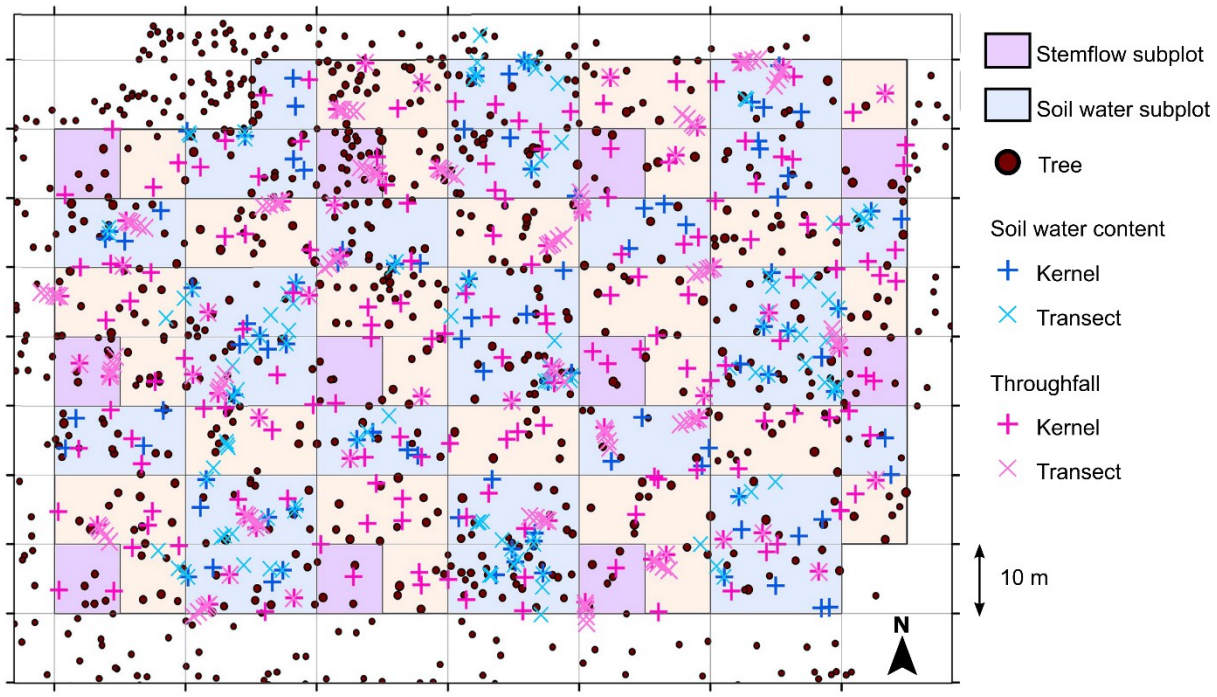

Figure 1: Experimental setup in the 1-ha forest plot subdivided by a 10 m × 10 m grid yielding 100 subplots. Stemflow is measured on all trees within the pink subplots. Throughfall and soil water content are measured in a stratified random design with transects on (a) all 100 subplots for throughfall and (b) 49 selected subplots for soil water content (see Section 2.2 for more details).

per-area stemflow of the stemflow subplots was assumed to be representative of the total plot mean stemflow. In order to assess the funneling of precipitation towards the tree stem and compare between different events, we calculated the funneling ratio (R_F) for each tree and each event according to Herwitz (1986):

$$R_F = \left(\frac{V_{SF}}{P_g \cdot A_{tree}}\right), \quad (1)$$

where V_{SF} refers to the collected stemflow volume for each tree, P_g to gross precipitation and A_{tree} to the tree basal area (at breast height). Essentially, the funneling ratio compares the volume of water collected by the tree with the volume of water that would have been received by a rain collector of the same size as the tree basal area (Herwitz, 1986), thus showing how many times the local stemflow input exceeds open precipitation.

Gross precipitation measurements were taken manually from 5 funnels placed in an adjacent open grassland (distance 250 m), sampled at the same time as each net precipitation sampling. From March 16 to October 7, gross precipitation was also recorded automatically with an iMetos AG/CP/DD 300 weather station (PESSL Instruments GmbH, Weiz, Austria).

Interception loss is calculated as the difference of net precipitation, composed of throughfall and stemflow, and gross precipitation.

In order to compare precipitation in 2015 with the long-term record, we used data on precipitation collected over the last 30 years (1986-2015) at two nearby German Weather Service precipitation gauges (DWD climate data center, www.dwd.de/cdc), both also located on the lee side of the Hainich mountain range in (i) Hörselberg-Hainich-Behringen (ID 336, located 12 km to the southeast) and (ii) Muehlhausen-Windeberg (ID 5593, 20 km to the northeast).

2.2.3 Measurement and processing of soil water content, bulk density and field capacity

Soil water content was recorded every 6 min by a wireless sensor network (SoilNet; Bogena et al. (2010)) equipped with SMT100 frequency domain sensors (Truebner GmbH, Neustadt, Germany). Sampling points were selected based on a stratified random design (Figure 1), which

is independent of the throughfall design above. Because collecting stemflow potentially influences soil water content immediately downslope, we chose 49 subplots located upslope of the stemflow subplots in a checkerboard-like pattern. Each was equipped with two random kernel measurement points. Furthermore, 24 transects were established at random, with three measurement points 0.1 m, 2 m and 6 m from the kernel. In order to increase the number of measurements points proximal to tree stems, we added 40 additional measurement points within 1.2 m of tree stems. In total, 210 soil water content measurement points were established. They were installed successively, 177 (84 %) in fall 2014 and 33 (16 %) in fall 2015. At each measurement point, two sensors were installed at 7.5 cm and 27.5 cm depth, representing topsoil and subsoil. Sensors were oriented pointing uphill in the presumed direction of water flow, with the long axis parallel to the surface and the blade oriented vertically, to minimize disturbance of water flow. In this study, we show the monitoring time series of the year 2015.

For analysis of soil water response to precipitation, we identified 15 summer rain events from June to August, 2015, by identifying singular peak points in the spatial median soil water content time series. Event states were defined as the soil wetting peak after events, and drained states as the minimum soil water content before event wetting started. Eleven of these summer rain events took place before July 30 and thus also were included as net precipitation events.

Undisturbed ring soil samples (volume V_s = 100 cm^3) were collected ~0.5 m from each sensor position at the time of sensor installation (84 % of samples in fall 2015, 16 % in fall 2015). Water content at field capacity was determined gravimetrically from the weight difference between the undisturbed samples after letting them saturate with water for 72 h and subsequently placing them in a sand box with a hanging water column imposing a pressure of –60 hPa for 72 h. Soil bulk density (ρ_b, g cm^{-3}) was calculated from the dry weight ($m_{s\,dry}$, g) of the soil core after drying for 24 h at 105 °C.

We approximated soil porosity ($n_{s\,app}$) from bulk density, assuming a constant density of the soil mineral component of ρ_m = 2.66 g cm^{-3} as

$$n_{s\,app} = \left(1 - \frac{\rho_b}{\rho_m}\right). \quad (2)$$

We refer to drainage porosity as the approximated air-filled porosity at field capacity, given by the difference of approximated porosity and water content at field capacity.

2.2.4 Statistical analysis

For metrics and correlations of throughfall and soil water content, we used only the stratified random (kernel) measurement points and excluded transect measurement points. We used quantile-based metrics and tests to characterize and compare patterns in the data. To assess the spread of the samples, and while allowing for comparison between different variables, we use the coefficient of quartile variation (CQV):

$$\mathrm{CQV} = \left(\frac{Q_3 - Q_1}{Q_3 + Q_1}\right), \tag{3}$$

where Q_1 and Q_3 are the first and third quartile of the sample.

Spearman's rank correlation was used for all correlations of spatial and temporal patterns. Differences between data samples were tested using the Wilcoxon rank sum test. Stability of throughfall and stemflow was assessed as the temporal autocorrelation of spatial patterns, by mutual correlation of individual measurement points among all events.

To investigate differences in soil water content between areas near the tree stem and further away, we included all measurement points (random and transect) in order to obtain a larger sample for tree proximal locations. We separated the data into two groups depending on their distance to the next tree, defining proximal as being located at a distance < 1 m and distal as a distance > 1 m from the nearest tree. This resulted in a sample of $n = 55$ for the stem proximal group and $n = 127$ for the stem distal group.

All data was processed and analyzed in R version 3.2.1 (R Core Team, 2016).

2.3 Results

2.3.1 Hydrological characterization of the measurement period

The hydrological year 2015 was the second driest of the past 30 years (1986-2015) at both nearby German Weather Service precipitation stations. Each winter (11/2014 - 04/2015) and summer (05/2015 - 10/2015) were the 3rd driest of the last 30 years. Both seasons received roughly only 67 % (Hörselbach-Hainich-Behringen) and 75 % (Mühlhausen-Windeberg) of the average precipitation. The preceding hydrological year (2013/2014) and the final winter months of 2015 received average precipitation.

2.3.2 Net precipitation patterns

The precipitation event sizes, i.e., cumulative gross precipitation, of the 16 manually sampled precipitation events, ranged widely between 1 mm and 35 mm, with 60 % of events having been smaller than 5 mm (Figure 2, Table 1) and the largest third of the events contributed 77 % to the total received rainfall. Throughfall varied substantially in space, especially for small events. The temporal stability of the throughfall pattern was strong and did not depend much on the event size (Figure 3). Throughfall decreased significantly with canopy density for some events (Table 1). Throughfall in tree stem proximal areas (< 1 m from stem) was similar (on average 98.7 %) of throughfall in stem distal locations during the observed precipitation events.

Stemflow contribution to the overall water budget was small, but increasing with event size from 0.01 % for the smallest precipitation event (1 mm) up to 3 % for the largest event (35 mm; Table 1). Another characteristic of stemflow is the funneling ratio (R_F), which expresses the concentration of gross precipitation onto the tree's basal area via stemflow. Funneling ratios were > 1 for events > 3 mm and reached 32 for the largest event. Local stemflow input rates exceeded gross precipitation regularly (more than 50 % of the time) by more than fivefold.

Table 1: Summary of properties of observed precipitation events, ordered by size. The lower part of the table summarizes the fluxes (totals) and properties (medians) of all events falling into the respective sizes classes: small (P_g < 3 mm), medium (3 mm < P_g < 10 mm), large (P_g > 10 mm). Asterisks indicate significant correlations.

Date of Record	P_g [mm]	P_{TF} [mm]	CQV P_{TF} [-]	$\rho_{TF\ can}$ [-]	P_{SF} [mm]	CQV P_{SF} [-]	R_F P_{SF} [-]	E_I [%]	Event Size
2015-06-14	1.1	0.3	0.60	-0.36***	0.00	0.00	0	77	small
2015-05-10	1.2	0.1	1.00	-0.14	0.00	1.00	0	89	small
2015-07-21	1.6	0.6	0.33	-0.27	0.00	0.00	0	58	small
2015-06-28	1.8	0.5	0.34	-0.18	0.00	1.00	0	65	small
2015-06-20	2.1	0.4	0.64	-0.22	0.00	0.60	1	74	small
2015-05-30	2.8	1.7	0.18	-0.21	0.01	0.47	4	37	small
2015-06-18	3.3	1.7	0.28	-0.10	0.02	0.57	3	47	medium
2015-06-02	3.7	1.8	0.24	-0.41***	0.01	0.78	2	50	medium
2015-05-13	4.1	2.7	0.17	-0.05	0.04	0.65	6	33	medium
2015-07-11	4.6	2.7	0.13	-0.13	0.04	0.44	5	40	medium
2015-07-25	5.7	3.9	0.15	-0.07	0.1	0.58	9	30	medium
2015-07-08	13.3	9.4	0.07	-0.23**	0.37	0.74	15	26	large
2015-07-15	13.9	8.3	0.18	-0.15	0.36	0.78	11	63	large
2015-07-28	20.1	13.7	0.16	-0.27	0.89	0.71	23	24	large
2015-06-24	23.0	13.9	0.16	-0.24**	0.67	0.74	13	34	large
2015-07-20	35.2	29.2	0.07	-0.10	1.87	0.71	32	10	large
	10.4	3.5	0.47	-0.22	0.02	0.54	0	69	small
	21.4	12.7	0.17	-0.10	0.19	0.58	5	40	medium
	105.5	74.5	0.16	-0.24	4.16	0.74	15	26	large

Abbreviations: P_g: gross precipitation; P_{TF}: median throughfall; CQV P_{TF}: coefficient of quartile variation of throughfall; $\rho_{TF\ can}$: Spearman's ρ for the correlation between canopy cover and throughfall; P_{SF}: stemflow; CQV P_{SF}: coefficient of quartile variation of stemflow; R_F: funneling ratio of stemflow; E_I: interception loss.
Levels of significance: *** : p < 0.01; ** : p < 0.05

Temporal stability of collected stemflow volumes increased substantially with event size and patterns were extremely stable (ρ > 0.95) for the large event class (Figure 3).

In summary, positions receiving high or low throughfall and stemflow compared to the spatial mean did not change considerably over time, and only for stemflow with event size. Hence, patterns of precipitation input to the soil on the investigated forest plot were relatively stable and may potentially have caused stable soil water content distributions.

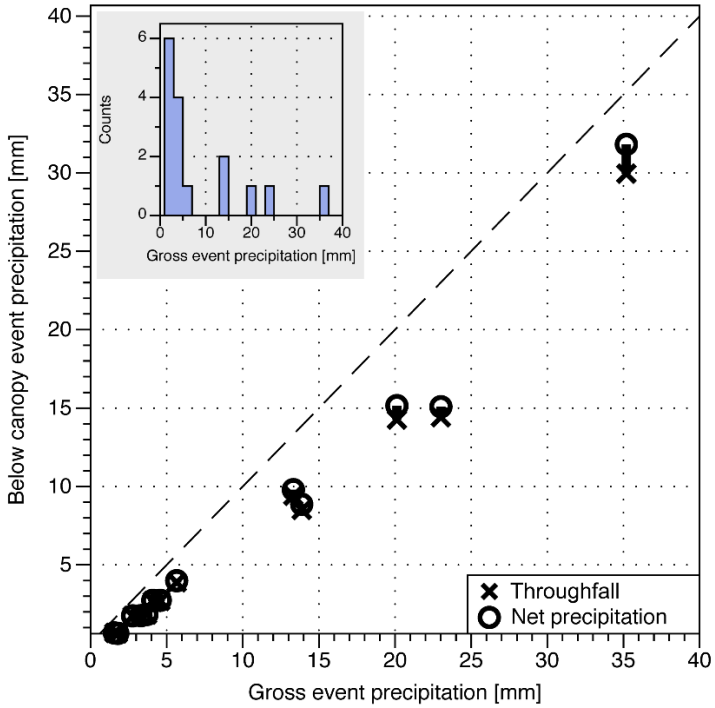

Figure 2: Total net precipitation (sum of throughfall and stemflow) and throughfall in relation to gross precipitation for all measured precipitation events in 2015. Frequency distribution of the size of precipitation events is given in the small subfigure.

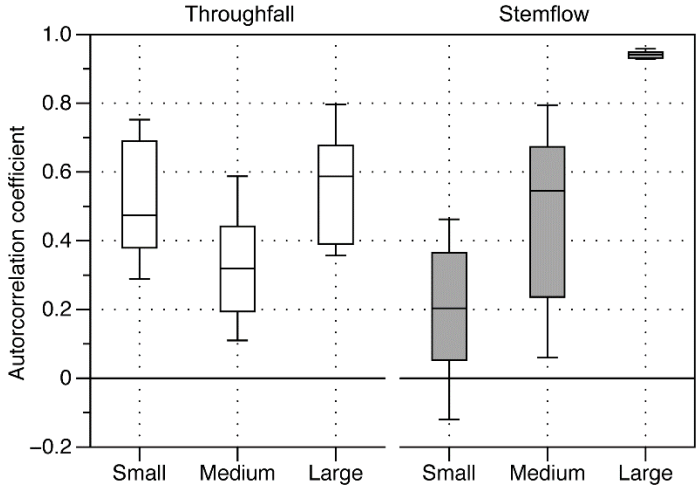

Figure 3 Autocorrelation coefficients (Spearman) of (left) throughfall and (right) stemflow separated by rain event size (small, medium and large precipitation events). Individual measurement points between pairs of events falling into the event size categories were correlated as indicated in Table 1.

2.3.3 Patterns of field capacity and soil porosity

Soil porosity decreased about 13 % from topsoil to subsoil, whereas field capacity declined only about 4 % (Table 2**)**. Compared to the precipitation components (throughfall: CQV = 0.29, stemflow: CQV = 0.61), the spatial variation was relatively small for the sampled soil properties with CQVs of 0.1 or less. Field capacity varied almost twice as much in subsoil (CQV = 0.1) than in the topsoil (CQV = 0.06).

Interestingly, field capacity varied substantially between locations proximal and distal to tree stems (Table 3). This difference was significant both in the topsoil and subsoil, with larger differences observed in the subsoil (topsoil: 3 vol-%, subsoil: 8 vol-%).

Porosity had lower spatial variation overall than field capacity. Also, porosity varied less in the subsoil (CQV = 0.04) than in the topsoil (CQV = 0.05). As total porosity was insignificantly different between positions proximal and distal to tree stems, but field capacity was lower proximal to stems, drainage porosity is significantly increased in stem-proximal areas.

Table 2: Soil properties measured at available soil water content sampling points (n = 182), given as median together with the CQV (Equation (3)).

	Topsoil		Subsoil	
	Median	**CQV**	**Median**	**CQV**
θ_{FC} [%]	43.5	0.06	41.7	0.10
$n_{s\ app}$ [%]	55.6	0.05	48.3	0.04
$n_{s\ app} - \theta_{FC}$ [%]	11.8	0.28	6.2	0.45

Abbreviations: CQV: Coefficient of quartile variation; θ_{FC}: water content at field capacity; $n_{s\ app}$: porosity approximated from bulk density; $n_{s\ app} - \theta_{FC}$: macropore volume

Table 3: Median soil properties proximal (< 1 m) and distal (> 1 m) to tree stems and their difference. Asterisks indicate significant differences (proximal – distal).

	Topsoil			Subsoil		
	Proximal	**Distal**	**Difference**	**Proximal**	**Distal**	**Difference**
Sample size	55	127		55	127	
θ_{FC} [%]	42.5	43.7	-1.2*	39.2	42.8	-3.6**
$n_{s\ app}$ [%]	56.2	55.8	0.3	47.9	48.3	-0.4
$n_{s\ app} - \theta_{FC}$ [%]	13.6	12.1	1.5*	8.7	5.5	3.3**

Abbrevations: θ_{FC}: water content at field capacity; $n_{s\ app}$: porosity approximated from bulk density; $n_{s\ app} - \theta_{FC}$: macropore volume

Levels of significance: *** : $p < 0.001$; ** : $p < 0.01$; * : $p < 0.05$

2.3.4 Soil water content time series

Soil water content showed a characteristic trough during the growing season from May to September (Figure 4). Soil water content in the topsoil was generally lower than in the subsoil and showed stronger temporal variation, whereas subsoil water content varied more in space. During the growing season, water content did not reach a spatial median of less than 10 vol-% in the topsoil and 15 vol-% in the subsoil. These are high values, considering the dry summer of 2015, exceeding soil water content measured in the adjacent grassland site (data not shown). This may be partly due to the fine soil texture and could also result from tree root water uptake from within the weathered bedrock. The peak water content after precipitation events during the growing seasons were 25 vol-% in the topsoil and 35 vol-% in the subsoil, well below the winter soil water content. Wintertime spatial median topsoil water content, varying between 35 vol-% and 40 vol-%, almost reached median field capacity (43 vol-%; Figure 4), whereas subsoil median soil water content surpassed median field capacity of 42 vol-% after infiltration events in winter at 40 vol-% to 45 vol-%, suggesting short periods of inhibited drainage.

2.3.5 Impact of net precipitation patterns on soil water content patterns

The most direct comparison of precipitation input and soil water response is comparing soil water content measurement points with nearby throughfall measurement points. Both sets of measurement points were chosen using independent stratified random designs, and 10 pairs of points happened to be located within 1 m of each other by chance. We compared measured throughfall depth with soil moistening (expressed as water content increase pre-event to event peak) at these paired measurement points during twelve summer rain events in June and July, 2015, where we also had measured throughfall (Figure 5). Results show that throughfall and soil moistening were related for single precipitation events of different sizes. This is an indication that net precipitation inputs are traceable in soil water dynamics.

To test for a direct impact of stemflow on soil water content, we compared soil water content response to rain events in areas close to (< 1 m) and distant from (> 1 m) trees during 15 summer rain events from June to August, 2015. For small and medium events (categorized as in Table 1) with little stemflow, soil moistening did not differ between measurement points near and far

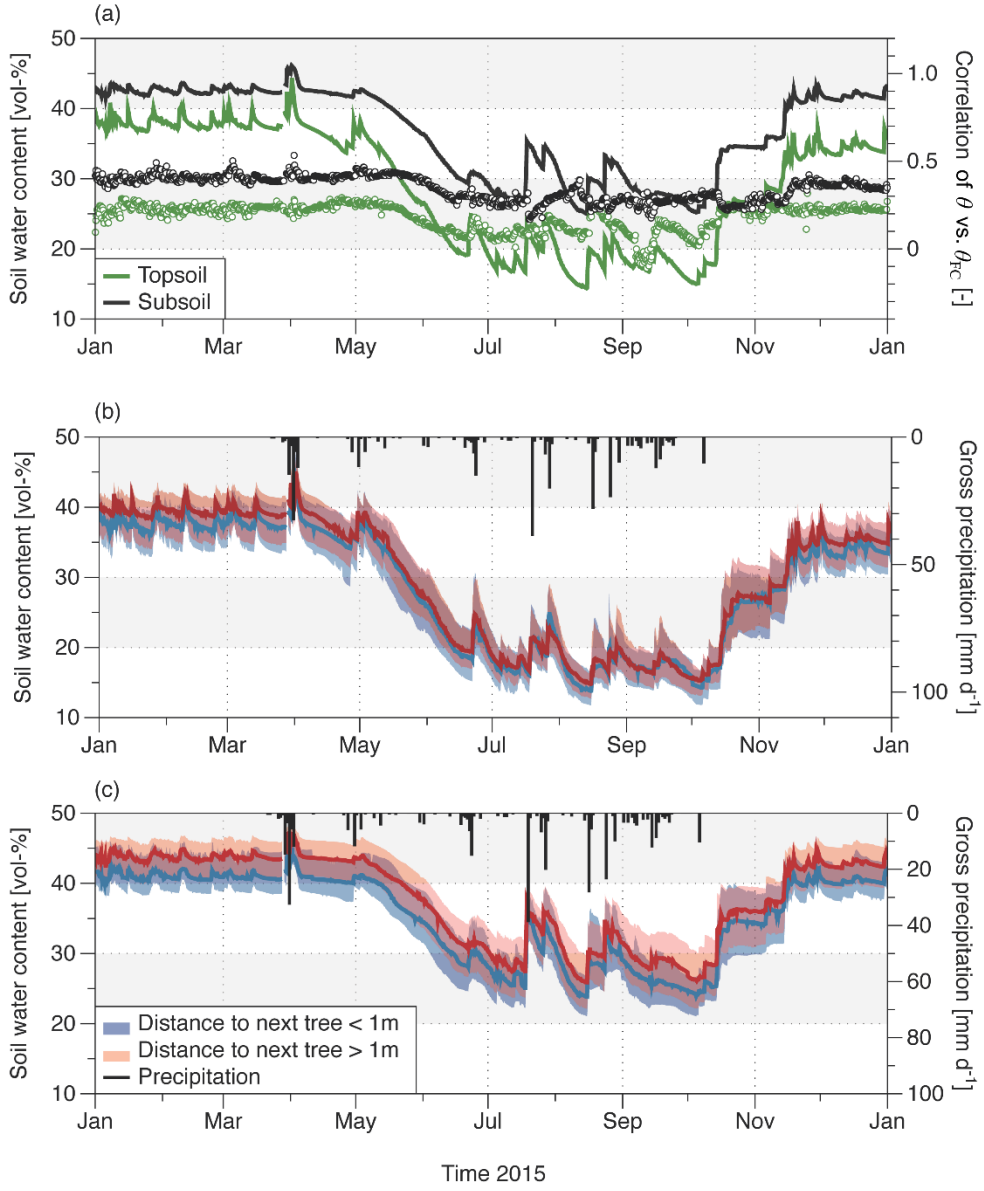

Figure 4: Soil water content time series for 2015. (a) Spatial median of topsoil and subsoil water content (lines) together with the Spearman's ρ for the correlation between soil water content and field capacity obtained at roughly 0.5 m distance from the sensors (dots). Lower panels: Median and quartiles, divided in groups proximal (< 1 m) and distal (> 1 m) to tree stems (b) in the topsoil and (c) in the subsoil. Daily precipitation sums are given for April to October. Abbreviations: θ: soil water content; θ_{FC}: soil water content at field capacity; ρ: Spearman's coefficient of rank correlation.

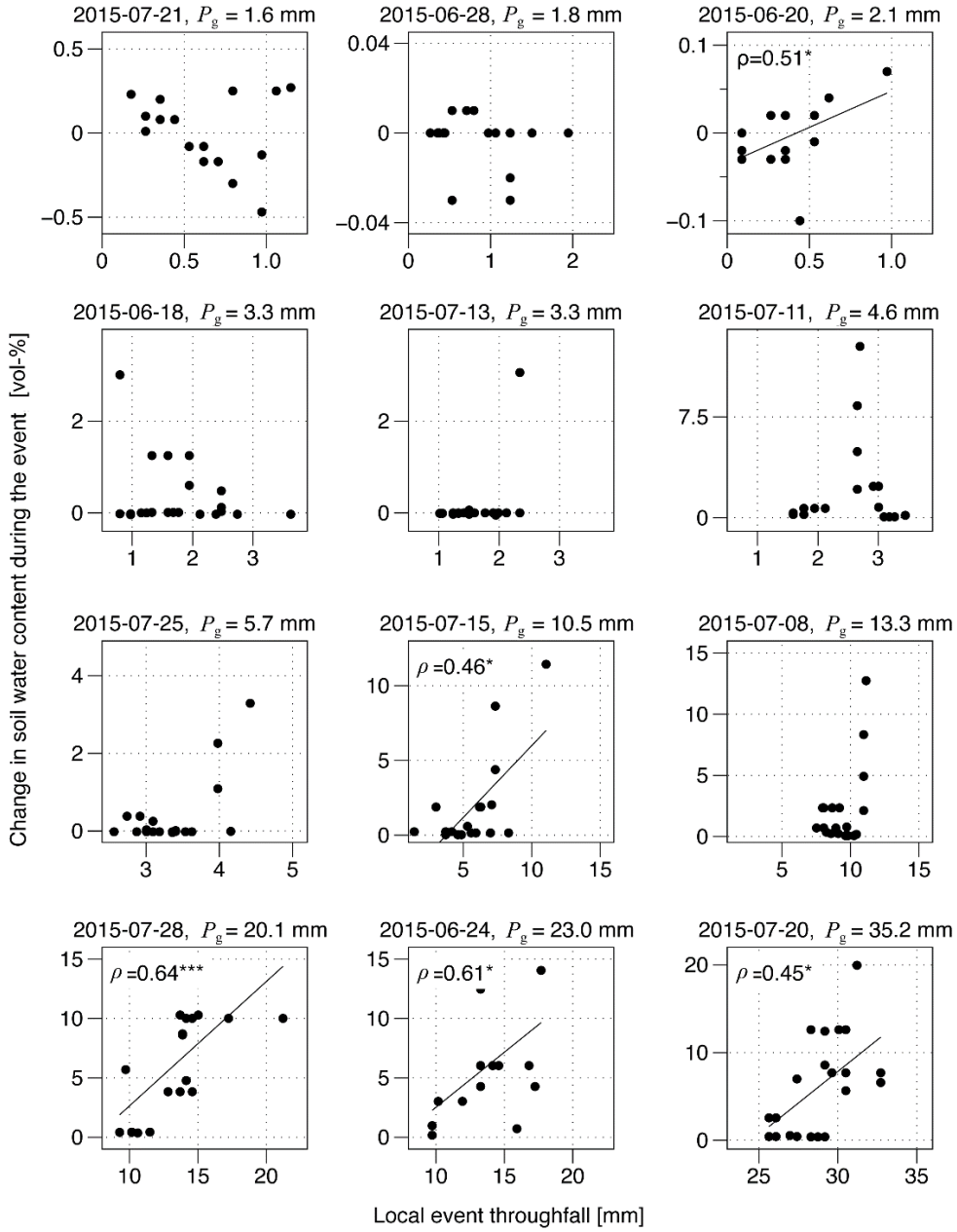

Figure 5: Correlation of cumulative throughfall obtained at a given position and event with nearby soil water content increase (between lowest soil water content before and peak water content after the event) for single measurement points at neighboring positions (distance < 1 m) for twelve precipitation events of different sizes at given dates in summer 2015 ordered per net precipitation size. The events are the overlap of the net precipitation campaign events and summer soil moistening events (see methods, Section 2.2) plus one additional event at 2015-07-13, where throughfall and gross precipitation, but no stemflow, were sampled. Abbreviations: P_g: gross precipitation; ρ: Spearman's coefficient of rank correlation.

from tree stems (difference 0.1 vol-% in the topsoil, no difference in the subsoil). In contrast, for large rain events (P_g > 10 mm) that yielded substantial stemflow, soil median water content increase was on average somewhat higher proximal to trees compared to further away: The difference of the group median was 0.2 vol-% in the topsoil and 0.3 vol-% in the subsoil and the difference between the maximum value in each group was 5.8 vol-% in topsoil and 6.4 vol-% in subsoil. This indicates that hotspots of soil water content increase were typically situated at stemflow-influenced locations.

In the preceding analyses, we considered approximate local relationships between net precipitation and soil water content attempting to draw a most direct link between them. However, a synchronous measurement of precipitation input and soil water response at the same spot is impossible. We therefore evaluated the connection between precipitation and soil water content using statistical characterization of the large amount of high-resolution data we collected and their spatial and temporal variation.

In order to quantify how temporal stability of soil water content was influenced by precipitation events, we compared the similarity of spatial fields of water content at time points before and after rain events (Figure 6**).** We selected the time points of minima and maxima of soil water content (i.e., before and after a rain events) and called the two groups ‘drained states’ and ‘event states’. Separately for each group, we then calculated the rank correlation between the spatial fields of soil water content (temporal autocorrelation coefficient, y-axis, Figure 6) for all occurring time lags (x-axis, Figure 6). Thus, all correlation coefficients presented in Figure 6 are separated by at least one drying and moistening cycle. Regardless, the autocorrelation persisted even for long time lags, indicating that spatial patterns of soil water content were very stable over time. Interestingly, drained soil water patterns were more strongly autocorrelated than at event states (wetted soil). Also, autocorrelation of the drained states deteriorated less with increasing time lags, even when several drying and moistening cycles took place in the meantime. This was the case for both topsoil (Figure 6) and subsoil (data not shown). The persistence time of the event state, i.e., the amount of time until the soil water pattern correlates more strongly with the one at the following drained state than with the one at the previous event state, was < 12 h for 50 % of events, and > 3 d for only 25 % of the observed events. These

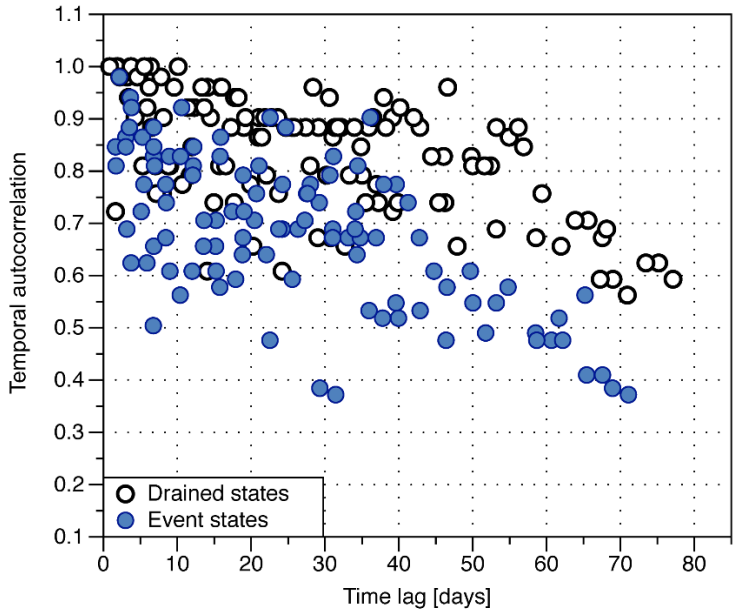

Figure 6: Autocorrelation of topsoil water content at different time points, separated for time points at soil moistening maxima after rainfall (event states) and time points at soil drying minima (drained states), during 15 summer soil moistening events. Given are Spearman's correlation coefficients between spatial soil water content fields, separated by the time lag indicated on the x-axis.

observations suggest that the soil water content pattern at event states reflected both the spatial throughfall pattern and its temporal stability.

Figure 7 shows the relationship between the median and the coefficient of variation (m-CQV) of the spatial soil water content distribution. The m-CQV relationship was negative, meaning that variation increased as average soil water content decreased, and was slightly concave. Particularly in drier topsoil, spatial variation increased strongly in response to rain events. The blue lines in Figure 7 show three examples of soil water content variation responding to wetting and drying due to rain events. The variation increased strongly during wetting (upward branch), but decreased even quicker, as soon as wetting stopped and the soil drained, thus forming a clockwise hysteresis loop. There, the high variation in net precipitation appears to add onto the soil water pattern, almost doubling its variation, which implies the creation of spots with very high water content. However, the disturbance of the local soil water pattern by rain events was of very short duration. For example, the trajectory of the m-CQV relationship (June 23-29) depicted in Figure 7 covered a total of 6 d, with the rising leg comprising 6 h and the majority of the falling leg lasting only 2 d. Thus, the soil water distribution fell back quickly into a pattern

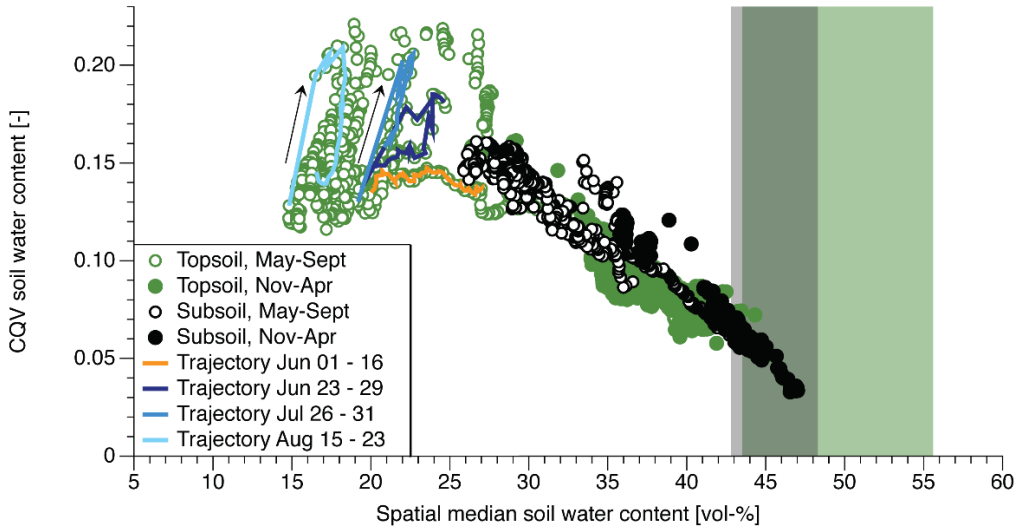

Figure 7: Observed median and coefficient of quartile variation (CQV) of spatial soil water content distribution for the soil water measurements in Figure 4 (a). The shaded areas indicate the water content spectrum corresponding to macro-porosity (between field capacity and porosity) for topsoil (green) and subsoil (grey).

dominated by local factors after initial drainage following rain events. Subsoil water content was much less strongly affected by precipitation, which was expected.

2.3.6 Impact of patterns of field capacity on soil water content patterns

During wintertime, spatial soil water content correlated very well (with ρ ranging from 0.35 to 0.5) with corresponding field capacity obtained near the soil sensor locations (~0.5 m; Figure 4 (a)), particularly in the topsoil. This suggests that spatial variation in soil water content was substantially influenced by soil water retention at this depth during moist conditions. In summer, the correlation between field capacity and soil water content in the topsoil was much weaker, but increased during each rainfall event, when soil water content moved closer to field capacity. This may be an effect of reduced spatial differentiation in soil water retention in the wet soil range. In contrast, subsoil water content in summer was increasingly related with field capacity when the soil dried (for example, between mid-July and mid-August). The rapid decrease of Spearman's ρ between subsoil field capacity and soil water content fields after summer rain events in Figure 7 indicates, that precipitation events destroyed an established soil water content pattern that was related to soil water retention.

Soil water content in the subsoil differed systematically and significantly between proximal and distal positions from tree stems during all drained states (Figure 4 (c)). The temporal median of this difference was greater and less variable in the subsoil (-2.6 vol-%, CQV 0.14), compared to the topsoil (-1.1 vol-%, CQV = 0.33). At both depths the difference was more pronounced in winter, where a local influence of root water uptake can be excluded as potential causative factor. Instead, the decrease of soil water content near trees corresponded closely with significantly lower field capacity close to tree stems, in particular for the subsoil (see above). This difference was prevalent throughout the time series and only disappeared periodically shortly after bigger precipitation events, probably due to the influence of stemflow.

2.4 Discussion

The primary aim of this study was to detect the impact of net precipitation patterns on soil water content patterns. Our data show only a short-lived impact of net precipitation patterns on soil water content patterns. The direct comparison of soil water content response to throughfall reveals only a weak relationship between the two. We can therefore state three main findings, which will be discussed in the following: (1) soil water content patterns are primarily controlled by the soil environment, and specifically are strongly affected by soil hydraulic properties, (2) precipitation heterogeneity influences soil water patterns for short times after precipitation events and (3) we find systematic patterns of soil water content and properties depending on the distance to a tree.

2.4.1 Water retention strongly affects soil water patterns

The spatial distribution of soil water content is mainly shaped by the soil itself. Patterns are characterized by a high temporal stability. This applies in particular to drained states. Then, spatial soil water content returns to the same static pattern, indicating that the driver must be a local property which is stable over time. In addition, the drained states are subject to much less variation than event states. This becomes most obvious when tracking events in the m-CQV diagram, which start from and return to the lower part of the graph. Accordingly, the graph can be separated into two sections: the event-driven section, which is characterized by dynamic and

high variance (examples represented by blue event trajectories) and the static, soil driven section (orange trajectory and lower envelope of the point cloud), which shows the typical parabolic curve commonly observed for the m-CQV relationship, going from low variance in the wet range to a maximum in intermediate wet conditions to again low variance in the dry range (Famiglietti et al., 1999; Brocca et al., 2009; Rosenbaum et al., 2012).

The wet range of the m-CQV curve is formed in winter. Here, soil water content correlates well with soil water retention properties (e.g. field capacity). The low variance in the wet range can thus be explained by the low variation in field capacity. Hence, gravity-driven flow drains the soil quickly after wetting events, and soil water potentials can be expected to be almost balanced.

In the intermediate wet range, the parabolic, soil-driven part of the m-CQV relationship reaches a maximum. A substantial part of this is formed during an extended drying period in spring (orange trajectory with lowest variation), demonstrating that evapotranspiration does not increase soil water content variation at our site much. This might be due to equilibrating soil water potentials by adaptive root water uptake or redistribution fluxes in the soil matrix, and suggests that the remaining variance is due to a continued effect of soil water retention. This idea is also supported by theoretical work, showing that a maximum of the m-CQV curve in the intermediate wet range can be explained by the wider spectrum of soil water retention functions in that moisture range alone (Vereecken et al., 2007).

Field capacity (soil water content retained at -60 hPa) explains a substantial proportion of the spatial pattern of soil water content in our forest plot. The correlation is consistently significant over the soil water content time series, even in drier soil. However, the correlation is not strong, which is expected, given that the soil property samples were only collected once and do not originate from the exact same spot as the soil water content measurements. Soil structure can vary substantially at a small spatial scale as well as over time because of its connection with biological activity. Thus, data from sampling in 2014 might become less representative over the course of the year 2015.

It is noteworthy that soil porosity is less variable than field capacity at both depths, a pattern that is most evident when comparing locations proximal and distal to tree stems. This implies that differences in field capacity on our plot have strong impacts on soil hydraulic properties and

reflect shifts in pore size distribution in a pore size range that is typically affected by biological processes. Studies investigating soil water distribution frequently comprise soil texture, and rarely soil hydraulic parameters, yet those that do find a clear dominance of these properties among the factors explaining soil water content patterns, which is in agreement with our results. For example, Choi et al. (2007) explained 50 % of large scale soil water content variance in their first principal component by soil porosity, wilting point and field capacity, while they also tested soil texture and study extent. Martínez García et al. (2014) tested soil water retention parameters, different climates, soil textures and vegetation and found that variation in soil water content was strongly controlled by the shape parameter of the van Genuchten-Mualem model (Van Genuchten, 1980), as also reported by Vereecken et al. (2007) and Qu et al. (2015). Other studies have found relationships between saturated soil hydraulic conductivity and porosity (Lawrence and Hornberger, 2007; Martinez et al., 2013), both of which relate to macroporosity and drainage dynamics. A lot of studies were unable to clearly attribute a particular factor as the main driver of soil water content patterns using the data they had available, but indicated that soil hydraulic properties or water retention might play an important role (Schume et al., 2003; Teuling et al., 2005; Keim et al., 2006; Famiglietti et al., 2008; Baroni et al., 2013; Bertoldi et al., 2014; Brocca et al., 2014).

Our results suggest, that soil water retention, especially in the dynamic wet range shaped by soil structure, plays a key role in controlling soil water content variability, even in the presence of substantial heterogeneity of precipitation input, and support with data previous propositions by Keim et al. (2006) and Zucco et al. (2014). Processes balancing soil water within the soil are probably strong and proceed rapidly. Thus, even though lateral processes play a role, near-saturation flow is probable to have a vertical dominance. This likely also affects the fate of input fluxes below ground.

2.4.2 Net precipitation effect on soil water content is short-lived

Our data show only a short-lived impact of net precipitation patterns on soil water content patterns. This is supported by the high temporal stability of soil water patterns after drying periods (drained states) even after long time lags, as well as a sharp increase of variation in soil water content in response to rainfall (event states). It implies that spatial variability in net

precipitation is added to the temporally stable, locally-governed soil water content pattern for a limited time of hours to days following rainfall. Accordingly, the relationship between median soil water content and coefficient of quartile variation (m-CQV) at our site has a strong dynamic component characterized by high variance in the dry to intermediate summer state produced by precipitation events. This dynamic range is subject to clockwise hysteresis, demonstrating the effect of heterogenous infiltration as observed by Rosenbaum et al. (2012).On the moistening branch, spatial variability rises quickly with the introduction of spatially variable net precipitation patterns. The drying branch is formed by processes which equalize soil water potentials such as drainage, transpiration and lateral soil water redistribution. Those equalizing processes reduce variations in soil water content during the drying process and move the m-CQV relationship back towards the soil dominated static pattern described above (Fatichi et al., 2015).

Our findings are in contrast to the frequent proposition that throughfall and stemflow drive soil water content distribution (Pressland, 1976; Schume et al., 2003; Keim et al., 2006; Zimmermann et al., 2009; Zehe et al., 2010; Bachmair et al., 2012; Guswa, 2012), which was however limited by available experimental data. The short-lived nature of the net precipitation-induced soil water content pattern might be one reason that studies to date had difficulties linking the two processes in field settings (Pressland, 1976; Raat et al., 2002; Liang et al., 2007).

Our observations are however consistent with modelling studies. Coenders-Gerrits et al. (2013) came to a very similar result by modeling soil water content of a hillslope with heterogeneous throughfall input in a three-dimensional model based on the Richards' flow equation: Throughfall patterns had a very short-time impact on modelled soil water content patterns, whereas most of the time, bedrock topography was the driving factor, which they anticipated might also act as a substitute for heterogeneous soil properties. Bouten et al. (1992) used a quasi-three-dimensional model also with the Richards equation, and concluded that soil physical properties rather than throughfall variation was the main driver of modelled soil water content patterns. Notably, both models also found that despite the short-lived influence of throughfall on soil water patterns, heterogeneous net precipitation still had a strong impact on soil water fluxes, especially at infiltration 'hotspots'. Generally, hotspots of infiltration have the potential to trigger preferential vertical and non-equilibrium macropore flow (Schume et al., 2003; Bachmair et al., 2012), which would not result in a proportional increase of soil water content in the matrix. A

quick response of the macropore system (wet or dry) and enhanced macropore flow have been reported in particular from sites with fine-textured soils, such as ours, which are often strongly aggregated (Schume et al., 2003; Jost et al., 2012; Jarvis et al., 2013). This is in line with earlier research emphasizing the role of spatial net precipitation patterns for subsurface stormflow and hydraulic system response dynamics (Keim et al., 2006; Blume et al., 2009; Guswa and Spence, 2011).

Our observation period is limited to one year and the memory effect in soil water was strong over extended lag periods, compared to other studies (Vanderlinden et al., 2012). Further longer lasting effects of net precipitation and soil structure may be revealed in a multi-annual field study.

2.4.3 Less soil water around tree stems due to systematic changes in soil structure

A remarkable implication of the strong influence of soil properties on soil water content at this site is the non-intuitive distribution of soil water observed around tree stems. Soil water content was reduced around tree stems, especially in the subsoil. Former studies had reported increased water content in stem-proximal soil areas (Pressland, 1976; Chang and Matzner, 2000; Bialkowski and Buttle, 2015) or anticipated it (Gersper and Holowaychuk, 1970; Návar, 2011). Some studies did observe drier soils next to trees, but did not further discuss this fact (Rutter, 1964; Buttle et al., 2014). We can exclude transpiration and net precipitation input as explanation for this effect for three reasons: (1) the significant difference in soil water content between positions proximal and distal to tree stems is also present throughout the winter season, when transpiration is negligible; (2) throughfall is almost equal between positions proximal and distal from stems and stemflow acts as additional water source, thus water inputs are similar or higher close to stems compared to further away; and (3) the difference in soil water content between stem-proximal and distal areas is significant in the subsoil, where water input patterns are less pronounced. Instead, the lower field capacity near stems suggests enhanced drainage in stem proximal regions, leading to lower soil water content.

Beech trees at our site seem to directly or indirectly intervene with pedogenic processes and significantly decrease field capacity around stems. There has been little notice so far of soil pore structure showing spatial organization around single trees. We are aware of only one study (Rashid et al., 2015) that derived soil hydraulic properties from tension disk infiltrometers at a limited number of stem proximal (n = 3) and distal (n = 4) locations. In agreement with the observations presented here, they found lower soil water content, higher macro-porosity, and enhanced saturated hydraulic conductivity in stem proximal compared to stem distal locations.

Shallow-rooting trees are known to compact soil underneath them (Augusto et al., 2002; Eviner and Chapin, 2003), which has been observed in spruce stands. As the shallow soils at our site reduce rooting depth, even for typically deeper rooting species like beech, soil compaction could be potential explanation for lower field capacity near stems. However, because total porosity was not reduced in tree proximal areas, soil compaction is likely not the main cause for the observed shift in the pore spectrum.

Single tree effects on chemical soil properties have frequently been reported. Both chemical soil properties and biota vary spatially at the individual tree scale, as well among tree species (Boettcher and Kalisz, 1990; Aponte et al., 2013) as depending on the distance to the tree stem (Zinke, 1962; Lodhi, 1977; Falkengren-Grerup, 1989; Koch and Matzner, 1993; Rosier et al., 2016). Decreasing pH closer to tree stems was repeatedly associated with acid stemflow input, especially around beech trees (Koch and Matzner, 1993). Preferential flow and low pH in soil solution have been shown to increase pedogenic processes by enhancing transport of solutes (Bogner et al., 2012). A more progressed decalcification due to lower pH in seepage and thus a deeper chemical weathering close to the tree stems could potentially affect the soil structure near stems. Recently, soil water repellency of particle coatings has been associated with soil pH in stemflow affected areas in a beech stand (Krueger et al., 2016). This, besides root water uptake, may have contributed to the observed drier soils in stem proximal areas during dry conditions in summer, but does not explain the same pattern in winter. Soil pH is a also a major driver of soil microbial activity and community composition (Lauber et al., 2009). Shifts in soil microbial communities and soil organic carbon with tree proximity have been observed (Nacke et al., 2016) and equivalent changes in soil functions may be expected. Also, enhanced abundance of root associated biopores, potentially sustained by repeated macro-pore flow during stemflow

(Schwärzel et al., 2012), may facilitate the transfer of oxygen into deep soils which may positively affect subsoil microbial activity.

At the ecosystem scale, tree species effects on soil physical properties and hydrological dynamics have repeatedly been studied (Augusto et al., 2002; Schume et al., 2003; Jost et al., 2012). Eviner and Chapin (2003) described the impact of different tree species on soil structure and water retention due to rooting behavior, organic matter and associated soil biota. Thompson et al. (2010) showed that infiltration capacity was positively related to aboveground biomass in semi-arid sites, but less so in water-limited environments. However, effects of plant productivity gradients caused by species diversity on infiltration capacity have also been found in temperate grasslands (Fischer et al., 2015; Gould et al., 2016).

In general, existing research does not allow us to draw firm conclusions about the reasons for our observed soil water and soil structure patterns near tree stems. More work on understanding the local drivers of tree stems on soil physical properties is merited in order to understand effects on soil patterns and potential effects on seepage fluxes. Stemflow infiltration has been observed to have a tendency to quick, vertical flow (Durocher, 1990; Spencer and van Meerveld, 2016). Potentially, the enhanced abundance of macropores resulting from the reduced field capacity close to tree stems found at this site may affect the ability of the soil to channel stemflow fluxes to greater depth (Taniguchi et al., 1996; Návar, 2011; Schwärzel et al., 2012; Coenders-Gerrits et al., 2013).

2.5 Conclusion

We presented a data set of highly-resolved forest stand precipitation, soil water content, and soil property data from a 1 ha mixed beech forest plot. Our results strongly suggest that, contrary to common assumptions, soil hydraulic properties (here by proxy of field capacity) are the dominant driver for spatial patterns of soil water content at the plot scale. Summer precipitation events only temporarily introduce additional variation to the very stable soil water content pattern. This supports earlier modelling work with data, but disagrees with a frequently raised hypothesis on the effect of net precipitation on soil water content raised in the forest hydrology literature. However, although soil water patterns are not strongly affected, vertical fluxes are

expected to respond to net precipitation patterns and more experimental work is warranted to confirm the connection between net precipitation patterns and seepage.

Field capacity was a strong driver of spatial variation of soil water content, and together with overall similarity in total porosity, this indicates a shift of the water retention curve within the wet range. Our field data support earlier modelling studies proposing a strong influence of soil water retention characteristics on soil water content variability. At the same time, our data indicate that distribution of soil structure (i.e., pore size range affected by biologic processes) plays a crucial role in shaping soil water content distribution at our site. Therefore, quantitative assessment of spatial fields of soil structural properties, including spatial autocorrelation, will greatly improve interpretation of soil water patterns in the future.

The importance of soil structure becomes particularly obvious when comparing the significantly drier stemflow-influenced areas around tree stems with wetter stem distal areas, a pattern that is due to decreased field capacity and an increased fraction of air-filled pores at field capacity. The effect of the distance from tree stems on the spatial organization of soil hydraulic properties is an aspect unaccounted for so far. The local combination of high soil macroporosity and high precipitation input near tree stems may have substantial effects on subsurface storm flow and ground water recharge. A systematic spatial organization of these properties, as observed in the stemflow-impacted areas around tree stems, is a phenomenon which has received little notice so far. Whether this setting can be observed at other sites and for longer time spans, and how it affects water and nutrient flow and biological activity, are questions worthy of further attention.

3 Neighborhood and stand structure affect stemflow generation in a heterogeneous deciduous temperate forest

3.1 Introduction

In forests, precipitation is intercepted by the canopy and reaches the soil partitioned into throughfall and stemflow. The different pathways of precipitation through the forest canopy create a strongly heterogeneous pattern of water input to the soil, with consequences for soil hydrobiochemistry (Levia and Frost, 2003; Zimmermann et al., 2007). These pathways compartmentalize the forest floor into cold and hotspots of infiltration, with a strong subsequent impact on subsurface flow and biogeochemical processes (Liang et al., 2007; Guswa and Spence, 2011; Coenders-Gerrits et al., 2013). Thus, an understanding of forest canopy precipitation partitioning processes is highly important for our conceptual understanding of forest ecohydrology systems.

Although stemflow constitutes a minor fraction of net precipitation, research shows that stemflow is important for a site's hydrological functioning (Pressland, 1976; Durocher, 1990; Levia and Frost, 2003; Hildebrandt et al., 2007; Staelens et al., 2008; Levia and Germer, 2015; Carlyle-Moses et al., 2018). Stemflow introduces a strong additional heterogeneity to subcanopy precipitation. Stems potentially act as funnels and can make trees prominent hotspots of canopy drainage. Concentrated water inputs to the soil can trigger macropore flow (Flühler and Roth, 2004), bypassing the soil and thresholding subsurface storm-flow processes that contribute to deep percolation (Taniguchi et al., 1996; Liang et al., 2007). This effect has been called double funneling of trees (Martinez-Meza and Whitford, 1996; Johnson and Lehmann, 2006; Li et al., 2009; Liang et al., 2011; Schwärzel et al., 2012; Spencer and van Meerveld, 2016) and renders

trees important players in the hydrological functioning of forests, on top of their role with respect to soil water depletion.

Correctly depicting variance of stemflow and understanding its mechanisms can be of utter importance, because according to the hotspots and hot moments hypotheses (McClain et al., 2003), maximum fluxes have the strongest impact on the system (rather than site averages). However, few studies have provided measures of stemflow spatial (i.e., tree-to-tree) variation (Hanchi and Rapp, 1997; Zimmermann et al., 2015). Most stemflow studies focus on a few trees to exemplify a site's possible stemflow processes. This is probably because elaborate sampling is required to capture stemflow variance: a random and representative sample is needed, encompassing a high coverage and extent within the study stand. The limited data that are available show that stemflow variation is substantial, and higher for stemflow than for throughfall (Van Stan et al., 2020). Thus, stemflow contributes importantly and even primarily to net precipitation heterogeneity and flux hot and cold spots and moments. At the same time, some research suggests that tree-to-tree stemflow variation is stable in time (Chapter 2), meaning that during different precipitation events, the same trees produce relatively high or relatively low stemflow. Although few studies have explicitly investigated this temporal stability in stemflow, a great deal of research has been conducted to link tree traits to stemflow yield to understand spatial (i.e., tree-to-tree) variability, and thus inherently implied temporally stabile drivers. Most prominently, tree diameter (or circumference, basal area, crown projection area) has been identified as a factor shaping tree-specific stemflow within an event (Reynolds and Henderson, 1967; Aboal et al., 1999; André et al., 2008; Krämer and Hölscher, 2009; Takahashi et al., 2011). However, stemflow yield still shows a great deal of between-tree variation after accounting for tree size (Reynolds and Henderson, 1967; Takahashi et al., 2011; McKee and Carlyle-Moses, 2017), as trees' traits related to morphology and crown architecture additionally affect individual tree stemflow. For example, factors such as many and steeply inclined branches (Herwitz, 1987; Návar, 1993; Martinez-Meza and Whitford, 1996; Iida et al., 2005b; Levia et al., 2015), smoother bark (Aboal et al., 1999; Iida et al., 2005b; Van Stan and Levia, 2010; Van Stan et al., 2016), leaf hydrophobicity (Iida et al., 2005b), low LAI/few leaves (Takahashi et al., 2011; Molina and del Campo, 2012; Levia et al., 2015) and more woody surface (Levia and Germer, 2015; Levia et al., 2015) have been found to enhance stemflow production.

So far, most of the investigations have targeted species-specific variables. However, some canopy traits are also affected by stand structure: trees have been shown to strongly adapt their growth to the space occupation of neighboring trees (Schröter et al., 2012; Juchheim et al., 2017). Different competition strategies and typical phenotypes of different species complement each other in mixed forest, allowing for more efficient niche and space occupation (Frech et al., 2003; Juchheim et al., 2017). Thus, neighborhood characteristics such as species composition, diversity or size heterogeneity could also impact tree traits related to stemflow. Stand and neighborhood properties might directly and indirectly influence stemflow formation of the individual tree. This pattern could also persist on a larger scale, forming forest patches of structure-induced enhanced and reduced stemflow.

Nevertheless, neighborhood effects have hardly been considered for stemflow analyses. Some studies have included canopy position (Reynolds and Henderson, 1967; Aboal et al., 1999; Terra et al., 2018) or neighboring tree proximity (McKee and Carlyle-Moses, 2017) in tree stemflow models, whereas Krämer and Hölscher (2009) tested species composition effects on area average stemflow. Other studies have discussed a shading effect in the lower canopy (André et al., 2008; Takahashi et al., 2011) as a possible explanation for their stemflow results. However, a systematic study explicitly focusing on neighborhood effects on stemflow in a quantitative approach is currently missing.

In this contribution, we tackle spatio-temporal patterns of stemflow in conjunction with spatially distributed tree and neighborhood variables using a spatially stratified design. Additionally, by assessing stemflow area based on 11 small (100 m^2) subplots, we obtain a first assessment of effects impacting areal integrated stemflow patterns at the subplot scale.

Based on the above design, we assess the temporal stability of spatial stemflow patterns and test the impacts of stand structure and neighborhood parameters (additional to tree size) on individual stemflow yield as well as whether these factors even out for stemflow variation at a larger scale.

3.2 Methods

3.2.1 Site description and sampling design

The measurement site is situated in a gently sloping forested area in the Hainich low mountain range in central Germany. It is a site of the Hainich Critical Zone Exploratory within the Collaborative Research Center AquaDiva (Küsel et al., 2016). Annual rainfall ranges between 600 and 900 mm. The mixed beech forest is part of a national park and is unmanaged, with a high age and species heterogeneity. Within a 1 ha sampling plot, 11 respective subplots of 10 m × 10 m were chosen in a regular pattern and stemflow was measured on all trees within the subplots (Figure 8). A total of 65 trees were such selected with the following species composition: 80 % were beech trees (*Fagus sylvatica*), 12 % were sycamore maple (*Acer pseudoplatanus*), and *Acer platanoides*, *Fraxinus excelsior*, *Carpinus betulus* and *Ulmus glabra*

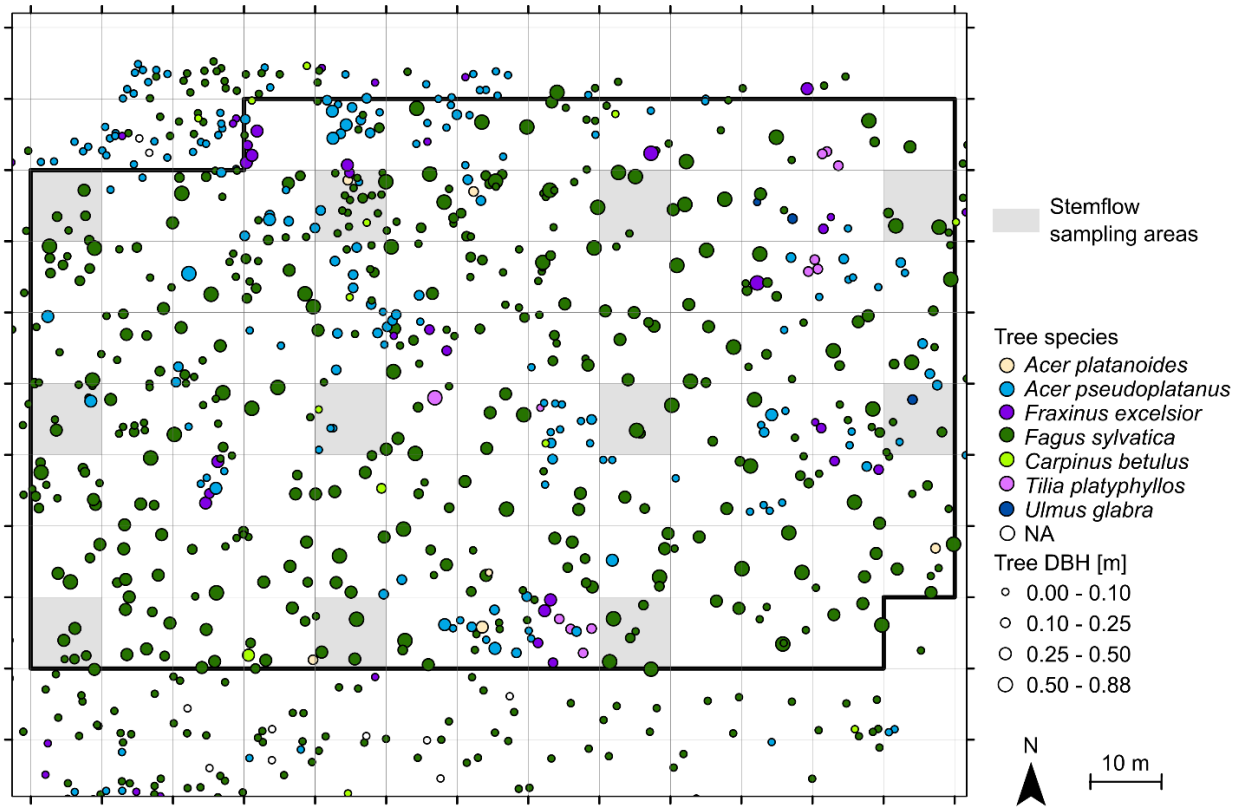

Figure 8: Position of the 11 subplots (grey shaded areas, 10 m × 10 m) in which stemflow was sampled within the forest plot.

also occurred. The diameter at breast height (DBH) showed a negative exponential distribution, with 54 % of the trees having a DBH that was less than 0.1 m and a maximum DBH of 0.81 m. Tree metrics within the subplots were representative of the larger-scale stand (see the Appendix, Section 3.6).

3.2.2 Field sampling

3.2.2.1 Measurement of stand properties

Trees within the plot and a 10 m buffer zone around the plot were surveyed and given and identification number (ID). The position of each tree was determined using a total station (Topcon, Tokyo, Japan) combined with a differential GPS (Topcon, Tokyo, Japan). Tree height was measured using an ultrasonic sensor (Haglöf Vertex, Haglöf, Järfälla, Sweden), and tree circumference at breast height was measured with a measuring tape in 2014. The trees' DBH and basal area values were calculated from their circumference at breast height, assuming a circular tree trunk. The leaf area index was measured in summer 2015 using a LAI-2000 (LI-COR, Lincoln, Nebraska USA).

3.2.2.2 Neighborhood of individual trees

From the stand properties we derived metrics describing the neighborhood of the 65 individual trees. “Neighborhood” was defined as the area around the tree with a radius of the mean tree distance on the plot:

$$r = 2\sqrt{\frac{\frac{A_{\text{plot}}}{n_{\text{trees plot}}}}{\pi}}, \tag{4}$$

where r is the mean tree distance (which equals 4.7 m on our plot), A_{plot} is the plot area and $n_{\text{trees plot}}$ is the total number of trees on the plot. Within this radius, we counted the number of trees in the neighborhood, their cumulative basal area, and the neighborhood’s relative height ($h_{\text{n rel}}$), as follows:

$$h_{\text{n rel}} = \frac{h_{\text{tree max}}}{h_{\text{tree } j}}, \tag{5}$$

where $h_{\text{tree max}}$ is the height of the highest tree in the neighborhood, and $h_{\text{tree},j}$ is the height of reference tree *j*. Note that relative height, as a neighborhood property, increases for taller neighborhoods.

3.2.2.3 Subplot characteristics

We calculated heterogeneity measures for each stemflow subplot. We used the Simpson index of biodiversity *D* (Simpson, 1949), as it is suitable for small sample sizes, $-\log_e D$ transformed, as recommended by Buckland et al. (2005):

$$D = \sum_i \left(\frac{n_i}{\sum_i n_i}\right)^2, \tag{6}$$

where n_i is the number of individuals of species *i* per unit area.

Additionally, we derived a size heterogeneity index *H*, which was calculated according to Krämer and Hölscher (2009) as

$$H = \frac{\frac{q_{0.75,s} - q_{0.25,s}}{q_{0.5,s}}}{\tilde{s}}, \tag{7}$$

with

$$s = h_{\text{tree}} d_{\text{tree}}, \tag{8}$$

Here $q_{x,s}$ is the x^{th} quantile of *s*, and h_{tree} and d_{tree} are the height and DBH of a tree respectively.

3.2.2.4 Gross precipitation and stemflow measurement

Gross precipitation and stemflow were measured as described in (Chapter 2). For gross precipitation, five funnel-type collectors were used, which were placed ca. 250 m from the forest plot on an adjacent grassland, ca. 50 m from the forest edge. Precipitation (in mm) was derived by referring the precipitation volume in the collectors to the area covered by the funnel and taking the median of the five parallel measurements.

Stemflow was collected on all trees within the 11 designated subplots (see above) into containers by way of collars made from lay-flat hose wrapped around the trees and sealed with silicone. Precipitation was sampled on an event basis from May to August in the years 2014, 2015 and

2016, recording all occurring events. Sampling started ca. 2 h after the event ended. Measurements lasted several hours. If measurements were interrupted by new rainfall, events were treated cumulatively. Over the entire period a total 39 events were recorded. Events during which overflow of containers could have occurred for at least one stemflow measurement were excluded from the data analysis. For the statistical model analysis (see below), we also excluded very small events (< 0.5 L median stemflow per tree), leaving 26 of the 39 sampled precipitation events. Subplot stemflow was calculated as the sum of stemflow collected from all trees on that subplot.

The stemflow funneling ratios were calculated from the individual stemflow volumes as follows (Herwitz, 1986):

$$R_{\mathrm{F}} = \left(\frac{V_{\mathrm{SF}}}{P_g \cdot A_{\mathrm{tree}}}\right), \tag{9}$$

where R_{F} is the funneling ratio, V_{SF} is the stemflow volume, P_{g} is the gross precipitation and A_{tree} is a tree's basal area (at breast height). It shows, the degree to which a tree concentrates the rainfall to a point water input to the soil.

Normalized tree/subplot stemflow $V_{\mathrm{SF\,n}}$was calculated from the individual tree stemflow volume ($V_{\mathrm{SF}\,j,e}$) for event *e*, and the event's median stemflow volume ($\widetilde{V_{\mathrm{SF}\,e}}$), according to Vachaud et al. (1985):

$$V_{\mathrm{SF\,n}} = \left(\frac{V_{\mathrm{SF}\,j,e} - \widetilde{V_{\mathrm{SF}\,e}}}{\widetilde{V_{\mathrm{SF}\,e}}}\right), \tag{10}$$

3.2.3 Statistical analysis

3.2.3.1 Descriptive statistics of stemflow patterns

To examine temporal stability of stemflow patterns, we correlated individual/subplot stemflow yields pairwise for all events falling into an event size class, thereby obtaining a set of correlation coefficients for each event size class. In order to account for non-normal distribution of stemflow, we used Spearman rank correlations. Thus, sets of high (or low) correlation

coefficients signify that the same (or different) trees/subplots produce above and below average stemflow yields during each event, demonstrating high (or low) temporal stability.

3.2.3.2 Linear mixed effects models

In order to determine the effect of potential driving factors for stemflow yield, linear mixed effects models (LMMs) were used. LMMs are multivariate linear regression models that allow the user to control for repeated sampling. Quantified factors, the impact of which is to be tested in the model, are called fixed effects. Qualitative information of repeated sampling, referring to individuals, time points or treatments, are called random effects. Random effects can explain parts of the residual of the fixed effects model by calculating different intercepts for different category levels. In a random slope model, random effect category levels can also change the slopes of the linear regression of certain fixed effects (so-called interactions). In this way, repeated sampling cannot bias the fixed effects models. R software (R Core Team, 2016) was used for all data processing and analysis. Linear mixed effects models were developed using the lme4 (Bates et al., 2015) and lmerTest (Kuznetsova et al., 2016) packages, pseudo-R^2 values were calculated using the MuMIn package (Barton, 2018).

We developed models at two spatial scales: (1) individual tree scale and (2) aggregated subplot scale, in both cases assessing how precipitation, tree size and neighborhood affect stemflow. For (1) we fitted P_g, tree DBH, tree height, neighborhood number of trees, neighborhood basal area and neighborhood relative height as fixed effects and precipitation event ID, event year, tree ID, tree species and subplot ID as random effects. For (2) we fitted P_g, as well as the number of trees, number of species, the Simpson diversity index, stand basal area, maximum DBH, size heterogeneity and LAI on the subplot as fixed effects and precipitation event ID, event year and subplot ID as random effects. Table 4 and Table 5 summarize the fixed and random effects of both models. We grouped measured precipitation events into size classes (small: < 3 mm, medium: 3–10 mm and large: > 10 mm) similarly to Chapter 2. Because of the exclusion of events with a median stemflow less than 0.5 L, fewer events representative of the small and medium size class remained in our data set; therefore, we expanded the range for the small events class to 5 mm, yielding 5 small, 7 medium and 16 large events. Thus, at each scale

(individual tree and subplot scales), four linear effects models were developed, three for the individual event size classes and one including all events.

3.2.3.3 Data selection and transformation for linear mixed effects models

All data were checked for a normal distribution and were log-transformed if necessary (stemflow volumes and tree DBH). To be able to account for zero stemflow values, one was added to the stemflow data before transformation. All data were standardized automatically using the "scale" function in R. This normalization allows for the assessment of the single effects' impacts by comparing the slopes (fixed effects) and intercepts (random effects) fitted for each factor. All tested metrics are listed in Table 4 (fixed effects) and Table 5 (random effects).

3.2.3.4 Model development

The model development involved the improvement of the mixed effects model by optimizing or excluding effects until only significant effects remained and the model had a low error. This was done successively by repeated comparison of two models which differed in one aspect only; the model that was significantly better in terms of the AIC (Akaike information criterion) was chosen. The model development was conducted here in two main steps (Figure 9). Step (1) was

Table 4: Distributed parameters of tree, neighborhood and subplot properties used as fixed effects in the linear mixed effects models of the named scale.

Fixed effect parameter		Used on scale	Median	IQR	Maximum	Minimum
Tree (n = 65)	DBH [m]	tree	0.11	0.22	0.81	0.05
	height [m]	tree	16.0	13.4	36.2	4.5
Neighborhood (n = 65, 70 m²)	# trees	tree	4	6	16	0
	basal area [m²]	tree	0.17	0.37	0.64	0.00
	relative height	tree	1.55	1.64	6.84	0.00
Subplot (n = 11, 100 m²)	# trees	subplot	5	2	21	2
	# species	subplot	1	1	5	1
	Simpson's index	subplot	0.00	0.47	0.82	0.00
	basal area [m²]	subplot	0.28	0.41	0.83	0.02
	maximum DBH [m]	subplot	0.55	0.26	0.81	0.10
	size heterogeneity index	subplot	1.37	0.79	16.84	0.56
	LAI	subplot	3.93	0.66	4.95	3.40

Abbreviations: DBH: diameter at breast height; #: number of; LAI: leaf area index

Table 5: Type, number and range of values of categorical variables used as random effects in the linear mixed effects models on the named scale.

Random effect parameter		Used on scale	Number of levels	Levels
Event	ID	tree & subplot	26	Event identification number (1-26)
	Year	tree & subplot	3	2014, 2015, 2016
Tree	ID	tree	65	Tree identification number (1-65)
	Species	tree	5	*Acer platanoides,* *Acer pseudoplatanus,* *Carpinus betulus,* *Fagus sylvatica,* *Fraxinus excelsior,* *Ulmus glabra*
Subplot	ID	subplot	11	Subplot identification number (1-11)

Abbreviations: ID: identification number

the development of the random effects model: starting with a complete model including all possible fixed and random effects, the significance of random effects was tested separately for each effect. Here, selection started with the effect with the highest standard deviation, testing all possible interactions, the simple effect (no interaction) and the exclusion of the effect. Only significant random effects were retained. Step (2) was the development of the fixed effects model from the established random effects model. Here, selection started with the effect with the lowest slope estimate, testing whether the model improved significantly with inclusion of the effect. Only significant fixed effects were retained.

3.3 Results

3.3.1 Event and stemflow characteristics

We recorded 38 precipitation events with a total P_g (gross precipitation) of 626 mm (Table 6). Roughly half of the events fell into the "large" class (P_g > 10 mm). Overall, only a small fraction of rainfall (1.8 %) was converted to stemflow, but the contribution changed with event size (Figure 10). Small and medium events (50 % of the events) only contributed 4 % of total stemflow in our study area. Most of the stemflow (96 %) was derived from events classified as "large". Moreover, 80 % of the stemflow was generated in the largest 30 % of events, and 30 %

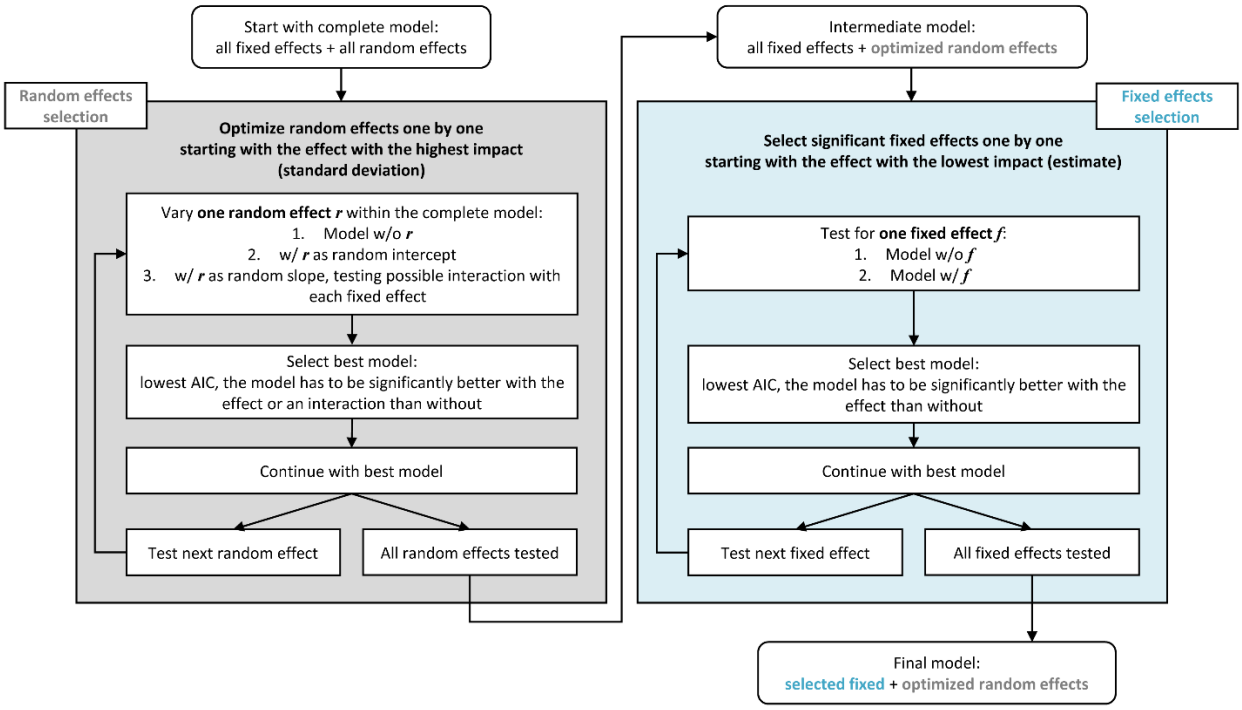

Figure 9: Workflow of the linear mixed effects models' development steps, consisting of (left) first the optimization of the random effects and (right) second the selection of significant fixed effects.

of the total measured stemflow was generated in one single large precipitation event of 65 mm (30 May 2014).

Event funneling ratios increased with event size (Figure 11, left) from a median of 1 for small events to a median of 7 for medium events and 14 for large events. Maximum values range from 60 for events with a rainfall of less than 30 mm to over 200 for the largest recorded event with a rainfall of 65 mm. As funneling ratios increase with event rainfall, local input near stems increases relative to gross precipitation with event size. Thus, large events not only contribute most to total stemflow, but additionally enhance the funneling effect. Non-beech trees on our plot are as productive on average as the beech trees (Figure 11, right).

The coefficient of quartile variation (CQV) for all events averaged out at 0.65, for large events it increased to 0.7. Between subplots, variation for all events as well as for large events amounted to 0.55 (Figure 12, left).

Spatial patterns of stemflow were temporally stable (Figure 12, right; Figure 13; Figure 14). This is especially true for large rainfall events (Figure 12, right). The median correlation coefficient

Table 6: Overview of collected stemflow precipitation events. Measured stemflow depth refers to cumulative stemflow of one event of all trees that could be evaluated. Events that were excluded from the linear mixed effects modelling are labelled and the reason for the exclusion given (see Methods section for more detail). Gap filled stemflow is only available for events included in the modelling analysis. The overall gap rate was 6.2 %, missing a mean of 5.2 % of the calculated total stemflow.

Event properties					Stemflow depth			
					Measured		Gap-filled	
ID	Date	P_g [mm]	Size class	Excluded for	P_{SF} [mm]	P_{SF}/P_g [%]	P_{SF} [mm]	P_{SF}/P_g [%]
21	6/14/2015	1.1	small	median too low	< 0.01	0.01	-	-
17	5/10/2015	1.15	small	-	< 0.01	0.03	> 0.01	0.03
31	7/21/2015	1.57	small	-	< 0.01	0.14	> 0.01	0.14
25	6/28/2015	1.79	small	median too low	< 0.01	0.08	-	-
23	6/20/2015	2.05	small	median too low	< 0.01	0.08	-	-
9	6/5/2014	2.35	small	median too low	< 0.01	0.20	-	-
19	5/30/2015	2.76	small	median too low	0.01	0.40	-	-
22	6/18/2015	3.31	medium	median too low	0.01	0.44	-	-
5	5/19/2014	3.66	medium	median too low	0.05	1.24	-	-
20	6/2/2015	3.71	medium	-	0.01	0.19	0.01	0.19
18	5/13/2015	4.09	medium	-	0.04	0.89	0.04	0.94
27	7/11/2015	4.58	medium	median too low	0.04	0.77	-	-
16	7/26/2014	4.69	medium	-	0.04	0.84	0.04	0.86
39	6/28/2016	5.27	medium	-	0.01	0.10	0.01	0.11
32	7/25/2015	5.66	medium	-	0.09	1.57	0.09	1.67
13	7/11/2014	6.31	medium	-	0.17	2.74	0.18	2.92
1	5/4/2014	8.24	medium	-	0.06	0.79	0.11	1.29
11	7/2/2014	10.3	large	-	0.04	0.42	0.05	0.46
10	6/11/2014	10.5	large	-	0.27	2.56	0.29	2.72
6_7	5/26/2014	11	large	-	0.23	2.09	0.23	2.13
26	7/8/2015	13.32	large	-	0.37	2.75	0.39	2.93
38	6/21/2016	13.68	large	-	0.13	0.94	0.13	0.94
28_29	7/15/2015	13.87	large	-	0.36	2.60	0.36	2.62
36	6/16/2016	16.92	large	-	0.17	1.01	0.19	1.10
43	8/2/2016	19.63	large	-	0.24	1.24	0.25	1.26
40	7/4/2016	19.79	large	-	0.17	0.88	0.17	0.88
33	7/28/2015	20.12	large	-	0.84	4.17	0.90	4.48
34	5/25/2016	20.8	large	median too low	0.49	2.36	-	-
24	6/24/2015	23.01	large	median too low	0.66	2.86	-	-
37	6/16/2016	23.15	large	-	0.31	1.33	0.31	1.33
41	7/14/2016	24.12	large	-	0.67	2.77	0.67	2.77
35	5/31/2016	25.02	large	-	0.66	2.64	0.70	2.79
42	7/25/2016	33.51	large	median too low	0.98	2.94	-	-
30	7/20/2015	35.19	large	overflow	1.79	5.07	-	-
15	7/23/2014	35.81	large	-	1.15	3.20	1.29	3.60
14	7/14/2014	42.24	large	overflow	0.91	2.15	-	-
8	5/30/2014	64.99	large	-	3.53	5.43	3.58	5.51
12	7/10/2014	86.8	large	overflow	3.69	4.25	-	-

Abbreviations: P_g: gross precipitation; P_{SF}: stemflow net precipitation

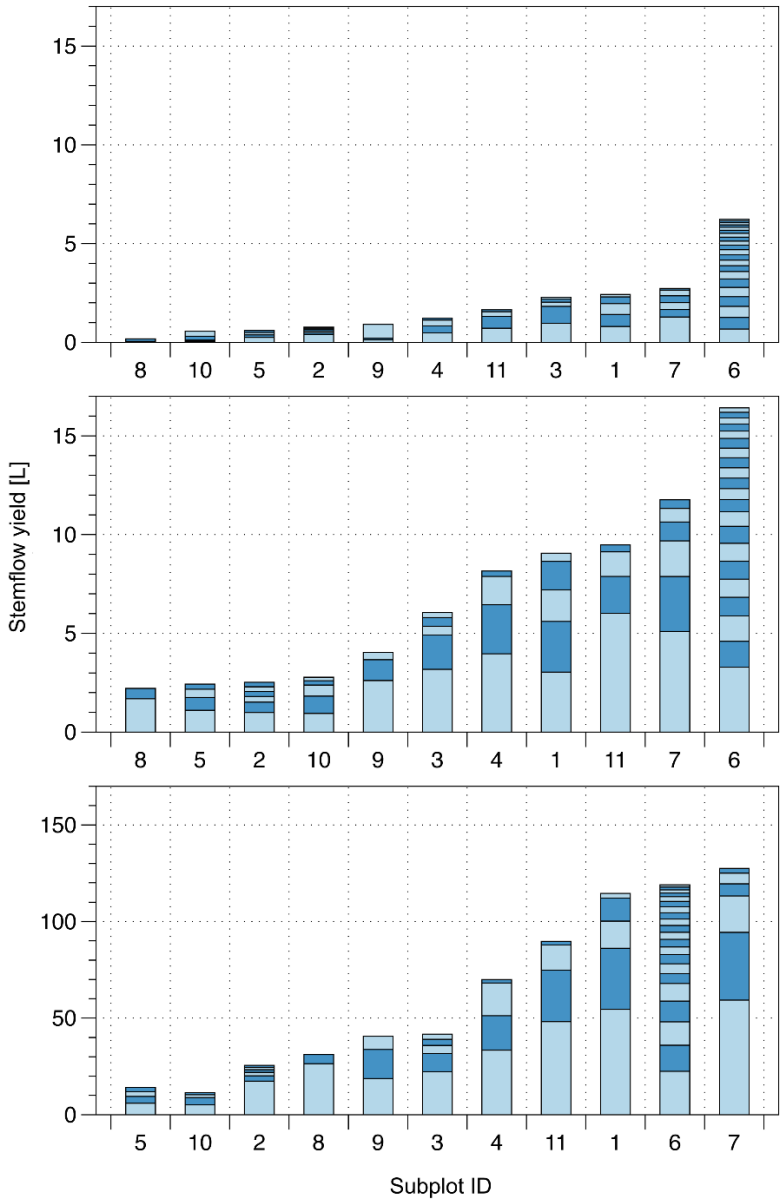

Figure 10: Ranked cumulated subplot stemflow (bars) per event for each event size class (top: small, < 5 mm, middle: medium, 3-10 mm, bottom: large, > 10 mm) and the contributions of individual trees (alternating light and dark blue sections of each bar).

between stemflow in events of the large event class is 0.9 and is significantly ($p \ll 0.001$) higher than in small or medium events both on the tree and the subplot scale. This indicates that systematic drivers of stemflow are active for large events at both scales. Additionally, higher stemflow ranks did not always correspond to higher DBH ranks (Figure 13, Figure 14).

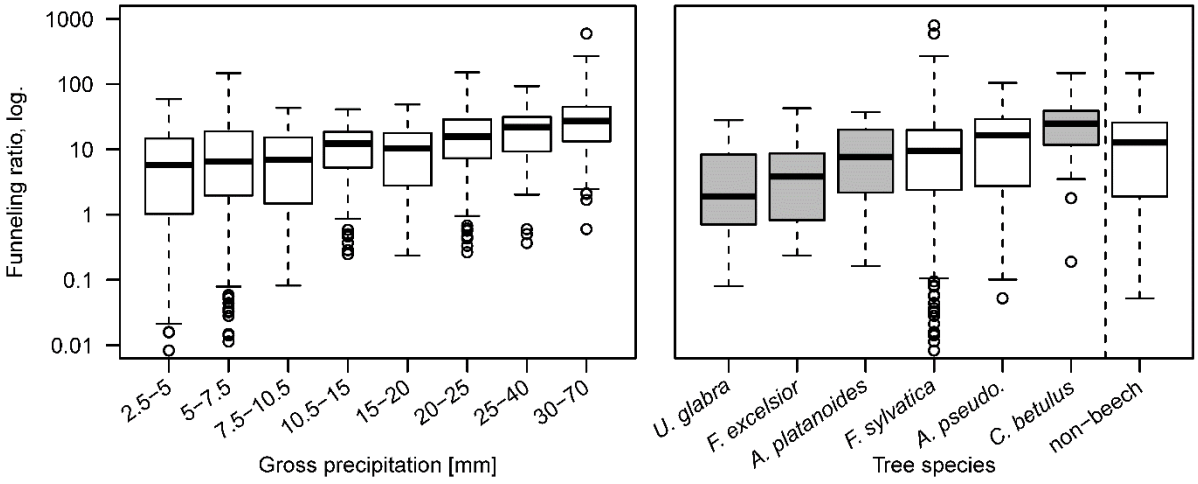

Figure 11: Event funneling ratios of individual trees (n = 65), (left) in relation to event gross precipitation, (right) in relation to tree species. Grey shaded boxplots contain the data of less than three tree individuals.

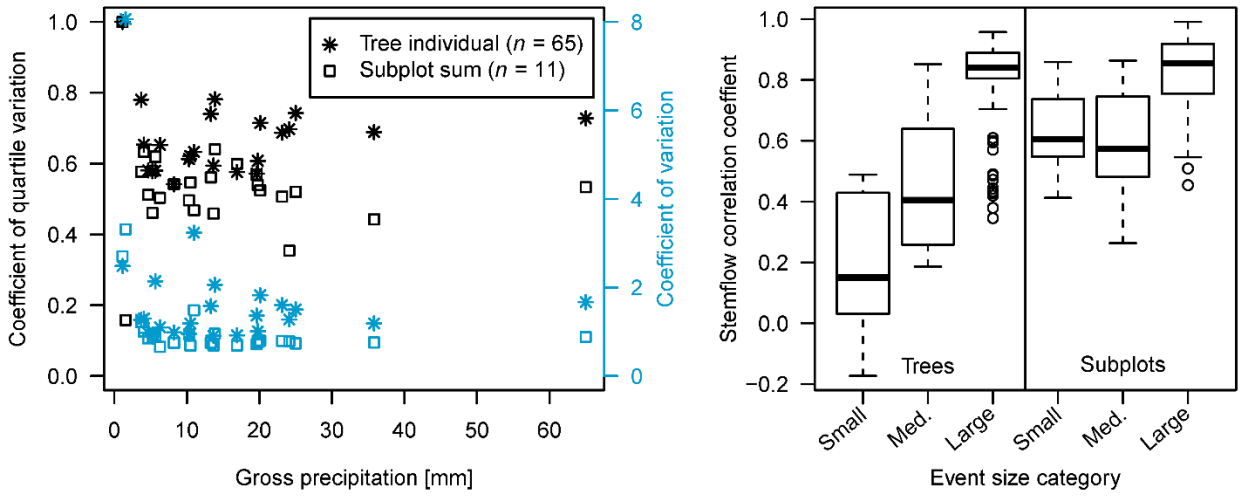

Figure 12: (Left) Coefficients of quartile variation and coefficients of variation for stemflow of individual trees and subplots for all recorded precipitation events in relation to gross precipitation. (Right) Temporal stability of stemflow on the tree and the subplot scale, calculated as pairwise correlation coefficients (Spearman) of tree/subplot stemflow between all different precipitation events of one event size class.

3.3.2 Site, vegetation and neighborhood factors affecting stemflow

3.3.2.1 Individual tree models

All linear mixed effects models for individual tree stemflow cover much of the variation in observed stemflow yields (R^2 = 0.77–0.91, Table 7). However, for medium events, most of the variance is explained by the random effects, which implies that the non-measured individual and site properties had a large overall effect on stemflow, whereas included factors were not as important.

Considering modelled fixed effects, as expected, event rainfall (P_g) is the most important and significant effect in all event size classes (Table 7). For small and medium events, P_g explains most (99 % and 83 % respectively) of stemflow in the fixed effects. However, for large events, P_g is less important whereas tree size (i.e., DBH) becomes more important: 48 % of stemflow is explained by P_g and 37 % is explained by DBH in the fixed effects in large events.

Neighborhood properties (number of trees, basal area or relative height) have a significant impact on stemflow for the small events, and they are a trend in medium and large events (p = 0.077 and 0.055 respectively). The neighborhood parameters that are important vary with the event class, whereas the direction of the effects (i.e., increasing or decreasing stemflow) is consistent in all event classes. Neighborhood effects increase with event size from small to large events, while gross precipitation concurrently decreases from small to large events. Thus, neighborhood properties affect stemflow more strongly for large events. During large events, the number of trees in the neighborhood increases stemflow, whereas stemflow is decreased by a larger basal area and taller trees in the neighborhood. Overall, neighborhood "crowding" (i.e., parameters indicating high biomass, like neighborhood basal area) tends to decrease stemflow production per tree with one notable exception: the number of trees in a neighborhood increases stemflow yield.

Additional neighborhood effects may be hidden in the random effects which encompass unquantified but systematic effects of repeated measurements within a group or individual. Of those, subplot ID is almost never significant (Table 7). Instead, event ID is the strongest random effect for all models, accounting for rain event characteristics not captured by total event rainfall.

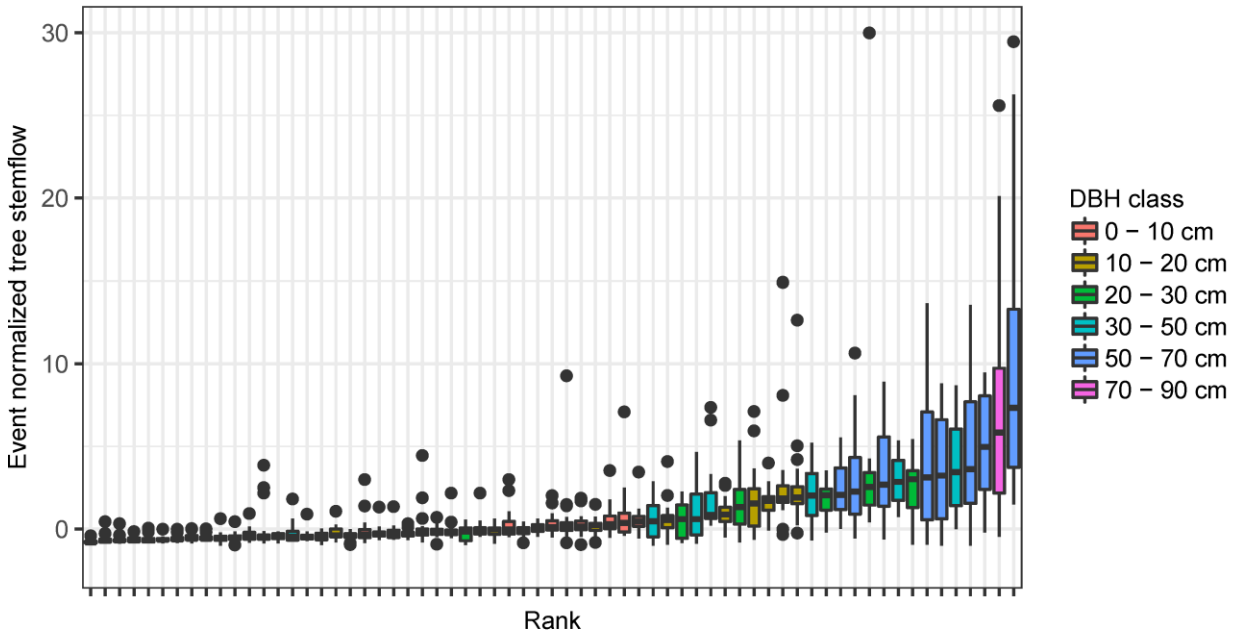

Figure 13: Temporal stability of individual tree stemflow over all sampled events. Trees are ranked according to their median event normalized stemflow and colored according to DBH (diameter at breast height).

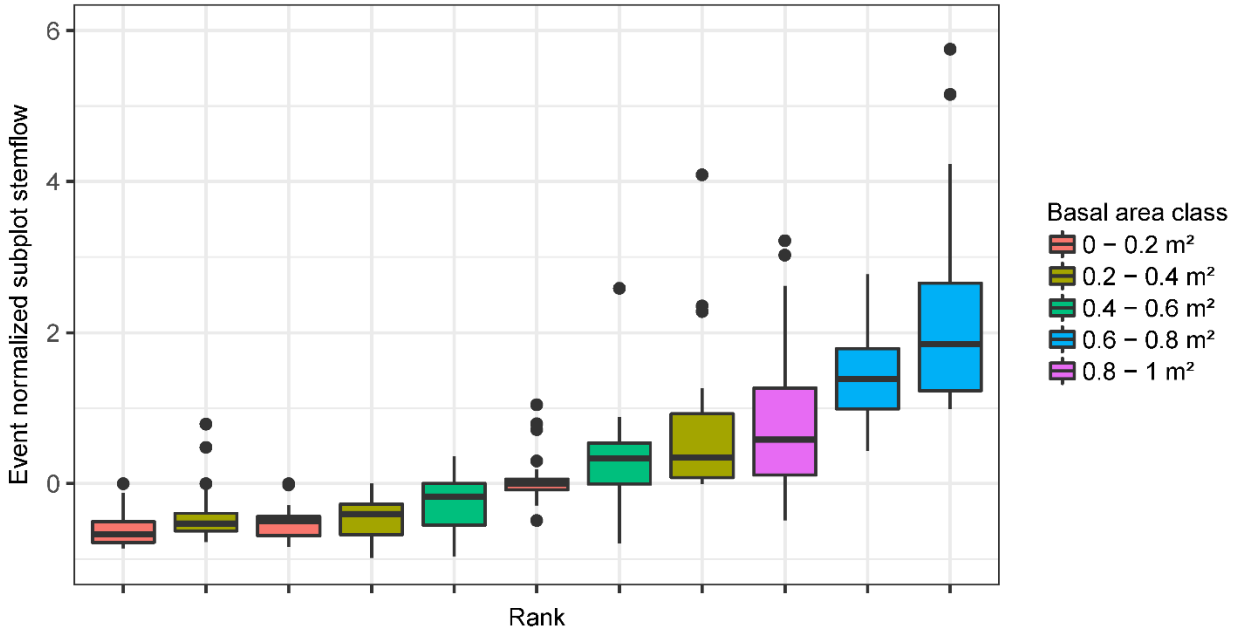

Figure 14: Temporal stability of 100 m² subplot stemflow over all sampled events. Subplots are ranked according to their median event normalized stemflow and colored according to basal area.

The interaction with tree diameter shows that the prominent relationship between tree diameter and stemflow changes with the individual event properties. The second strongest effect is tree ID, which acts as proxy for tree parameters other than those quantified in the fixed effects, e.g. tree morphological features. Interaction of P_g with tree ID indicates that individual trees may yield more or less stemflow, depending on the event precipitation. Furthermore, tree species is only a significant random effect for large events, interacting with DBH, showing that the relation

Table 7: Results of the linear mixed effects models for individual tree stemflow yield: Slope estimates and significance levels of significant fixed effects, standard deviations of random effects and their interacting fixed effects (random slopes). The four models include (i) all precipitation events, (ii) small precipitations events with rainfall < 5 mm, (iii) medium precipitation events with rainfall 3-10 mm, (iv) large precipitation events with rainfall > 10 mm. Pseudo-R^2 are given for each full model (fixed and random effects), for the fixed effects model separately and for the random effects model separately. Note that data was scaled before model development.

		All events	Small events	Medium events	Large events
R^2					
Full model		0.91	0.86	0.77	0.84
Fixed effects		0.19	0.73	0.11	0.51
Random effects		0.72	0.12	0.66	0.33
Relative effect size					
Fixed effects	**Gross precipitation**	↑ 0.28 ***	↑ 7.72 ***	↑ 1.04 *.	↑ 0.28 ***
	Tree DBH (log.)	↑ 0.25 ***	-	↑ 0.17[1]	↑ 0.22 *
	Tree height	-	-	-	-
	Neighborhood # trees	-	↑ 0.1 **	-	↑ 0.05 .
	Neighborhood basal area	↓ 0.05 **	-	-	↓ 0.04 .
	Neighborhood relative height	-	-	↓ 0.05 .	-
Random effects (interaction)	**Event ID**	0.68 (Tree DBH)	0.24 (Tree DBH)	0.40 (Tree DBH)	0.17 (Tree DBH)
	Event year	0.23 (N. # trees)	-	0.04 (Tree height)	-
	Tree ID	0.15 (Tree height)	0.17 (-)	0.41 (Gross precip.)	0.16 (Gross precip.)
	Tree species	-	-	-	0.06 (Tree DBH)
	Subplot ID	0.09 (Gross precip.)	-	-	-
	Residual	19.0	0.37	0.30	0.19

[1] Effect was not significant, but necessary for the model's convergence

Abbreviations: DBH: diameter at breast height; log.: log-transformed; # : number of; n.: neighborhood; precip.: precipitation; rel.: relative

Levels of significance: *** : $p < 0.001$; ** : $p < 0.01$; * : $p < 0.05$; . : $p < 0.1$

between DBH and stemflow is species-specific. Event year only appears in the model for medium sized events with a very small contribution. Overall, the random effects reflect the substantial importance of tree properties other than DBH for generating stemflow, specifically individual tree morphology and position (tree ID) and tree species.

3.3.2.2 Subplot-scale models

All mixed effects models for subplot stemflow explain a large proportion of variance, which are higher than for the individual tree models above (R^2 = 0.85–0.95, Table 8). Similar to the

Table 8: Results of the linear mixed effects models for subplot stemflow: Slope estimates and significance levels of significant fixed effects, standard deviations of random effects and their interacting fixed effects (random slopes). The four models include (i) all precipitation events, (ii) small precipitations events with rainfall < 5 mm, (iii) medium precipitation events with rainfall 3-10 mm, (iv) large precipitation events with rainfall > 10 mm. Pseudo-R^2 are given for each full model (fixed and random effects), for the fixed effects model separately and for the random effects model separately. Note that data was scaled before model development.

		All events	Small events	Medium events	Large events
R^2					
Full model		0.95	0.89	0.85	0.93
Fixed effects		0.21	0.76	0.40	0.74
Random effects		0.74	0.13	0.45	0.19
Relative effect size					
Fixed effects	**Gross precipitation**	↑ 0.33 ***	↑ 7.44 ***	↑ 2.03 *	↑ 0.32 ***
	# trees (log.)	↑ 0.30 ***	↑ 0.42 ***	↑ 0.43 ***	↑ 0.42 ***
	# species	↓ 0.13 **	-	↓ 0.23 ***	↓ 0.50 ***
	Simpson's index	-	-	-	↑ 0.23 **
	Basal area	-	-	-	↓ 0.13 **
	Maximum DBH	↑ 0.12 ***	-	-	↑ 0.30 ***
	Size heterogeneity index (log.)	↓ 0.08 ***	-	↓ 0.06 *	↓ 0.12 ***
	LAI	-	-	-	↓ 0.07 ***
Random effects (interaction)	**Event ID**	0.76 (# species)	0.31 (# species)	0.36 (Simpson's in.)	0.20 (Maximum DBH)
	Event year	-	-	-	-
	Subplot ID	-	-	-	-
	Residual	0.21	0.34	0.21	0.12

Abbreviations: #: number of; log.: log-transformed; DBH: diameter at breast height; LAI: leaf area index; ID: identification number; in.: index

Levels of significance: *** : $p < 0.001$; ** : $p < 0.01$; * : $p < 0.05$; . : $p < 0.1$

individual tree models, in medium events, the random effects explanation more of the variance than the fixed effects.

P_g and the number of trees on the subplot are the most important fixed effects (Table 8). Their relative contribution shifts from small and medium events to large events, with P_g losing andnumber of trees gaining importance (ca. 95 % and 5 %, 75 % and 15 %, 15 % and 20 % for small, medium and large events respectively). For all event sizes, P_g, number of trees and maximum DBH increase stemflow, whereas subplot basal area, LAI and most of the diversity measures (both number of species and size heterogeneity index) decrease it. The exception is the Simpson species diversity index, which also increases subplot stemflow.

Only one random effect, event ID, is significant for all subplot models (Table 8). Neither event year nor subplot ID played a role in any of the models, indicating that plot properties were sufficiently captured by the fixed effects. This is further supported by the high proportion of fixed effects contributing to the explained variance, specifically in large events ($R^2 = 0.93$, thereof 0.74 for the fixed effects model and 0.19 for the random effects model, Table 8).

3.3.2.3 Comparison of tree- and subplot-scale models

At both the individual tree and subplot scales, the model encompassing all events was dominated by the random effects, although in both small and large events most of the variance was explained by (different) fixed effects. This shows that driving factors differ between event size classes; therefore, we will focus mainly on event class models.

Generally, R^2 values are higher for the subplot than for the individual tree model. Thus, the subplot-scale model was better able to explain the data variation. Moreover, the R^2 values of the fixed effects are higher at the subplot scale, whereas the R^2 values of the random effects (as well as the model residual within the random effects) were higher in the individual tree model.

The regression slopes between predicted and observed data are slightly smaller than 1 at both scales, indicating a bias towards underestimation (see the example for large events in Figure 15). The model bias of the subplot model (slope of 0.92) is lower than that of the individual tree model (0.87). Consequently, when calculating subplot stemflow from individual tree model predictions, the prediction bias is slightly worse (slope of 0.9) than that of the subplot level

model itself (Figure 15). The same procedure allows for the evaluation of the role of the tree ID at the subplot scale. Remember that the tree ID in the individual tree models could potentially include neighborhood effects, specifically morphology (enhancing individual stemflow without affecting the neighbor) or shading (enhancing individual stemflow at the expense of the neighbor). For this, we calculated subplot sums of stemflow predicted by the individual tree model with and without including the tree ID random effect in the model. The regression slope for the prediction without the tree ID was only 0.86 (vs. 0.9 with the tree ID included, see Figure 15). The difference is not significant but a trend exists, showing that tree ID contributes to increasing stemflow in one (or several) individuals on the subplot without decreasing it in others.

In general, similar patterns emerge for different event size classes at the tree scale and at the subplot scale: P_g is a strong driver for stemflow at both scales and loses influence with increasing event size, although more so at the plot scale. Instead, tree or stand characteristics affect stemflow, especially in large events. On both the individual tree and subplot scale, absolute tree size and the number of trees most strongly increase stemflow, whereas neighborhood/subplot

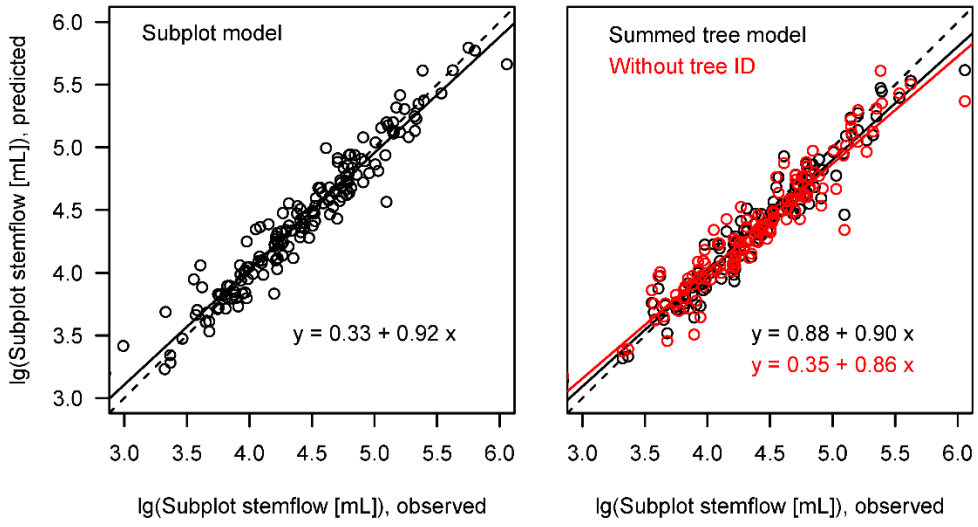

Figure 15: (Left) Predicted stemflow per subplot using the subplot linear mixed effects model in relation to observed values for the large event class, (right) stemflow sums per subplot predicted by the individual tree linear mixed effects model in relation to observed values. The right panel shows additionally the predicted values when excluding the tree ID random effect from the individual tree model. Dashed lines give the 1-to-1-line, continuous lines show the linear regressions, equations are given in the graph.

basal area slightly decreases stemflow. Species become relevant at both scales especially for large events. Event ID is the strongest random effect on both scales, whereas subplot ID was not significant as a random effect at either scale.

However, we also observe small differences between the individual tree- and subplot-scale model patterns: for individual tree models, apart from P_g, individual tree size is most important for large events and neighborhood effects play a minor role. In contrast, for the subplot model, several stand structural parameters affect stemflow. Especially, the number of species and the number of trees are more important than P_g and tree size. Notably, while the size heterogeneity index significantly decreases stemflow for large events at the subplot scale, we found no effect of the equivalent measure (relative height) on the individual tree scale.

3.4 Discussion

Stemflow varied substantially in space both at the individual tree as well as at the subplot scale. At the same time, the greatest share of stemflow volume was created during large events, when spatial patterns of stemflow were particularly temporally stable, both at the individual tree as well as at the plot scale. This shows that in addition to throughfall, the temporal stability of which has been repeatedly reported, stemflow patterns are equally or even more stable in time (Chapter 2). Furthermore, funneling ratios increased with increasing event size. Our findings confirm that (1) spatial patterns in stemflow are systematic and can therefore be explained by tree or stand properties, which we try to identify in this study, and (2) large events generate the majority of total stemflow, have the highest funneling ratios, and spatial patterns are the most pronounced and stable.

3.4.1 Tree size only affects stemflow during large events with fully developed flow paths

Tree metrics are the most important fixed effects for large events (but are less important for small events), which is likely related to the establishment of fully connected stemflow paths. Fully connected flow paths lead to the built-up of stable, systematic patterns of stemflow and increased funneling ratios, relating strongly to tree properties. This agrees with previous research

on stemflow generation processes: although some studies conceptualized stemflow invoking a bucket concept, where tree (André et al., 2008) or bark (Aboal et al., 1999) storage need to saturate before stemflow is initiated, a more dynamic picture is given by Herwitz (1987), Crockford et al. (1996), Levia and Frost (2003) and Levia et al. (2010) which fits well with our observation. Levia and Frost (2003) state that "stemflow generation can begin before the woody frame is completely wetted" due to preferential flow lines resulting from tree morphology or angled rain. Levia et al. (2011) and Van Stan et al. (2016) go one step further, describing the development of new flow paths with progressing rainfall duration, as additional tree surfaces are wetted. Additionally, Levia et al. (2010) observed higher delays in stemflow channeling at rainfall variation for larger trees of the same species. In either of these cases, stemflow generation depends on critical event size thresholds. This view is supported by our findings: for small events, factors shaping spatial stemflow patterns are mostly random and of low temporal stability, indicating that flow paths are not yet well established. Medium events are characterized by increased temporal stability of spatial ranks, but low explained variance in the fixed effects, indicating that flow paths are only partly developed. For large events, tree traits related to water collection or channeling capability are the most important factors explaining individual tree stemflow, which indicates that flow paths are fully established. Together, these results suggest that increasingly established flow paths with increasing event size invoke spatially stable patterns of stemflow that are more related to tree attributes and less to event properties.

3.4.2 Neighborhood and stand properties affect stemflow

3.4.2.1 Stand structure effects largely explain subplot stemflow

For large events, all proposed stand structural parameters are significant at the subplot scale. Subplot ID has no random effect; thus, selected stand characteristics in the fixed effects capture the stemflow generation processes on the subplot scale well, also including those unexplained morphological factors which are hidden in the tree ID on the individual tree scale. Furthermore, the subplot-scale model explains more variance than the individual tree model.

For large events on the individual tree scale, neighborhood effects only appeared as trends, which may have been related to different neighborhood variables, such as number of trees vs.

basal area, working in different directions. However, the subplot models reveal that those neighborhood effects identified at the individual tree level act in the same way at the subplot level: the number of trees still increases the stemflow on the subplot level, whereas basal area reduces it. This shows that a tree's neighbors systematically affect its stemflow and that those patterns do not cancel each other out when considering community stemflow at the subplot scale. Moreover, this suggests that the tree morphologic properties hidden in the tree ID on the individual tree scale are actually associated with stand and neighborhood dynamics.

It is not surprising that stand structure in a recruiting forest is organized in a patchy fashion. Due to the enormous competition for light a climax forest cannot regenerate, except in spatial and temporal niches, e.g. due to the invasion of clearings due to the death of mature trees or other environmental heterogeneities (Horn, 1971). Consequently, regeneration patterns in an undisturbed forest, like the one observed here, organize into a juxtaposition of patches with different stand ages, species compositions and structures. This structural mosaic is also obvious from the variation in our subplot-scale stand metrics and our data suggest that it propagates to ecohydrological functioning.

In conclusion, neighborhood effects were better covered by subplot properties than by the metrics of the individual neighborhood. Accordingly, knowledge of stand structure proves to be advantageous for stemflow assessment.

3.4.2.2 Tree density positively affects stemflow, while shading plays a subordinate role

Number of trees is the most prominent positive contributor to stemflow on the subplot level, confirming the intuitive rule that more trees produce more stemflow. Similarly, Reynolds and Henderson (1967) found higher interception in denser stands, which potentially becomes stemflow after a certain rainfall threshold. Accordingly, Molina and del Campo (2012) report increased stemflow for higher stand densities. Levia and Frost (2003), Levia et al. (2015) and Levia and Germer (2015) argue that more woody surface area (hit by raindrops and providing stemflow pathways) is a main prerequisite for enhanced stemflow. This implies that – next to bigger trees or trees with more branches – a higher number of trees also potentially increases stemflow. Interestingly, the number of trees in the neighborhood also increases individual tree stemflow, which is far less intuitive than the equivalent at the subplot scale. The number of

neighbors could also enhance a tree's stemflow by promoting steeper branching angles in dense stands (Schröter et al., 2012; Juchheim et al., 2017), which are known to yield more stemflow (Návar, 1993; Levia et al., 2015) (see below). Molina and del Campo (2012) similarly observed increased stemflow production in denser stands at the individual tree scale in a Mediterranean climate but attributed the effect to evaporation protection under dense canopies, as they varied density in their study by thinning and could therefore exclude canopy morphology as a reason. Alternatively, dripping on smaller trees may contribute to stemflow generation (see below).

In additional to higher tree density, reduced leaf area also increased stemflow, potentially by increasing the exposed woody surface. This agrees with former studies on the effect of tree properties on stemflow generation (Van Stan and Levia, 2010; Takahashi et al., 2011; Molina and del Campo, 2012; Levia et al., 2015); rain intercepted by leaves is rather redirected away from the stem and becomes throughfall, as leaves are not steeply inclined toward the branch, especially when they are wet.

The most frequently proposed direct neighborhood impact in the literature is a rain shading effect, where exposed canopies collect more precipitation than less exposed ones (Takahashi et al., 2011; Terra et al., 2018). André et al. (2008) discussed the fact that small trees overtopped by larger neighbors might be deprived of a great part of rainfall. Similarly, amongst others (Crockford and Richardson, 1990; Návar, 1993; Aboal et al., 1999), Levia and Frost (2003) found higher stemflow production in the upper canopy. However, in Reynolds and Henderson (1967), medium height, co-dominant and subdominant trees were the most efficient with respect to stemflow production. Pointing in the same direction, smaller trees are often reported to have higher stemflow funneling ratios (Murakami, 2009; Van Stan and Levia, 2010), and our data support this.

Relative height as a fixed effect was never significant in our models. In contrast, the combination of number and size (basal area) of neighboring trees impact a single tree's stemflow. Our data also suggest that the highest or largest tree does not automatically yield the most stemflow (tree height was not retained in the tree-scale model and ranks of DBH and stemflow yield are not the same). The highest trees are the best competitors for light, which implies tree traits which are not beneficial for stemflow production: small crowns, few branches and a low DBH per height ratio

(Juchheim et al., 2017). Moreover, thick leaf layers in the light canopy could divert rainfall from the tree, as a high LAI reduces stemflow production (see above).

In conclusion, stemflow is enhanced by tree density, and is limited by trade-offs between trees when basal area increases. Thus, we find the positive impact of tree density much stronger than the shading effect between trees, which, in contrast, is much weaker than expected.

3.4.2.3 Neighborhood influences stemflow indirectly by shaping tree morphology

Apart from the neighborhood effects revealed by those factors characterizing the neighborhood (as discussed above), there is a "dark figure" of potential neighborhood interactions hidden in the random effects at the tree scale, specifically event year, tree ID and subplot ID. The year of the measurement covers canopy dynamics as growth and canopy gaps due to windfall and broken branches, changing both the tree and its neighborhood. The subplot ID represents the properties of the small tree community that the respective tree is situated in which are not covered by the fixed effects describing the neighborhood. The tree ID comprises all kinds of tree traits (canopy architecture) and canopy position effects (shading or exposure) which are not covered by the fixed effects.

Of those random effects, tree ID is the most prominent significant random effect in all event classes. Interestingly, when predicting subplot-scale stemflow using the individual-scale model for large events, the subplot stemflow is underestimated, and more so than by predicting the subplot stemflow using the subplot-scale model. Therefore, the tree ID-induced variance at the tree scale does not cancel out at the subplot scale. This further supports the conclusion that interactions are not shading, but more likely stemflow-enhancing tree morphology effects.

Neighborhood impacts stemflow indirectly, as it shapes the growth of a tree's canopy (Horn, 1971; Schröter et al., 2012; Juchheim et al., 2017) and stands representative for small tree communities, as species and ages do not mix randomly, but appear in clusters. At the same time, the morphology of a tree substantially affects stemflow: Aboal et al. (1999) found, that bigger crown projection area, the position in the canopy and smoother bark yielded higher stemflow volumes. Návar (1993) reported higher stemflow yields for trees with many, steeply inclined branches from the top part of the crown. (Iida et al., 2005b) attributed branching angles to changes in precipitation partitioning and more branches and, thus, higher crown length to higher

stemflow. In a study on beech saplings, Levia et al. (2015) identified, from a set of properties, besides woody surface, more and steeper branches and fewer leaves as significantly promoting stemflow.

As every tree is a dynamic imprint of its direct environment, the neighborhood and its temporal development drive a tree's traits. Our results suggest that this reflects on stemflow yield. Additional measurements of canopy architecture would be required to confirm the potential effects of stand density on tree morphology in our plot.

3.4.3 Tree diversity increases stemflow, possibly due to effective canopy space occupation

Most of the parameters capturing the diversity and heterogeneity of the stand decrease stemflow, with the notable exception of the Simpson index. This may be related to the fact that our forest plot is beech dominated, and the fully-grown beech trees concurrently produce a great deal of stemflow (André et al., 2008; Krämer and Hölscher, 2009; Van Stan and Levia, 2010).

Our results are in line with observations by Krämer and Hölscher (2009), who found a decrease in stemflow with species diversity (Shannon index) in a nearby forest and attributed this result to the high beech proportion at their site being a strong driver for stemflow. Schroth et al. (1999) also observed reduced stemflow in mixed stands, although they argued that this finding would strongly depend on the species involved and their traits

However, in forest stands dominated by stemflow-prolific tree species, increasing stand heterogeneity implies both a decrease in tree size and introduces less stemflow-producing species. Thus, heterogeneity measures need to be interpreted with caution, especially when measurements from representative trees are used.

The parameter “number of species” rather reflects a reciprocal of the number of large beech trees on the subplot than a measure of species richness. This is because most trees (80 %) are beech and the number of species is strongly related to the number of small trees (DBH ≤ 0.11 m, $R^2 = 0.88$) on the subplots. Moreover, size heterogeneity reduces stemflow generation during medium and large events. Stronger size heterogeneity implies the coexistence of both very large

and very small individuals, where, in terms of stemflow, the smaller individuals potentially add little to the effect of the prolific large tree(s).

Furthermore, Juchheim et al. (2017) showed a significant change in beech morphology when mixed with other species, of a kind potentially enhancing stemflow. Therefore, intermixture of other tree species in beech-dominated forests may have a positive impact on stemflow production, specifically for the beech trees, but not necessarily for the intermixed non-beech trees.

Notably, the Simpson index at the subplot scale is positively related to stemflow. The Simpson index is a relative measure of species diversity that corrects for the number of individuals considered (Buckland et al., 2005). The Simpson index illustrates not just the mere number of species, but the balanced species abundance; therefore, it is sensitive to the strong beech dominance that we find on most subplots (Magurran, 2004). The Simpson index only significantly increases stemflow for large events, where flow paths are established, and individual tree trait effects on stemflow develop their full potential. Frech et al. (2003) showed that more diverse tree communities are very efficient in using the canopy space. As different species use different strategies to compete for resources, they form variable canopy shapes which makes it easier for trees of different species to move closer together. A more efficient occupancy of canopy space increases woody surface area, the existence and exposition of which has been shown to be the core of stemflow promotion (see above) (Levia and Frost, 2003; Levia and Germer, 2015; Levia et al., 2015). Additionally, beech trees growing in concert with other species are more likely to develop crown morphologies with a higher number of branches (Juchheim et al., 2017), which further promotes stemflow (Levia et al., 2015).

3.5 Conclusion

In this study, we investigated possible neighborhood effects on stemflow yield on the individual tree and subplot (patch) scale. Our unmanaged and mixed-species forest produced a high spatial variance in individual tree stemflow. Spatial patterns of stemflow were temporally stable, especially for large events. The spatial variance persisted with the same order of magnitude on small forest patches of 10 m × 10 m.

Tree size was not the only relevant trait for stemflow generation. Neighborhood and stand properties contributed importantly to stemflow distribution. On both investigated scales, stemflow increased with the number of trees in the neighborhood. Tree density particularly increases woody surface area – a key to stemflow promotion, providing rain receiving area and flow paths. Because neighborhood effects did not cancel out at the subplot scale, tree morphology (crown architecture) must have enhanced subplot stemflow. As canopies react plastically towards their surroundings, neighborhood impacts tree morphological features, including those affecting stemflow. In contrast, shading within the canopy was much less important: relative height did not affect stemflow, only neighborhood and stand basal area, representing larger trees, slightly reduced stemflow which suggests a weak shading effect. Furthermore, barely decreased stemflow variance at the subplot scale indicates that shading effects are probably minor.

All impacts are most obvious for large precipitation events. Tree, stand and neighborhood effects are more important as event size increases. We conclude that the full development and connection of drainage flow paths through the canopy taps the full potential of systematic factors in forest structure impacting stemflow yield. Because of positive effects on forest density, unmanaged and mixed-species forest could be more stemflow-productive than managed ones. This is supported by the positive effect of the Simpson diversity index on small stand stemflow. More research is required to understand systematic effects of forest management on stemflow.

3.6 Appendix of Chapter 3

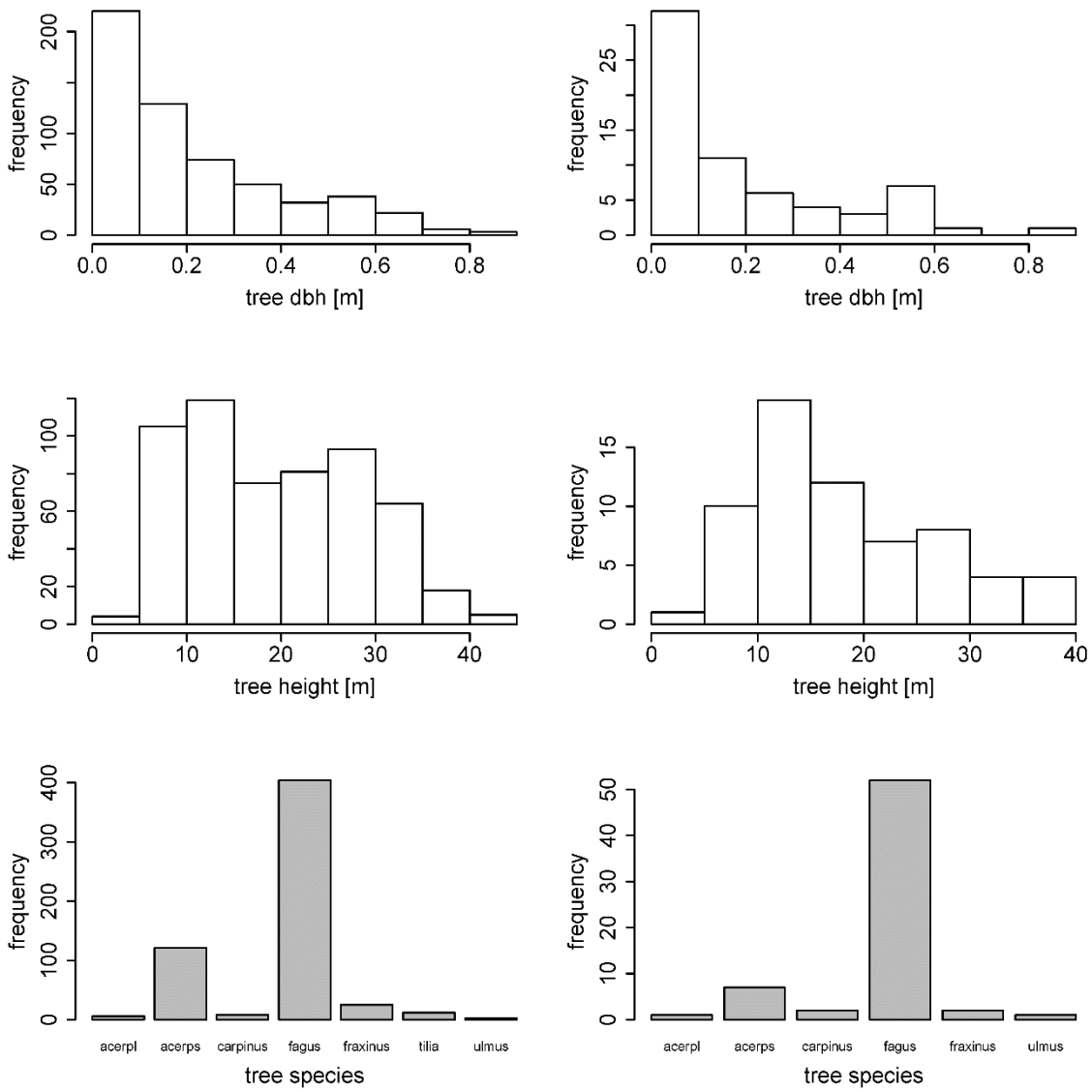

Figure 16: Histograms of stand properties on the whole 1-ha-plot (left, n = 581) and the eleven 100-m²-subplots on which stemflow was measured (right, n = 65).

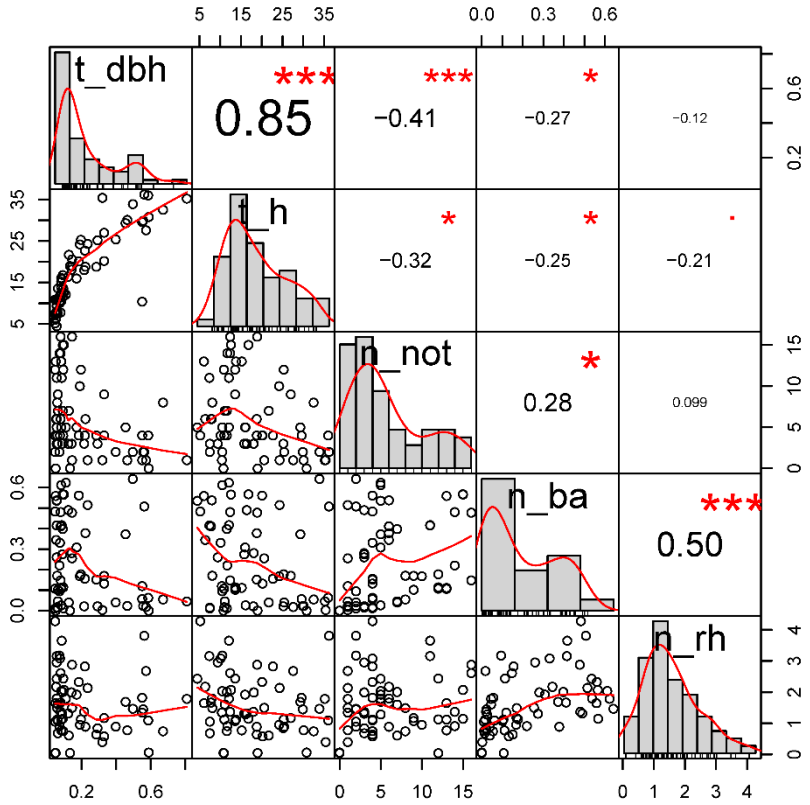

Figure 17: Distributions and correlations of variables included as fixed effects in the linear mixed effect models of individual tree stemflow. Abbreviations: t_dbh: tree diameter at breast height; t_h: tree height; n_not: number of trees in the neighborhood; n_ba: neighborhood basal area; n_rh: neighborhood relative height.

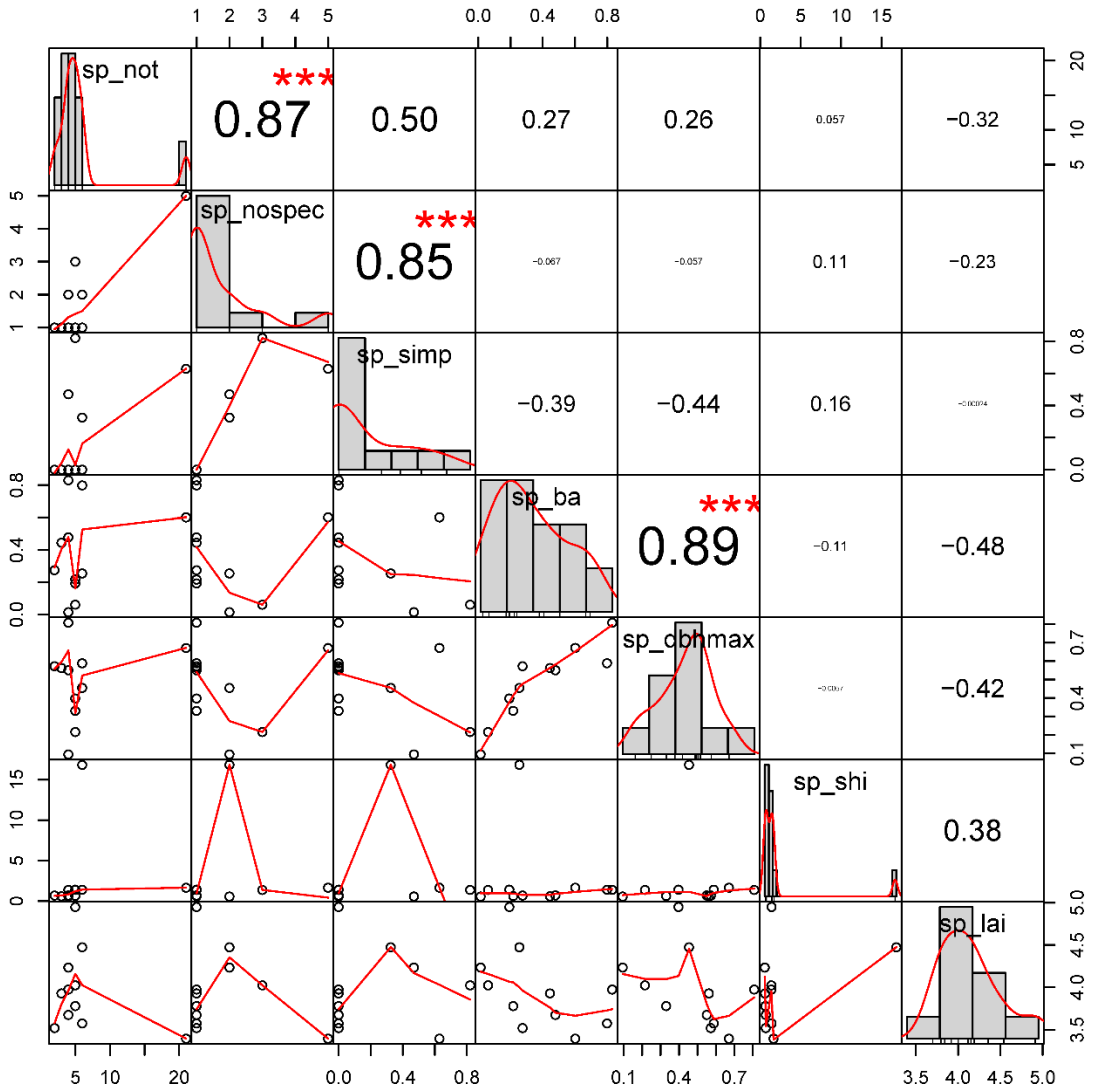

Figure 18: Distributions and correlations of variables included as fixed effects in the linear mixed effect models of subplot stemflow. Abbreviations: sp_not: number of trees in the subplot; sp_nospec: number of species in the subplot; sp_simp: Simpson's diversity index of the subplot; sp_ba: basal area of the subplot; sp_dbhmax: diameter at breast height of the biggest tree on the subplot; sp_shi: size heterogeneity index of the subplot; sp_lai: subplot leaf area index.

4 Infiltration hotspots and tree-induced soil microsites: The role of stemflow in net precipitation patterns at the soil level

4.1 Introduction

Stemflow has received much attention in forest ecohydrology research in recent times. As stemflow concentrates rainfall to the soil by a 3-37 fold of the median precipitation annually, and funneling can be much stronger for individual events and trees (Levia and Germer, 2015), it seems to be obvious that stemflow fluxes play a special role in water and nutrient turnover in some ecosystems. Also, indication has been found that stemflow is likely to trigger preferential flow in forest soils, enhancing the effect of soil bypass flow and dual porosity flow behavior (Martinez-Meza and Whitford, 1996; Taniguchi et al., 1996; Johnson and Lehmann, 2006; Li et al., 2009; Liang et al., 2011; Schwärzel et al., 2012).

The preferential treatment of stemflow has been criticized, as stemflow funneling can be close to zero for many trees and contribute little (0-5 %) of the overall precipitation input on a larger scale (Van Stan and Gordon, 2018). Yet, little proof so far exist of the role stemflow actually plays for subsurface flow mechanisms, soil water fluxes, or even water and nutrient input concentrations to the soil. While subsurface processes are very hard to observe, especially if they take place locally (making them hard to find) and short-term (making them hard to capture), it is also difficult to recapitulate input fluxes, as they are usually measured divided into throughfall and stemflow. Thus, the fate of net precipitation fluxes is unknown already at the point of infiltration (Carlyle-Moses et al., 2018; Van Stan II and Allen, 2020). As stemflow spreads on the forest floor near the tree trunk, and throughfall and stemflow add up in these stemflow

infiltration areas, considering throughfall and stemflow in concert could either obliterate or enhance the hotspot effect attributed to stemflow.

Yet, the difficulty is to define the stemflow infiltration areas (Carlyle-Moses et al., 2018). Stemflow infiltration has been assessed in the field by observation of marks on the soil surface (Tanaka et al., 1990; Iida et al., 2005a; Rashid and Askari, 2014), soil water content dynamics (Voigt, 1960; Buttle et al., 2014), literal observation of the infiltration process, during natural rainfall (Pressland, 1976; Návar, 2011) or irrigation (Buttle et al., 2014), or dye tracing experiments (Schwärzel et al., 2012; Carlyle-Moses et al., 2018). Also, calculation methods for stemflow infiltration areas were introduced, as by Tanaka et al. (1996), who fitted the radii of observed stemflow marks to a function of the tree's DBH, a model frequently used later on (Aboal et al., 1999; Iida et al., 2005a; Liang et al., 2011; Rashid and Askari, 2014). Another calculation method, which is based on stemflow intensity and soil hydraulic conductivity, has been proposed by Reynolds and Henderson (1967) and also repeatedly used since then (Herwitz, 1986; Návar and Bryan, 1990; Gómez et al., 2002; Carlyle-Moses et al., 2018). Stemflow infiltration areas are given either as area per tree, ranging from 0.0314 m^2 (Návar, 2011) to 1.52 m^2 (Herwitz, 1986), or as the width of a ring around a tree, with results between 0.09 m (Gómez et al., 2002) and >>1 m (Rashid and Askari, 2014) throughout methods and ecosystems. Carlyle-Moses et al. (2018) recently hypothesized, that stemflow infiltration areas have been generally overestimated by obtaining them from extreme conditions. This is supported by statements made by Durocher (1990), saying that stemflow infiltrated in direct proximity to the tree trunk without overland flow, and Reynolds and Henderson (1967), who argued that general estimations "for the area of spread of stemflow [were] rather too large for most storms".

Gaining insight about percolation behavior of infiltrated stemflow is all the more difficult. While positively measuring water flux patterns in the soil is near to impossible, we can have a closer look at soil properties. In Chapter 2, I found soil water retention to be significantly lower in areas close to tree stems compared to the rest of the plot area. Other studies have likewise found altered soil properties at the base of trees, as for pH (Neite and Runge, 1986; Wilke et al., 1993; Jung and Chang, 2013), soil organic carbon (Gersper and Holowaychuk, 1971; Rampazzo and Blum, 1992; Nacke et al., 2016; Rosier et al., 2016), soil texture (Gersper and Holowaychuk, 1970; Rampazzo and Blum, 1992), and soil hydraulic properties (Rashid et al., 2015). Soil

properties give the framework for possible soil water dynamics, and their differences close to tree stems or further away would impact on the fate of input fluxes. What is more, soil properties can also be considered a record of processes they have been exposed to for some time. As aboveground flux patterns have been found to be highly stable in time (Raat et al., 2002; Keim et al., 2006; Staelens et al., 2006; Van Stan et al., 2020) (see Chapters 2 and 3), input flux patterns might weather and model the soil at different rates, leaving an imprint on soil properties.

In this study, I want to address the meaning of stemflow at the forest floor and within the forest soil. Therefore, based on the large, statistically distributed data set of net precipitation (n(throughfall) = 350, n(stemflow) = 65, n(events) = 24) and soil properties (n(profiles) = 210), this study's objectives are: (1) Investigating the role of stemflow for the spatial differentiation of area-based, all-year net precipitation infiltration into the soil combining throughfall and stemflow data, based on the physic-based, dynamic model of Reynolds and Henderson (1967).
(2) Characterizing tree-induced soil microsites, in respect to concerned soil properties and vertical and horizontal extend, in order to reveal their underlying formation processes.

In this manner, I aim to investigate if stemflow hotspots persist also during soil infiltration and percolation, with distinct impacts on the direct soil environment. This would set the prerequisite for, and make it likely, that those stemflow impacts continue into the deeper subsurface and therein ongoing water-related processes.

4.2 Methodology

4.2.1 Field measurements and sampling

The study site, sampling design, and sampling of the stand properties and net precipitation is equivalent to the descriptions in Chapter 2 and 3 and the sampling of soil properties is equivalent to Chapter 2.

4.2.1.1 Study site and sampling design

The field study took place in a mixed beech forest in the Hainich National Park in central Germany. The measurement plot was installed as part of the AquaDiva Critical Zone Exploratory

(Küsel et al., 2016) at the upper part of the gently sloping transect with a southeastern aspect at an elevation around 365 m a.s.l.. The climate is temperate with annual rainfall of 600 to 900 mm (Küsel et al., 2016).

The plot area of 1 ha was subdivided into 10 m × 10 m subplots. Measurements were carried out in a stratified design (Zimmermann et al., 2010; Zimmermann et al., 2016) based on the subplot grid. Throughfall was measured in all subplots, each with two randomly distributed samplers. Stemflow was measured on all trees within 11 subplots distributed within the plot in a regular pattern. The tree properties of the stemflow subplots (n = 65) were representative for the whole plot (n = 581).

The measurement plot comprises 581 trees with a basal area of 38 m^2. The stand consists of a majority of European beech (*Fagus sylvatica*, 67 %), Sycamore maple (*Acer pseudoplatanus*, 20 %) and European ash trees (*Fraxinus excelsior*, 9 %), accompanied by European hornbeam (*Carpinus betulus*), Large-leafed linden (*Tilia platyphyllos*), Norway maple (*Acer platanoides*) and Scots elm (*Ulmus glabra*). As the stand has been unmanaged since 1997 and was used for selective cutting before, the age and size structures are very heterogeneous, with a median DBH (diameter at breast height) of 0.15 m and a maximum DBH of 0.87 m. Trees with a DBH < 0.05 m were not included in the stand survey.

The soil on the study plot is a shallow, silty and clayey Cambisol (IUSS Working Group WRB, 2006) derived from a bedrock of finely interlayered lime- and marlstones with a thin loess cover. The median sand, silt and clay fractions are 3, 75 and 21 %, respectively; the median profile depth (depth to C-horizon) is 0.38 m.

4.2.1.2 Survey of stand properties

All trees with a DBH ≥ 0.05 m were considered. They were given an identification number and the species was determined. The position coordinates were detected using a differential GPS and total station (both Topcon, Tokyo, Japan). Tree circumference at breast height was measured with a measuring tape and then DBH and basal area calculated assuming the tree bole is circular in cross section. Tree height was measured with an ultrasonic sensor (Haglöf Vertex, Haglöf, Järfälla, Sweden).

4.2.1.3 Measurement of stand precipitation

Precipitation samples were taken on an event basis in campaigns from May to August in the years 2014, 2015 and 2016. All components (gross precipitation, throughfall and stemflow) were collected in samplers that were read out and emptied manually after each event. Between the ending of rainfall and the beginning of sampling, there was a waiting period of 2 h minimum. If rainfall started anew during sampling, sampling was stopped and started from the beginning as described above. The previous (partial) event was then added to the current one. Like that, single events had to be separated by a minimum of 8 h without rainfall.

Gross precipitation and throughfall were collected in funnel-type samplers. Gross precipitation samplers were placed on an adjacent grassland in about 250 m distance. Gross precipitation and throughfall depths were calculated referring the collected water amount to the funnel area (ca. 0.01 m^2). Stemflow was collected by collars of lay-flat hose cut open and wrapped around the tree. Collars were sealed with silicone and connected to a water barrel. Stemflow depth was calculated by referring the stemflow amount per subplot to the subplot area. Data gaps were closed using a tree stemflow linear mixed effects model described in Chapter 3.

A total of 39 events were recorded. Events, where overflow could have occurred, and very small events with almost no stemflow (median stemflow per tree < 0.5 L) were excluded, leaving 26 precipitation events (for a detailed list, see Chapter 3).

4.2.1.4 Soil sampling

Undisturbed ring soil samples of 100 cm^2 were taken at 210 locations on the forest plot, at 7.5 cm (topsoil) and 27.5 cm (subsoil) soil depth each. Sampling locations were distributed in a stratified random design with random transects (Zimmermann et al., 2010). To represent soil properties close to tree stems, only locations within 1 m from a tree were selected (n = 71). The sampling rings were driven into the soil with a Teflon hammer, carefully excavated and the soil surfaces prepared to be even. Additional 250 cm^3 samples were acquired for measurement of soil saturated hydraulic conductivity (K_s) as part of a master's thesis (5 locations in the two depths, 2 of them close to stems, 2 far from stems, and 1 in between, that will not considered here), that were not hammered into the soil, but pressed in with a shear press (Weckmüller, 2017).

Disturbed samples were taken at 50 locations on the forest plot, for each location at the depths of 5-10 cm (topsoil) and 25-30 cm (subsoil). 19 locations were within 1 m distance from a tree by chance.

4.2.1.5 Precipitation time series

Precipitation time series for rainfall intensity evaluation were gathered from two weather stations: (1) Weather measurements at the Eddy Flux Tower in the Hainich National Park provided by the Group of Bioclimatology, Faculty of Forest Sciences and Forest Ecology at the Georg August University of Göttingen, Germany. It is located at 10.4530 long., 51.0792 lat. with an elevation of 430 m a.s.l. in about 5 km distance to the study plot. Data was provided in 30-minute intervals for the years 2014 and 2015. (2) Weather measurements of the DFG (Deutsche Forschungsgemeinschaft), CRC 1076 "AquaDiva", subproject D03 ("Site management and central experiments", Principal Investigators K. Küsel and K.U. Totsche) at the Friedrich Schiller University Jena, Germany. The station is located at H1/Reckenbühl in the AquaDiva Critical Zone Exploratory at the Hainich ridge in about 1.5 km distance to the plot (Küsel et al., 2016). Data was provided in 10-minute intervals for the year 2016, and I aggregated them to 30-minute intervals.

To evaluate the events of the observation period at the plot in respect to the region's climate, the 30-year precipitation record (1986-2015) of the nearest weather station of the German national weather service (Deutscher Wetterdienst, DWD) "Mühlhausen/Thüringen-Windeberg", station ID 5593, located at 10.5123 long., 51.2712 lat., with an elevation of 345 m a.s.l. in about 20 km distance to the study plot.

4.2.2 Laboratory analysis of soil samples

4.2.2.1 Hydraulic properties

The undisturbed 100 cm^3 ring samples were saturated stepwise over several days. For measurement of field capacity, samples were placed in a lidded sand bed with the manual appliance of a hanging water column of – 60 cm, left to equilibrate for 72 h, and weighed again. Saturated hydraulic conductivity (K_s) was measured in the again saturated samples using the constant head method. The head was kept stable with a Mariotte's Bottle and the outflow per

time measured with a graduated cylinder and a stop clock. After all measurements, samples were dried in a drying oven at 105 °C for 24 h. They were left to cool down in a desiccator before measuring the dry weight to determine bulk density and calculate all weighted water contents.

The eight undisturbed ring samples of 250 cm^3 were saturated stepwise and then measured with the "Ksat" falling head K_s measurement system (METER Group AG, Munich, Germany).

4.2.2.2 Texture analysis

Disturbed samples were air-dried and the organic compounds destroyed with 15 % hydrogen peroxide solution, let sit under a fume hood for 16 h and after that placed in an 80 °C water bath for about 1 d. The emulsion was then sieved using stacked sieves of 2, 0.63, 0.2 and 0.063 mm (sand fractions). The silt and clay fractions were determined from density measurements with a hydrometer in a 1 L suspension of the sieve passing. After washing the sample twice with 15 drops of magnesium chloride in a centrifuge, it was dispersed mechanically in a mixer and chemically by adding 15 ml of sodium pyrophosphate. The hydrometer was read after 30 s, 1, 2, 5, 15, and 45 min, and 1, 2, 6, and 24 h.

4.2.2.3 Soil chemistry

Soil chemistry was measured in the 19 disturbed sample profiles that were by chance close to tree stems, and in 19 randomly selected tree-far profiles, to compliment them. The samples were air-dried, sieved for organic residues > 2mm, and grinded prior to chemical analyses.

From each soil sample, carbon content was measured for one subsample that had been incinerated at 450°C to destroy organic compounds, and one subsample that was left original, by an element analyzer using high-temperature combustion at 1200°C and subsequent chromatographic gas analysis ("Vario Max CN", Elementar Analysensysteme GmbH, Langenselbold, Germany). The first sample gives inorganic carbon content, the second the total carbon content, and the difference of the two gives the organic carbon content (c_{org}). Tungstic oxide was added to the sample prior to analysis as an oxidation catalyst, and result values were corrected after determining the dry weight of the material by drying it in an oven at 105 °C for 24 h.

For pH measurement, a soil sample was extracted in high-purity water, shook for 30 min by an overhead shaker, and then letting sit for another 30 min. The pH-value was derived from the electrical potential at a single-rod glass electrode ("pH 538", WTW by Xylem Analytics Germany Sales GmbH & Co. KG, Weilheim, Germany).

4.2.3 Statistical analysis

All analyses were carried out using R (R Core Team, 2016).

For descriptive statistics, quantile-based values were used: The median and the coefficient of quartile variation (CQV)

$$CQV = \left(\frac{Q_3 - Q_1}{Q_3 + Q_1}\right), \tag{11}$$

where Q_1 and Q_3 are the lower and upper quartile of the sample.

To test the significance of the difference between two samples, if normal distribution was given, a Student's t-test was used, if one of the samples was not normally distributed, the Mann-Whitney-test (two-sample-Wilcoxon rank sum test) was used.

4.2.4 Estimating tree microsite sizes with linear mixed effects models

For a first estimation, soil properties were divided into the two group tree-close and tree-far by the arbitrary distance of 1 m in Chapter 2. For each soil property with significant differences between tree-close and tree-far in this step, the most efficient distance from the tree stem to separate the categories tree-close and tree-far was further examined. For each soil property, a series of linear mixed effects models was set up using the packages lme4 (Bates et al., 2015) and lmerTest (Kuznetsova et al., 2016) in R (R Core Team, 2016), starting with a null model and following with testing different tree distances to categorize soil sampling locations into the groups tree-close and tree-far as a random effect. The tested distances from the tree stem (width of ring around the tree stem) were 0.1 m (*n* (close:far) = 10:410), 0.2 (28:392), 0.3 (56:364), 0.4 (58:362), 0.5 (74:346), 0.6 (104:316), 0.7 (112:308), 0.8 (126:294), 0.9 (136:284) and 1 m (158:262). The model qualifying best (depending on the Akaike information criterion, AIC) was assumed to best represent the differences in the soil property of question by the categorization

into tree-close and tree-far, and the respective tree distance was assumed the critical distance to define the size of the tree microsite for that soil property. If the critical tree distance was 1 m, distances > 1 m were additionally tested to see if the model further improved. K_s as a logarithmically distributed variable was log-transformed for the modeling.

4.2.5 Modeling of net precipitation infiltration areas

To estimate the spatial distribution of infiltration over the whole plot area, measured stemflow and throughfall were set in reference to an infiltration area.

The calculation was based on the stemflow measurement subplots, were stemflow had been assessed at every tree. The plot area was divided into areas, where stemflow infiltrated, mixing with throughfall, and areas, where only throughfall occurred: First, stemflow infiltration areas were calculated individually for each tree and each event, following different strategies (see scenarios below). Within the stemflow infiltration areas, the mean event throughfall value was added to stemflow inputs (except for the basal area scenario, where no mixing of stemflow and throughfall occurred). Then, for throughfall infiltration area, stemflow infiltration areas and tree basal areas where subtracted from the total area of the stemflow measurement subplots for each event. This area was divided by the 200 throughfall measurements in the random design, assuming their representativity.

Scenarios were calculated event-based and cumulated over all events (P_g = 358 mm).

4.2.5.1 Scenarios

1) **Funneling ratio scenario**: Stemflow infiltration area is calculated as the basal area of the tree it is collected by, as proposed by Herwitz (1986):

$$A_{\mathrm{i\,SF}} = \frac{\pi}{4}\, {d_{\mathrm{tree}}}^2 = A_{\mathrm{tree}}, \tag{12}$$

   where $A_{\mathrm{i\,SF}}$ is the stemflow infiltration area, d_{tree} is the diameter at breast height and A_{tree} is the basal area of a tree. There is no mixing of stemflow and throughfall.
2) **Annular infiltration area scenario**: Stemflow infiltrates within an annular area around the tree stem, calculated as

$$A_{\mathrm{i\,SF}} = (d_{\mathrm{tree}} + w)\, w\, \pi, \tag{13}$$

where w is the width of the infiltration ring around a tree. This is the scenario mostly present in literature, which I chose different suggestions of as sub-scenarios:

a) Infiltration ring with a width of 0.3 m

$$w = 0.3 \text{ m} \tag{14}$$

as proposed by Voigt (1960), based on soil water content measurements around the stem, and further used by Leonard (1961).

b) Infiltration ring with a width of 0.2 m

$$w = 0.2 \tag{15}$$

as proposed by Buttle et al. (2014), based on soil water content measurements in an irrigation experiment, and further used by Bialkowski and Buttle (2015).

c) Infiltration ring width based on the stemflow infiltration area measurements by Pressland (1976), as a logarithmic (because data proposes so) regression of DBH:

$$w = 0.115 \ln d_{\mathrm{tree}} + 0.45 \tag{16}$$

d) Infiltration ring radius as a function of DBH established by Tanaka et al. (1996) (based on the radius from the center from the tree, here altered to refer to the infiltration ring width):

$$w = (23.36 \ln d_{\mathrm{tree}} - 34.92) - \frac{d_{\mathrm{tree}}}{2} \tag{17}$$

and also/similarly used by Aboal et al. (1999), Iida et al. (2005a), Liang et al. (2007) and Rashid and Askari (2014).

The basal area is excluded from the infiltration area. Within the stemflow infiltration area, mean throughfall depth is added to stemflow inputs.

3) **Soil conductivity scenario**: Stemflow infiltrates depending on the infiltration capacity of the soil in combination with the stemflow intensity. Within the stemflow infiltration area, mean throughfall depth is added to stemflow inputs.

Stemflow intensity was calculated from the rainfall intensity as proposed by Carlyle-Moses et al. (2018), Gómez et al. (2002), Návar and Bryan (1990), Herwitz (1986) and

Reynolds and Henderson (1967). I used precipitation time series recorded by two nearby climate stations (Section 4.2.1.5). Manually noted start and end times of events from the precipitation campaigns on the study plot were compared with the precipitation data from the stations and showed a good match. Precipitation amounts per event were different at the two weather stations compared to the study plot, but showed a strong linear relationship with a R^2 of 0.95 and 0.74 for 2014-2015 and 2016, respectively. I therefore assumed the precipitation intensity to have similar relative time series at the sites. The precipitation time series were corrected according to the linear regressions with precipitation measured on the study plot to make rainfall intensities comparable between the two weather stations. All time steps with precipitation were grouped into three intensity categories by the frequency of their occurrence. For each tree, a precipitation threshold for the onset of stemflow was determined by finding the smallest precipitation event to yield stemflow for the particular tree. For each time step following on a half hour period without precipitation, this threshold was subtracted from precipitation (also over several time steps). The remaining time of a time step, in which precipitation was reduced because of the subtraction of the threshold, was calculated proportionally to preserve intensities during that time step. The resulting effective precipitation time series, specific for each event and tree, was used to proportionally calculate stemflow intensity using the three intensity categories.

As infiltration capacity of the soil, the K_s value measured on topsoil samples from 5-10 cm soil depth was assumed to be representative in the order of magnitude and the spatial distribution. The median K_s of sampling locations on the plot within 1 m distance from a tree was calculated to represent infiltration capacity near stems (n = 61, K_s = 151.07 mm h^{-1}).

Mean throughfall was set in relation to the precipitation intensity following the same procedure as for stemflow. Throughfall threshold was calculated as the intercept of the linear function of event gross precipitation from event mean throughfall. To account for throughfall in the stemflow infiltration areas, the mean throughfall per intensity category and event was subtracted from the infiltration capacity, leaving stemflow infiltration capacity. Stemflow infiltration area was then calculated for each intensity category, tree

and event according to stemflow infiltration capacity according to Carlyle-Moses et al. (2018):

$$A_{\mathrm{i\,SF}} = \frac{I_{\mathrm{SF}}}{C_{\mathrm{i\,SF}}}, \tag{18}$$

Where $A_{\mathrm{i\,SF}}$ is the stemflow infiltration area [m^2], I_{SF} is the stemflow input rate [L h^{-1}] and $C_{\mathrm{i\,SF}}$ is the stemflow infiltration capacity [mm h^{-1}], which is the difference of K_s and the throughfall infiltration.

For the precipitation input per stemflow infiltration area, for each event, tree and intensity category, the mean throughfall was added to the stemflow input. To sum up infiltration areas of the different intensity categories of one event, stemflow and throughfall infiltration areas were averaged for each data point (tree or throughfall collector) according to the time each intensity category persisted.

4.2.5.2 Cumulation over the plot

To get the relative, cumulative distribution over the plot, relative input volumes and areas were calculated and the columns cumulated after ordering the data according to the infiltration depth (L m^{-2}).

To achieve a regular data distribution in 1-%-intervals, the input volume was separated into (1-%) bins and the proportional area of each bin calculated stepwise.

4.3 Results

4.3.1 Characterization of precipitation and event sizes

By an inspection of precipitation behavior, the representativity of the weather during the precipitation campaigns for the general climate in the region was inquired.

Figure 19 approaches the statistical distribution of daily precipitation sums by setting the quantiles of the 30-year-climate and the weather during campaigns in relation. It shows a good

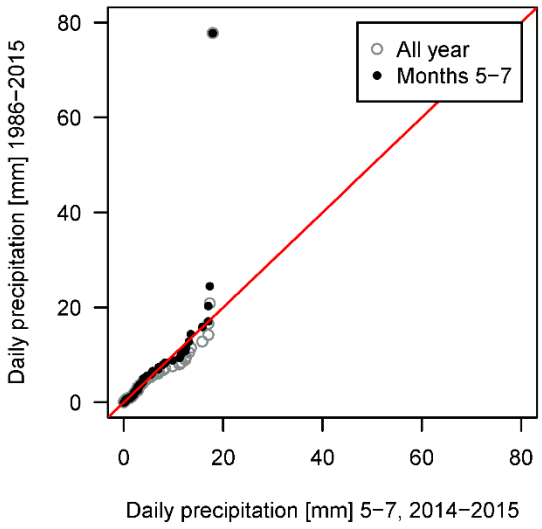

Figure 19: Quantile-Quantile plot of daily precipitation sums of the 30-year climate measured at the German Weather Service (DWD) station in Mühlhausen in relation to the weather during the periods when stand precipitation measurement campaigns took place (May to July 2014 and 2015).

agreement between precipitation within the two periods. A slight overrepresentation of events larger than 10 mm can be observed when comparing the campaign weather to all seasons, which disappears when considering the climate during only the summer months, as campaigns took place in summer. Only very extreme events within the last percentiles of the climate were not represented in the weather during the campaign. Yet, an extreme event of 65 mm was captured during the precipitation campaigns on 5/30/2014 and further evaluated (see a table of all recorded events in Chapter 3). The comparison of daily precipitation sums is practical, but has the disadvantage of an underestimation of large events (of > 10 mm), as large events are also likely to have a longer duration, and events spanning from before to after midnight are split up into two smaller events. The probability of catching a very large event during one calendar day in a 30-year-period is much higher as during an 8-month-period, which leads to the deformation of the quantile relationship as observed here.

Similar is the evaluation of the occurrence of events categorized as small (0-3 mm), medium (3-5 mm) and large (> 10 mm) in climate and during the observation period (Figure 20). The categories were defined by an equal number of occurrences during the campaign in 2015 (Chapter 2), yet Figure 20 (right) shows an overrepresentation of small events and a underrepresentation of large events in their occurrence also for the campaign periods. At the

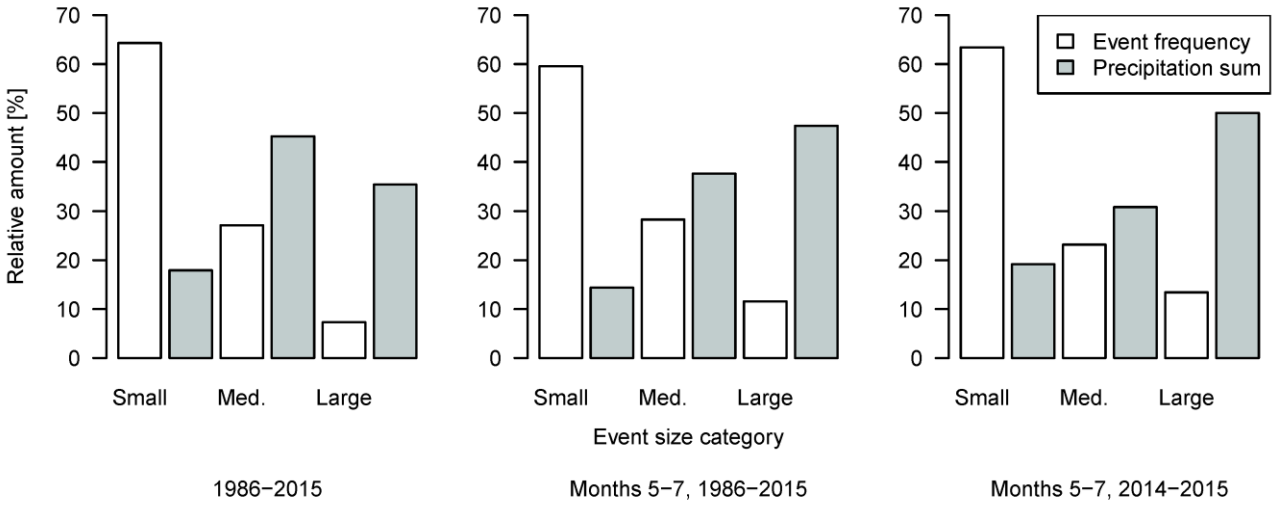

Figure 20: Relative distribution of the occurrence frequency and the precipitation sums of daily rain events over three event size classes (small: 0-3 mm, medium: 3-5 mm, large: > 10 mm) for the climate measured at the German Weather Service (DWD) station in Mühlhausen and the weather during the periods when stand precipitation measurement campaigns took place (May to July 2014 and 2015).

same time, the high relative amount of precipitation generated by large events shows the importance of large events for overall water input and fluxes, notwithstanding their underrepresentation in count.

Secondly, the relative amount of stemflow observed on the study plot is set in relation to global observations in literature to pigeonhole their representativity for global stemflow processes. The studies consulted show a high variability of stemflow at the different sites (Table 9). The mean values for forests from three different climates are all higher than the stemflow amount measured at the study site (which is 3.2 % in the 2015 events (Chapter 2), 3.0 % in all measured events 2014-2016 (Chapter 3), and 2.8 % in the data used for the current study and the linear mixed effects modeling of stemflow in Chapter 3). The evaluation of stemflow from this measurements is thus probably not overestimating the role of stemflow on a bigger scale, which could be much stronger at many other sites, though sites with very little stemflow might be underrepresented in stemflow literature in general (Van Stan and Gordon, 2018). It is impossible to give an estimation of the global role of stemflow on an area basis. Yet, Table 9 makes clear that stemflow is important at many sites and for a lot of different ecosystems, and that, of those, this study's data is within the center span.

Table 9: Stemflow values as percentage of gross precipitation for three different climates. The compilation is resumed from three stemflow reviews (as indicated). Excluded from this table were data from juvenile stands, plantations, agricultural systems or polluted sites. Two studies were excluded because they could not be accessed.

Original study	Resumed by	Ecosystem / Forest type	P_{SF} / P_g [%]
Tropical humid			
Herwitz (1986)	Levia and Frost (2003)	Tropical montane rainforest	13.6
Lloyd and de O. Marques F. (1988)	Levia and Frost (2003)	Tropical rainforest	1.8
Opakunle (1989)	Levia and Frost (2003)	Trees in a cacao plantation	2.0
Kellman and Roulet (1990)	Levia and Frost (2003)	Tropical dry forest	0.7
Veneklaas and Van Ek (1990)	Levia and Frost (2003)	Tropical montane rainforest	0.5
Marin et al. (2000)	Levia and Frost (2003)	Tropical rainforest	1.2
Hofhansl et al. (2012)	Levia and Germer (2015)	Tropical lowland rainforest	1.0
Chuyong et al. (2004)	Levia and Germer (2015)	Tropical rainforest	2.0
Oziegbe et al. (2011)	Levia and Germer (2015)	Secondary lowland rainforest	7.0
Dezzeo and Chacón (2006)	Levia and Germer (2015)	Tropical primary forest	8.0
Germer (2013)	Levia and Germer (2015)	Tropical open forest	8.0
Dawoe et al. (2018)	Carlyle-Moses et al. (2018)	Semi-deciduous tropical forest	1.5
Ghimire et al. (2017)	Carlyle-Moses et al. (2018)	Tropical secondary low-montane forest	1.7
González-Martínez et al. (2017)	Carlyle-Moses et al. (2018)	Tropical montane could forest	0.9
Group mean			**3.6**
Temperate humid			
Crockford and Khanna (1997)	Levia and Frost (2003)	Pine plantation	3.8
Crockford and Richardson (1990)	Levia and Frost (2003)	Dry sclerophyll forest	4.8
Olson et al. (1981)	Levia and Frost (2003)	Subalpine balsam fir forest	5.3
Liu et al. (2003)	Levia and Germer (2015)	Montane evergreen forest	2.0
Masukata et al. (1990)	Levia and Frost (2003)	Evergreen broadleaf forest	17.0
Tang (1996)	Levia and Frost (2003)	Slash pine forest	9.4
Taniguchi et al. (1996)	Levia and Frost (2003)	Japanese pine forest	0.9
Berger et al. (2009)	Levia and Germer (2015)	European beech forest	6.0
Pilegaard et al. (2003)	Levia and Germer (2015)	European beech forest	10.0
Lu et al. (2017)	Carlyle-Moses et al. (2018)	Sikang pine forest	4.9
Iida et al. (2017)	Carlyle-Moses et al. (2018)	Japanese redwood forest	3.2
Soulsby et al. (2017)	Carlyle-Moses et al. (2018)	Scots pine forest	1.3
Siegert et al. (2017)	Carlyle-Moses et al. (2018)	Yellow poplar and American beech forest	1.4
Group mean			**5.4**
Subtropical/Mediterranean semi-arid and arid			
Mauchamp and Janeau (1993)	Levia and Frost (2003)	Chihuhuan desert shrubs	29.0
Návar (1993)	Levia and Frost (2003)	Semi-arid shrubs	2.3
Martinez-Meza and Whitford (1996)	Levia and Frost (2003)	Chihuahuan desert shrubs	7.9
Whitford et al. (1997)	Levia and Frost (2003)	Creosotebushes	16.8
Návar et al. (1999)	Levia and Frost (2003)	Thornscrub community	3.0
Aboal et al. (1999)	Levia and Frost (2003)	Laurel forest	4.6
Rodrigo et al. (2003)	Levia and Germer (2015)	Holm oak forest	3.0
Bellot and Escarré (1991)	Levia and Germer (2015)	Holm oak forest	12.0
Cayuela et al. (2018)	Carlyle-Moses et al. (2018)	Mountain scots pine forest	1.2
Group mean			**8.9**
Total mean			**5.5**

4.3.2 Stemflow infiltration areas and spatial infiltration distribution

Infiltration areas (Figure 21) would be largely overestimated on the study site using the values or equations reported in literature, and even the basal area of a tree as reference area would still be an overestimation compared to the mean of the dynamically calculated infiltration areas depending on stemflow intensity and soil hydraulic conductivity. Consequently, funneling ratios are underestimated by 2-3 orders of magnitude (annular area models) and still 1 order of magnitude for the "classic" basal area funneling ratio from Herwitz (1986). It is also noteworthy that the range of stemflow infiltration areas is less for the dynamic model than for the basal area, meaning that the size of the infiltration area varies less than the size of the trees.

The relationship of cumulative precipitation input volume to cumulative infiltration area under the forest canopy (Figure 22) shows a rather even distribution: Ranking the data according to infiltration depth gives a smooth, symmetrical, slightly convex curve for throughfall. Stemflow adds some level of asymmetry to the picture, depending on the underlying sizes of stemflow infiltration areas: While annular infiltration areas around a stem of a fixed width only show a slightly more convex curve on the left side (scenarios 2a and 2b), it becomes steeper for an infiltration ring width that grows as a function of tree DBH (scenarios 2b and 2c), and the

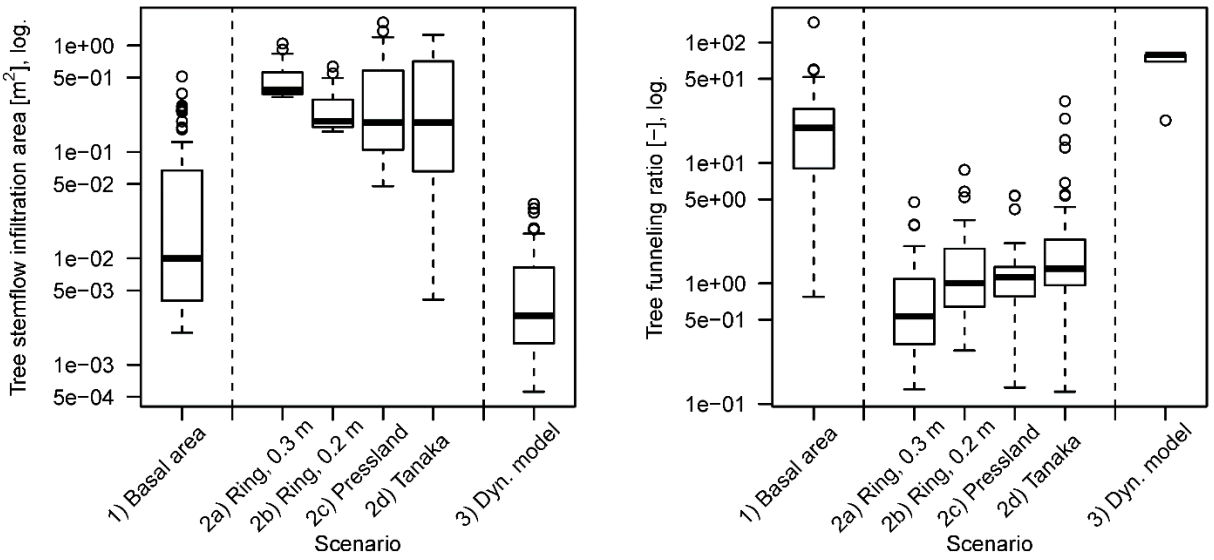

Figure 21: Stemflow infiltration areas and tree funneling ratios for all 65 trees, calculated based on the scenarios described in Section 4.2.5.

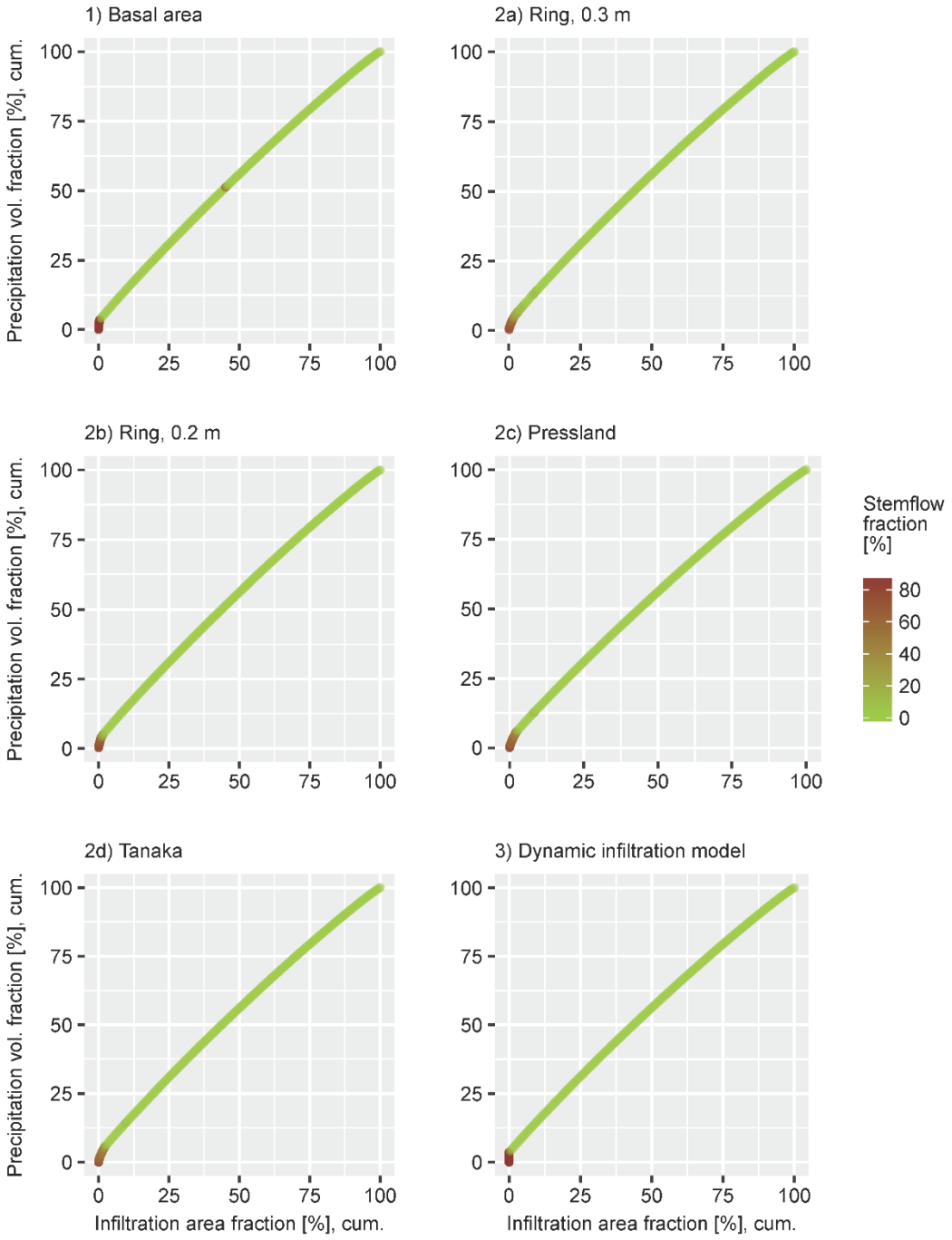

Figure 22: Cumulative net precipitation volumes infiltrating per area fractions of the study plot, also cumulative, ordered by infiltration depth [L m^{-2}] starting with the highest values. Stemflow fractions of the infiltration volumes are given in the color code. Relationships calculated for different scenario models of stemflow infiltration areas (1-3, as described in Section 4.2.5), applied to net precipitation data from the study plot.

funneling ratio and dynamic infiltration area scenarios (1 and 3) show an almost vertical start of the relation that abruptly switches to the smooth throughfall curve. This shows a shift along this gradient towards (1) an occurrence of higher infiltration depths (steep slopes) and (2) the separation of infiltration rates into two regimes of different characteristics. The color code in Figure 22 gives the percentage of stemflow in the infiltration input, showing that for scenarios 2a-d, stemflow blends in with throughfall, from a more stemflow-dominated input at higher infiltration rates, to a throughfall-dominated input on the majority of the area. For scenarios 1 and 3, there is no blending in – in stemflow infiltration areas, throughfall is negligible, and stemflow does not spread to throughfall-dominated areas.

For scenario 2a, the lowest stemflow fraction when mixing with throughfall is 9 % infiltrating at a rate of 325 L m^{-2} (sum of all measured events, maximum and minimum infiltration was 11941 and 160 L m^{-2}), and until then 28 % of precipitation inputs have infiltrated on 22 % of the plot area. For scenario 2d, all stemflow infiltrates within 5.7 % of precipitation on 2.3 % of the plot area and has an infiltration depth of 395 L m^{-2} (sum of all measured events, maximum and minimum infiltration was 11941 and 160 L m^{-2}) and a stemflow fraction of 31% before it changes to pure throughfall. For scenario 3, all stemflow infiltrates as 3.6 % of precipitation within 0.036 % of the plot area, with the infiltration depth dropping drastically from 254005 L m^{-2} to 358 L m^{-2} as highest throughfall infiltration depth (minimum throughfall infiltration depth was 160 L m^{-2}).

The drastic difference between the dynamic model of infiltration areas (Scenario 3) to all the other scenarios, including the funneling ratio (Scenario 1) shows best when considering infiltration depths (Figure 23) per percentage of total infiltration volume. While the total input volume is the same for all scenarios (the stemflow and throughfall measured on the forest plot), the maxima of infiltration depth are very different between scenarios. For scenario 3, maxima are multiples of the annular area scenarios and still twice as high as for the funneling ratio. What is more, this maximum holds for several percent of the input volume, while it only represents 1 % of input volumes for the other scenarios – in more detail, it holds for the total stemflow amount, that is 3.6 % of net precipitation, on a plateau which represents the infiltration capacity of the soil, and then abruptly falls to the throughfall dripping points. Thus, in the dynamic infiltration

scenario (scenario 3), hotspots of infiltration are much stronger and represent a much higher part of total inputs as they do in other scenarios.

When considering the relationship of precipitation input volume to infiltration area separated for different event sizes (Figure 24, left), it becomes obvious that an establishment of two input regimes is strongest for, and maybe only relevant in, large events. At the same time, the variation of inputs from the slow input regime is slightly higher for small events. This is also mirrored in a

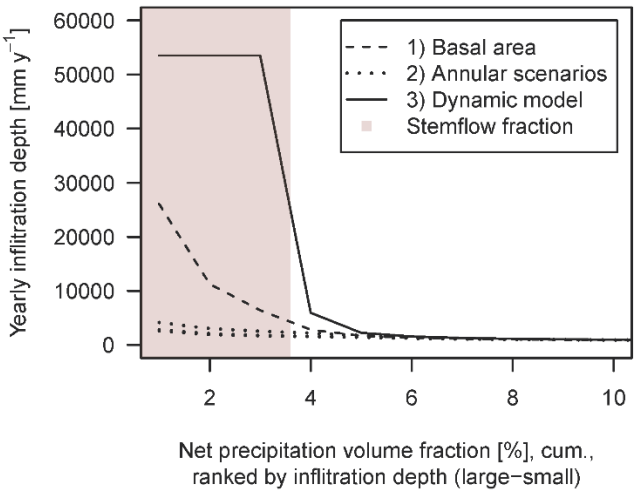

Figure 23: Infiltration depth of under-canopy-precipitation input to the forest floor per percent of total input volume, starting with the highest infiltration depth, for the 10 % of input volume with the highest infiltration depths, for the scenarios described in Section 4.2.5.

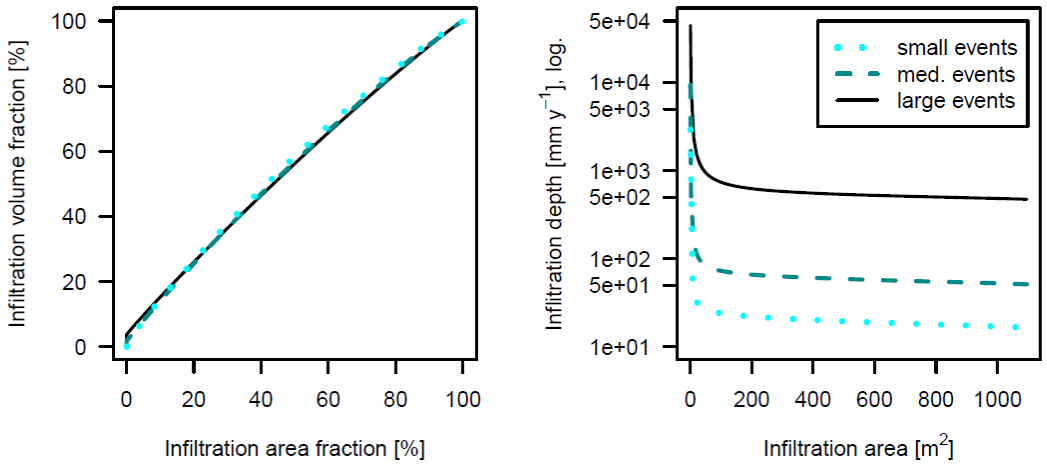

Figure 24: Infiltration area and volume relationships and yearly infiltration inputs per area for three event size classes (small: 0-3 mm, medium: 3-5 mm, large: > 10 mm).

higher variance and a higher degree of randomness I found for net precipitation at small events (Chapters 2 and 3). On a log scale, the infiltration depth per plot area has the same form for small, medium or large events (Figure 24, right), the only difference is a shift along the y axis – meaning, that for large events, precipitation input peaks are exponentially higher than bulk infiltration inputs compared to small and medium events.

4.3.3 Soil properties

4.3.3.1 Differences of soil properties in areas close to tree stems to further away

Comparison of the distribution of physical and chemical soil properties within the vicinity of tree stems and further away shows significant differences in field capacity and saturated hydraulic conductivity (K_s) in the subsoil, silt fraction in the topsoil, and organic carbon content in both top- and subsoil (Figure 25). The lower field capacity subsequently causes generally lower water contents close to tree stems (Chapter 2). Bulk density is higher in the subsoil compared to the

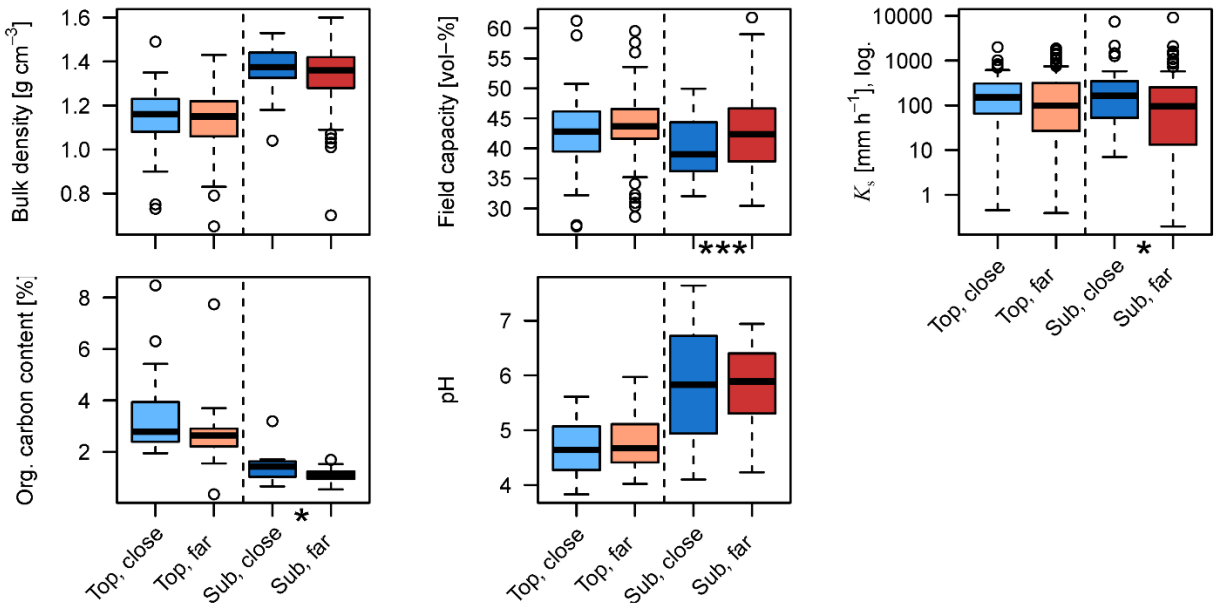

*Figure 25: Distributions of soil properties for locations in the topsoil (5-10 cm depth, "top") and the subsoil (25-30 cm depth "sub") close to trees (< 1 m distance to a stem, "close") or further from trees (> 1 m distance to a stem, "far"), n (close:far) in order or appearance: 63:136, 62:136, 64:136, 60:122, 19:31, 19:30 (for further information, compare Section 4.2.2.3). Asterisks mark a significant difference between tree-close and tree-far samples. Abbreviations: Field capacity: soil water content at – 60 hPa; K_s: the saturated hydraulic conductivity. Levels of significance: ***: $p < 0.001$, **: $p < 0.01$, *: $p < 0.05$.*

topsoil, what means that porosity is lower. Stem-close and -far areas are not significantly different in bulk density. In Chapter 2, I explained the differences in the field capacity and concurrently indifferent bulk density and porosity with a shifted pore size distribution towards more macropores in the vicinity of trees. The shift towards more macropores close to stems also facilitates saturated flow here, resulting in a higher K_s. The pattern differentiating stem-close and distant areas is much stronger in the subsoil. This also leads to a K_s in the subsoil equally high as in the topsoil. Yet, the special conditions in the vicinity of trees show in the whole soil profile. Organic carbon content is considerably higher here both in the top- and in the subsoil. A higher carbon input is thus vertically transported into deeper soil layers. pH values were not much different for stem-close and -distant locations. Yet, they are different for top- and subsoil. Subsoil pH values are in the range of clay dislocation, topsoil values are already past clay dislocation and in the range of cation depletion. The clay fraction is smaller in the topsoil compared to the subsoil; at the same time, silt fractions decrease with depth (Figure 26). The

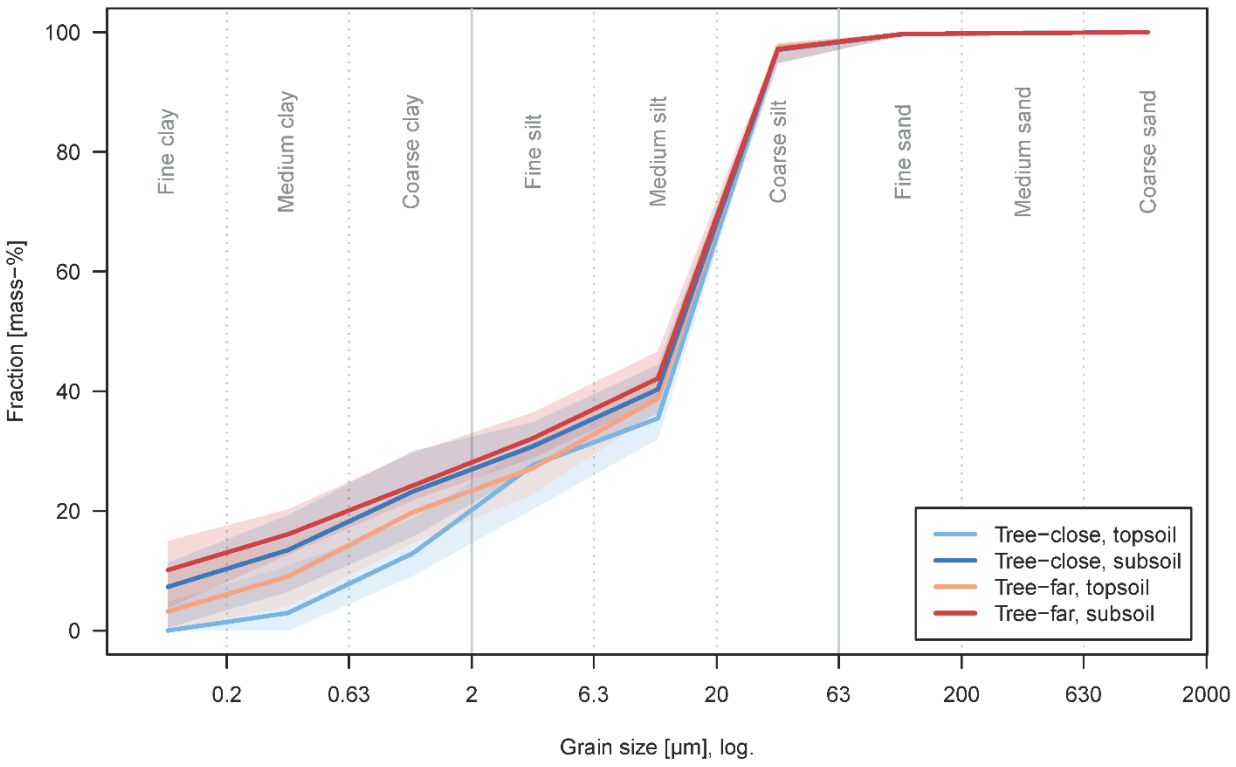

Figure 26: Grain size distribution curves: Medians and quartiles for the topsoil (5-10 cm depth) and the subsoil (25-30 cm depth) close to trees (< 1 m distance to a stem) or further from trees (> 1 m distance to a stem), n in order of appearance: 18, 25, 27, 28. The clay fraction is significantly different for tree-close and -far in the topsoil ($p = 0.03$).

sand fraction is overall very small (< 4 %), being a bit higher in the subsoil compared to the topsoil. The clay fraction is significantly lower in the topsoil close to stems compared to further away, while the other texture fractions show no significant differences.

4.3.3.2 Characterization of soil saturated hydraulic conductivity

Topsoil saturated hydraulic conductivity (K_s) at the study site, measured in a simple constant head setup on 100 cm^2 samples, has a mean value of 275 mm h^{-1} (median of 122 mm h^{-1}); in the vicinity of tree stems the mean is 251 mm h^{-1} (median of 150 mm h^{-1}). The 250 cm^2 pressed-in samples measured more carefully by Weckmüller (2017) had a mean K_s of 390 mm h^{-1} (median 382 mm h^{-1}) for four topsoil samples and of 363 mm h^{-1} for the two samples in the topsoil close to tree stems. I can therefore state that K_s was not overestimated by the simpler mass sampling and measurement methods. The overall higher K_s values obtained by the more careful measurement could be explained by the higher sampling volume, that give a higher chance to catch a big macropore in the sample, the presence of which is absolutely decisive for K_s. Using median values for my calculation of stemflow infiltration adds a second level of conservative measures.

4.3.3.3 Size of soil microsites

Proposing distances from the tree for the definition of soil microsites around trees showed different results for different soil properties and soil depths (Figure 27). In the topsoil, the critical tree distance was 0.3-0.4 m for soil organic carbon and 0.7 m for clay content; for every other soil property, a tree distance categorization did not improve the model. In the subsoil, the critical tree distance was 1 m for field capacity, 0.8 m for hydraulic conductivity (K_s) and 0.6 m for soil organic carbon. In coarse silt content, the model improved for a critical tree distance of 0.7 m, yet not significantly. Soil microsites at tree stems, thus, are non-uniform concerning different soil properties and tend to increase in size with soil depth at the study site.

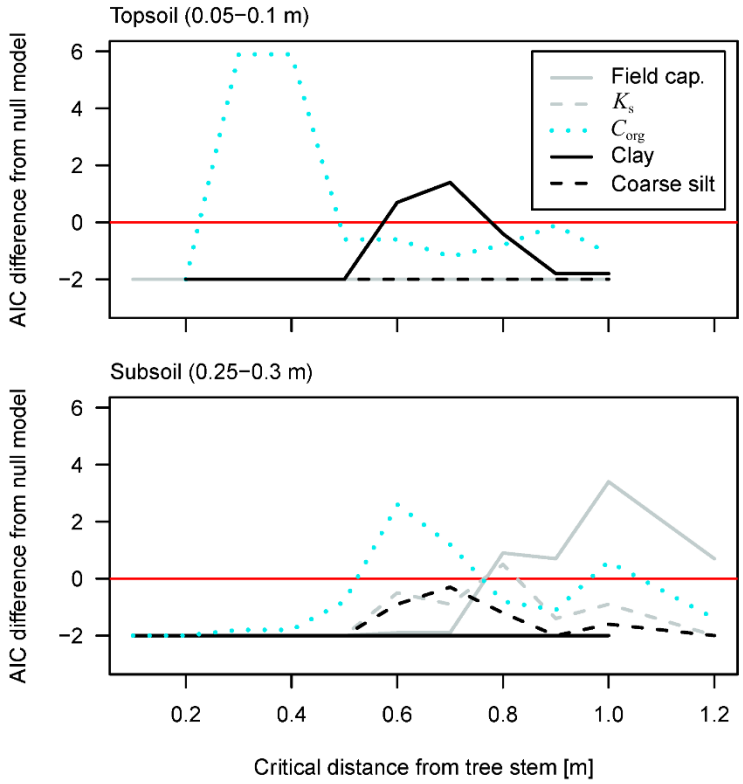

Figure 27: Results of Akaike Information Criterion (AIC) for linear mixed-effects models accounting for distance classes of increasing size (x-Axis). The y-axis gives the difference of AIC between the model containing tree distance classes (close and far) and the Null model (no distance classification included). A higher value than 0 implies model improvement. The highest positive values correspond to the size of the tree microsite for each soil property. Abbreviations: Field cap.: Soil water content at field capacity [vol-%]; K_s: Saturated soil hydraulic conductivity [mm h^{-1}] (log-transformed); C_{org}: Soil organic carbon content [%]; Clay: Clay content [%]; Coarse silt: Coarse silt content [%].

4.4 Discussion

4.4.1 Stemflow infiltration areas might be much smaller, and stemflow concentration much higher, than generally assumed

My results show much smaller stemflow infiltration areas calculated dynamically from precipitation intensity and soil infiltration capacity compared to other calculation methods. Notably, the derived infiltration areas are smaller than the basal area, implying that stemflow concentration is even stronger than Herwitz's often-used funneling ratio (Herwitz, 1986). This means that stemflow funneling has likely been generally underestimated.

Infiltration areas were mostly observed or calculated for single precipitation or irrigation events, often of large volumes and high rates (Reynolds and Henderson, 1967; Herwitz, 1986; Návar and Bryan, 1990; Návar, 2011; Schwärzel et al., 2012). As stemflow infiltration area sizes change depending on the stemflow rates, study findings vary strongly depending on the applied/examined precipitation or irrigation intensities. Additionally, observed infiltration areas have been derived from "infiltration marks" or "litter marks" in some studies (Tanaka et al., 1990; Iida et al., 2005a; Rashid and Askari, 2014), which can be attributed to maximum stemflow rates rather than averages: Maximum stemflow rates cause the maximum overland flow velocities and distances, which are able to transport litter and particles away from the stem. The same applies to dye tracer experiments: Dye will equally mark the maximum flow extend, corresponding to the highest stemflow rate, within the measurement period. Most approaches towards stemflow infiltration areas, thus, have been oriented towards the maximum extent of stemflow infiltration around a tree, or towards defining the total area that could ever receive stemflow input.

Therefore, to compare reported stemflow infiltration areas, it is important to consider the experimental settings. Taking this into account, my calculations using the dynamic model fit well with observed and calculated values reported in literature. In two dye tracer experiments, Schwärzel et al. (2012) and Carlyle-Moses et al. (2018) mapped stemflow infiltration areas. Schwärzel et al. (2012) applied a comparatively large quantity of water (180 L) to a tree stem within 3 h and found infiltration areas of 0.245 m^2. Carlyle-Moses et al. (2018) investigated three natural precipitation events ranging from 5.9. to 16 mm on three trees and found infiltration areas of 0.0017 m^2 per tree. This result is very similar to my study's result of 0.0029 m^2. In an additional calculation approach (using the same dynamic calculation), Carlyle-Moses et al. (2018) found a mean stemflow infiltration area of 0.0016 m^2 per tree. Results from low-intensity measurements and the dynamic calculation method thus are very similar (even though they cannot be directly compared, as they are based on different sites). Návar and Bryan (1990), Herwitz (1986) and Reynolds and Henderson (1967) calculated stemflow infiltration areas of 0.12-0.3 m^2, 0.13-1.52 m^2 and 0.13 m^2 with the same method, all for single events with very high precipitation intensities ($\geq$ 40 mm h^{-1}). Gómez et al. (2002) made the calculation for three olive trees of similar size for twelve events of varying size (average of 15 mm). The mean of the event

maximum stemflow infiltration areas for all events was 0.097 m^2, while the maximum was 0.373 m^2 (event of 77.1 mm). This illustrates how strongly maximum and mean infiltration areas differ. Stemflow infiltration areas of larger events in Gómez et al. (2002) align fairly well with the values calculated by Návar and Bryan (1990), Herwitz (1986) and Reynolds and Henderson (1967). Conclusively, despite different site, tree, and soil properties, values from observations of stemflow infiltration areas and calculations with the dynamic intensity/conductivity method result values all in the same order of magnitude for events with similar sizes or intensities.

Small stemflow infiltration areas result in high stemflow concentration at the soil surface. High infiltration concentrations imply a generally more variable infiltration pattern. Combining throughfall and stemflow inputs to derive an overall infiltration distribution, I found that this distribution is almost even, with the exception of stemflow. Stemflow infiltration depth is exceptionally high, but only refers to a very small fraction of infiltration volume (3.6 %) and soil surface area (0.036 %). Thus, my results confirm and stress the hotspot character of stemflow. Also, due to the small stemflow infiltration areas and the high stemflow infiltration depths, mixing of throughfall an stemflow is minor. Throughfall infiltration is negligible within stemflow infiltration areas (< 2 %), while on the major part of the plot area, stemflow infiltration does not occur. As small events are not important for overall rainfall distributions, and for larger events, throughfall and stemflow infiltration depths differ by several orders of magnitude (stemflow is a 80-fold of the highest throughfall dripping point), it can be stated that throughfall and stemflow indeed represent two totally different input types, which have been called “diffuse” and “point” inputs (Reynolds and Henderson, 1967; Durocher, 1990; Bialkowski and Buttle, 2015; Liang et al., 2015). These two input types could trigger two different subsurface flow regimes, a slow matrix flow and a fast-preferential flow. Stemflow has frequently been linked to preferential flow as well as enhanced deep percolation and recharge (Chang and Matzner, 2000; Johnson and Lehmann, 2006; Liang et al., 2009; Takahashi et al., 2011; Schwärzel et al., 2012; Buttle et al., 2014; Bialkowski and Buttle, 2015; Spencer and van Meerveld, 2016). Diffuse throughfall inputs, on the other hand, are more likely to infiltrate into the soil matrix and contribute to plant-available soil water storage. Stemflow and throughfall have conceptionally been assigned to different subsurface flow regimes in the past (Crabtree and Trudgill, 1985; Tang, 1996). Brooks et al. (2010) raised the “two water worlds” hypothesis, when they

discovered that precipitation fed two different subsurface pools, one soil matrix pool, which plants took up water from, and a second pool of mobile and preferential flow soil water, groundwater and stream water, which did not mix with the first pool and from which no plant water uptake occurred. Possibly, throughfall and stemflow could answer to these distinct pools.

As the areal distributed infiltration depths differ in magnitude, so do distributed net precipitation volumes and the areas they are relevant on. While stemflow still only constitutes 3.6 % of net precipitation on the study plot, it infiltrates on less than 0.1 % of the area, making a total area of 3.6 m^2 on the 1 ha plot of stemflow infiltration areas. Consequently, (1) stemflow is not a large proportion of inputs, yet if it, as anticipated, almost completely bypasses the soil and is not available for transpiration, it could constitute an important figure for groundwater recharge. (2) Because of the high nutrient loads of stemflow, a direct shortcut between stemflow and the groundwater could have a considerable impact on groundwater nutrient inputs. (3) The disproportionately high precipitation inputs have an impact on the small proportion of soil they apply to, creating microsites of soil formation at the stem bases of trees (Section 4.4.2).

4.4.1.1 Approaches for the determination of stemflow infiltration areas are inconsistent and constrained

Comparison of different methods and results of assessing stemflow infiltration areas in literature presents a number of obstacles. (1) Infiltration areas are often given for single events or irrigation/dye applications, often of large sizes and high intensities (Herwitz, 1986; Návar and Bryan, 1990; Návar, 2011; Schwärzel et al., 2012), making results exemplary rather than representative on a longer term. (2) Infiltration areas have been set in reference to different measures: tree DBH or species, and rain or stemflow sum or intensity. (3) Results have been provided in different measures: While a lot of studies give an actual area, others assume a annular infiltration of the stemflow and give the infiltration area's radius (center of the tree to outward border of the annular infiltration area) (Tanaka et al., 1996; Iida et al., 2005a; Rashid and Askari, 2014) or ring width (outward border of the tree stem to outward border of the annular infiltration area) (Voigt, 1960; Leonard, 1961; Herwitz, 1986; Gómez et al., 2002; Buttle et al., 2014; Bialkowski and Buttle, 2015). These different systems hinder comparison of results.

A frequent implication of approaches in literature is giving stemflow infiltration area as a function of DBH (Voigt, 1960; Leonard, 1961; Pressland, 1976; Majima and Tase, 1982; Aboal et al., 1999; Iida et al., 2005a; Liang et al., 2011; Buttle et al., 2014; Rashid and Askari, 2014; Bialkowski and Buttle, 2015). These studies conceptualize stemflow infiltration area as an annular area around the tree, which means that stemflow infiltration areas increase as a square function of DBH. This is also true for Herwitz (1986)'s funneling ratio. At the same time, stemflow often does not increase as a square function of DBH (Crockford et al., 1996; Aboal et al., 1999; Chuyong et al., 2004), and, additionally, varies considerably depending on gross precipitation and tree traits. Thus, in my results, stemflow infiltration areas calculated by the dynamic model correlate well with stemflow amounts, while the relation is scattered for other stemflow infiltration area calculation methods (data not shown). At the same time, stemflow infiltration areas calculated by other methods correlate well with DBH, while the relation is scattered for the dynamic model. Tanaka et al. (1996) tried to take care of this problem. They cite Rutter (1963), who found a linear relationship of stemflow to the square of DBH, therefore choosing a logarithmic function for the relation of DBH and the radius of the stemflow infiltration area. In my data, stemflow increased (already very scattered) linearly with DBH (as also in Van Stan and Levia (2010)), other studies did not find a relationship between DBH and stemflow at all (Buttle et al., 2014) – in summary, the relationship found by Rutter (1963) is not universal. Additionally, in this approach, the scatter in the relation of stemflow infiltration areas and stemflow still remains. The hypotheses of annular stemflow infiltration areas in general is unlikely to be true, because it would mean an isotropy of all stemflow impacting factors around the tree trunk. Factors like weather and tree architecture are usually not isotropic around the trunk, also not on average over time. Even at maximum stemflow, it is not to be expected that the whole stem circumference is wetted and acts as stemflow pathway (Levia et al., 2011), and even if it was, the whole stem circumference would not receive and channel an uniform amount of stemflow. Other factors of stemflow distribution around a stem are the architecture of the stem base, which consists of concave and convex segments for a lot of species (shape of the basal area), and topography, as stemflow has been found to travel further in downslope areas of a stem (Herwitz, 1986; Liang et al., 2011). Field studies observing annular stemflow infiltration areas often did not happen under natural condition, e.g. dye and irrigation experiments in which stemflow was artificially applied evenly all around the trunk (Schwärzel et al., 2012; Buttle et

al., 2014). While stemflow infiltration might occur annularly around the stem at some sites / for some species, and the concept is practical to calculate mean impact distances of stemflow from the tree stem, it is unfunctional for the calculation of stemflow infiltration areas and might be misleading, as neither the ring width nor the infiltration area are probable to increase proportionally to tree DBH.

The calculation of stemflow infiltration areas by the scenario 3 model is convincing because it is dynamic, physics-based and simple. The method has a temporal resolution, thus can be applied also to long-term precipitation time series and therefore be temporally representative. Stemflow infiltration areas are directly linked to stemflow input (instead of tree size), and can be assessed from the tree to the stand scale. The assumptions made for this approach are, as described by Reynolds and Henderson (1967) "that the steady state has been reached where stemflow volumes are linearly related to gross precipitation, the rate of stemflow is simply proportional to rainfall intensity, and infiltration rate into the soil is unaffected by time." Referring to these assumptions, Van Stan II and Allen (2020) recently criticized the method, naming explicitly the effects of unsaturated soils, air entrapment and hydrophobicity. I expect these effects to be small at the study site: (1) Microclimate in closed-canopy forest keeps the soil from drying completely in the summer. While the litter layer constitutes an additional interception storage resulting in loss of precipitation (Coenders-Gerrits et al., 2020), litter as well as the canopy cover also protect the soil from evaporative forcing (Metzger et al., 2014; Traff et al., 2015; Coenders-Gerrits et al., 2020). As hydrophobicity is related to dry matter (Hillel, 1998; Blume et al., 2010), it is likely to play a small role at this site. (2) Soil preferential flow of stemflow inputs has been frequently observed throughout climates and species (Johnson and Lehmann, 2006; Takahashi et al., 2011). It is also probable to play a role at this study site, as suggested by nearby observations (Tischer et al., 2020) and a generally high likelihood of preferential flow in clay-rich forest soils (Demand et al., 2019). The high hydraulic conductivity values observed on this study's site are based on small (100 cm^3) soil samples and are therefore largely confined to the soil matrix. Larger biopores and cracks come on top of the high measured conductivity values. Additionally, for preferential flow, the moisture state of the matrix is of minor importance, and dry or hydrophobic soils can even enhance preferential infiltration and flow (Beven and Germann, 1982; Hillel, 1998; Flühler and Roth, 2004). High occurrence of macropores and bimodality of water flow

dynamics due to dual porosity also allow entrapped air in soil pores to escape. (3) During long periods spent on-site, especially whilst measuring precipitation, overland flow or water logging were not observed. Also, no wash-off of litter or other "infiltration marks" were noticed. Nearby dye tracer stemflow experiments showed very small infiltration areas in accordance with the calculations in this study (Tischer et al., 2020). Generally, in bare, dry or sloped soils, a lateral spread of stemflow fluxes is more likely. Therefore, climate and land use might play a dominant role regarding stemflow infiltration areas. Agricultural systems do not provide a protection of the soil by canopy and litter cover, and might results in surface effects like hydrophobicity, silting and erosion, especially in warm climates. Care should therefore be taken when transferring stemflow infiltration observations from agricultural sites (Bui and Box Jr, 1992; Sansoulet et al., 2008; Cattan et al., 2009; Charlier et al., 2009; Rashid and Askari, 2014) to (near-natural) forests. Overall, determining stemflow infiltration areas in-situ is difficult, and a dynamic or spatiotemporal representative determination even is impossible. For lack of better methods to date, I consider the dynamic calculation method used here a good first approach, given a careful handling of input variables, as discussed in the following.

4.4.1.2 A conservative approach ensures representativity of small stemflow infiltration areas

Calculating the temporal mean instead of maximum stemflow infiltration areas resulted in much smaller areas in this study compared to the majority of other studies. These results depend strongly on the data used for the calculation. In the following, I want to discuss the input data and the consequent validity of this study's results.

Stemflow infiltration areas in my calculation strongly depend on rainfall intensity: Comparing rainfall characteristics of the measurement period to the local climate shows, that large events are slightly overrepresented in this study's data, showing the same pattern as the summer climate. The data is thus representative for summer conditions. Large summer events tend to be of higher precipitation intensities, resulting in larger stemflow infiltration areas. Therefore, it can be assumed that stemflow infiltration areas are still overestimated in this study considering the temporal mean of all times, when stemflow occurs. At the same time, it needs to be considered that inputs in small events are little, and stemflow does not exceed throughfall as much. Thus, in

total, small events have a negligible (to no) impact on cumulative rainfall amounts and the distribution of funneling over the plot (see results).

Stemflow infiltration areas in my calculation strongly depend on soil hydraulic conductivity: K_s at the study site can be quite high (> 1000 mm h^{-1}). The median of the samples, taken in high number on the plot (n = 182, 150 mm h^{-1}), is smaller than the mean, and is just one third of the larger-volume samples taken in smaller number and measured in a way that reduces potential disturbance of the sample. I chose to use the median of the mass approach to also stick to a more conservative measure of K_s, which again favors an overestimation of stemflow infiltration areas. Carlyle-Moses et al. (2018) said that "for most forest soils, K_s > 100 mm h^{-1} and may be > 1000 mm h^{-1}". Topsoil K_s values in forest studies have been reported to be 713 mm h^{-1} (Durocher, 1990), 415 (Schwärzel et al., 2012), 372 (Herwitz, 1986), 300 (Tang, 1996), 266 (Buttle et al., 2014), 81 (Gómez et al., 2002), 57 (Pressland, 1976) and 50 mm h^{-1} (Reynolds and Henderson, 1967). Therefore, even though K_s in forest soils can be quite high, high values are not representative for a lot of sites. This study's K_s measure lies within the lower range of the values reported in literature. Yet, results show, that despite of the comparably moderate K_s, the soil at this site is still able to discharge stemflow immediately, producing very small stemflow infiltration areas. I hope that thereby the results do not only speak for this specific site, but can also be seen representative for forested sites in more general.

4.4.2 Changed soil properties are in favor of accelerated soil formation at tree-induced microsites

Soil microsites at the bases of tree stems show distinctly different characteristics to the bulk forest area. They appear both in the top- and in the subsoil, concerning different soil properties.

4.4.2.1 pH is indifferent of tree distance

In contrast to much of the available literature on soil properties near stems, I found no differences of soil pH between stem close and distant areas at this study's site. Increased soil acidity has been reported repeatedly for soils close to tree stems (Gersper and Holowaychuk, 1971; Neite and Runge, 1986; Falkengren-Grerup, 1989; Wilke et al., 1993; Knoerzer and Gärtner, 2003; Rosier et al., 2016). Lower pH of soils close to tree stems is often set in reference

to stemflow being more acidic than rainfall, which has been a frequent observation in stemflow chemistry (Crabtree and Trudgill, 1985; Falkengren-Grerup, 1989; Návar and Bryan, 1990; Levia et al., 2011). Yet, low stemflow pH can also result from acidic air pollution, and many studies on effects of stemflow on soil properties were motivated by high pollution rates and acid rain in the 1970's to 1990's, which had dramatic effects on overall soil pH (Neite and Runge, 1986; Falkengren-Grerup, 1989; Rampazzo and Blum, 1992). At this study's site, stemflow pH is very similar to rainfall, with a tendency to be more alkaline (data not shown). Also elsewhere, stemflow has been observed to be more alkaline than rainfall (Shiklomanov and Levia, 2014), and the tree effect on soil pH has been found to be either acidic or alkaline depending on the tree species (Jung and Chang, 2013). In absence of pollution, stemflow pH largely depends on tree species, and the geology and land use of the surrounding landscape as sources of dry deposition. This study's site is situated away from industrial activity and in a limestone landscape. Stemflow pH is therefore not expected to have caused the observed differences in soil properties.

4.4.2.2 Clay dislocation shows accelerated soil formation at tree-induced microsites

Top- and subsoil textures distinctly differentiate tree microsites from the bulk area. They reveal that clay has been dislocated close to trees to a stronger degree than in further distance. Clay dislocation occurs during the advance of the soil formation process (in this study's setting). Consequently, soil formation has proceeded further close to trees. Clay dislocation is enabled by a pH of 5-6.5. pH shows no difference depending on tree distance in my study, consequently allowing for clay dislocation in equal measure. Instead, the differences in clay dislocation must be due to the larger water fluxes in near-stem areas, which enable clay dispergation and transport into deeper layers. Precipitation, i.e., water percolation, is a pedogenic factor, as is time, and consequently does higher percolation promote soil formation in time. Higher weathering indices and faster podsolisation have been observed in tree-proximal areas in other studies (Gersper and Holowaychuk, 1971; Rampazzo and Blum, 1992), both also indicators of advanced soil formation.

Texture differences are significant in the topsoil. Especially fine clay has been strongly decreased in the topsoil close to trees, as it is dislocated the easiest. Fine clay contents are also reduced in the topsoil tree-far, and in the subsoil tree-close, showing that clay dislocation has

taken place here as well. Clay coagulates again when it reaches soil areas still containing carbonate or when there are water flow obstacles. This explains, why clay dislocated from the topsoil close to trees is not found in the subsoil. The subsoil has also been already completely decalcified and shows no decrease in hydraulic conductivity, the whole near-stem soil profile shows a high fraction of macropores. Clay transport along flowlines and macropores into the deeper subsurface beyond the subsoil sampling depth of 0.25-0.3 m is therefore probable, especially with the locally extremely high water fluxes that can be expected close to trees due to stemflow. The same mechanism that caused the texture pattern in the topsoil – a stronger clay dislocation at tree microsites due to high water flow rates – could currently take place in the subsoil. Topsoil pH is already decreased below 5, thus clay dislocation here lies in the past. Subsoil pH, on the other hand, dropped below 6.5 with a median slightly below 6, indicating that, here, clay dislocation is currently possible.

4.4.2.3 Soil hydraulic properties and organic carbon show increased macroporosity and more pronounced structure at tree-induced microsites

A shifted pore size distribution with more macropores close to tree stems may have caused the observed lower water contents throughout the soil water content time series (Figure 4, Section 2.3.4), lower field capacity, and somewhat higher hydraulic conductivity.

Soil structure is the main driver of soil hydraulic properties besides soil texture, and is especially responsible for medium- and macropores. Soil structure is the systematic three-dimensional arrangement of soil particles due to physical (swelling and shrinking), chemical (electrostatic interactions, coagulation) and biological (gluing by organic compounds, bioturbation) processes, forming aggregates of typical composition and shape. The pore space between these aggregates is the main pathway for air, water and all related soil processes especially in clay soils (Hillel, 1998; Blume et al., 2010).

The changed hydraulic properties close to trees are prominent in the subsoil (0.25-0.3 m sampling depth). Subsoil structure at the study site is characterized by angular blocky aggregates consisting of flat faces and sharp corners. They are typical for clayey soils and develop due to swelling and shrinking (Blume et al., 2010). Clay contents are higher in the subsoil compared to the topsoil. Also, less bioturbation and general activity by larger organisms and plants can be

expected in the subsoil, which would remodel soil structure and create a loose, granular structure. These factors strengthen and conserve subsoil structure. Close to trees, higher organic carbon content further stabilizes soil aggregates (Blume et al., 2010), potentially accompanied by higher microbial activity (Rosier et al., 2016). Stronger shrinking and swelling of clay because of higher amplitudes in the drying-wetting cycle (compare soil water content time series in Figure 4, Section 2.3.4), growth and decay of roots and push-and-pull movements due to the tree swaying in the wind might additionally consolidate soil structure and increase secondary macropore spaces in a wider range around the tree stem.

Clay-rich forest soils on lime- and marlstones have been found to create high proportions of preferential flow (Demand et al., 2019). These results, which seem counterintuitive at first as clay soils have low hydraulic conductivities, make sense when considering the soil structure. They propose, that high rates of preferential flow are likely at the study site, especially close to tree stems. This also explains a saturated hydraulic conductivity in the subsoil equally high as in the topsoil, while it is usually observed to decline with depth (Herwitz, 1986; Schwärzel et al., 2012).

Organic carbon content is considerably higher close to trees both in the top- and in the subsoil. Higher carbon contents in tree-proximal areas were also observed by e.g. Rashid et al. (2015), Chang and Matzner (2000) and Gersper and Holowaychuk (1971) and might be the result of high organic loads in the stemflow (Chang and Matzner, 2000). Zinke (1962) explained the distribution of organic carbon by the amount of leaf litter, which I observed to accumulate around the tree stems at the study site due wind blow. Higher litter accumulations would again attract higher microbial biomass. Because of high water fluxes and a high proportion of macropores close to trees, higher organic inputs are also carried into deeper soil horizons. This is supported by findings of increased soil organic carbon in preferential flow lines (Bundt et al., 2001).

4.4.2.4 Extents of soil microsites at tree stem bases differ between properties

To study potential soil microsites at tree stems, I considered all locations within 1 m distance from the stem center as “tree close” in a first and simple approach (Chapter 2). In a second, more detailed study, I determined the critical distance from a tree to define the extent of the microsite,

based on the most significant difference, for each soil property. I observed a number of property changes at the tree-close soil microsites, yet, they differ in extent and combination. According to the results, (1) areas of altered soil properties do not coincide for different properties, (2) the soil microsites at tree stems are larger than the average stemflow infiltration area, and (3) soil microsites spread out with soil depth.

Areas of altered soil properties do not coincide for different properties. Thus, soil property changes close to trees are not strongly related to each other, could be shaped partly by different processes, or need different time spans to evolve. One major process shaping tree microsites is enhanced soil formation/weathering, forced by higher water fluxes due to stemflow. Clay dislocation is a typical consequence of advanced soil formation. Clay is dislocated from the topsoil in a ring of 0.7 m width around the tree stems. The impact distance of the other soil characteristic in the topsoil of tree-induced microsites, enriched organic carbon, is only half as wide (0.3-0.4 m). The process of carbon enrichment due to higher carbon inputs is thus relevant on a smaller area, or is partly compensated by higher mineralization rates (Chang and Matzner, 2000). What is more, the change in soil texture in the near-stem topsoil has no significant impact on soil physical and hydraulic properties here, and there is no correlation between texture and other properties (see the Appendix in Section 4.6 for correlation charts). In the subsoil, the change in texture is smaller, but there is a trend for a higher coarse silt content within an area of 0.7 m around the tree. Coarse silt constitutes the bulk of silt content at this study site, and might represent freshly weathered material from the bedrock or, alternatively, inversely represent clay dislocation. The extent of the enriched coarse silt content in the subsoil around the tree stem coincides with the extent of enhanced saturated hydraulic conductivity, and those properties are also correlated. A positive feedback would be possible due to the facilitation of clay transport by higher conductivities. Conductivity is not correlated to field capacity, yet, the latter shows a strong difference in stem-close compared to stem-far areas in the subsoil (ring of 1 m around the tree). Pore size profiles producing drainage or creating high saturated conductivities might not be identical, and stretch for different distances from the tree stem. Additional to the influence of enhanced water fluxes due to stemflow, macropore creation due to bioturbation or coarse root decay might impact hydraulic conductivity more strongly, while structuring features reducing field capacity probably comprise direct pressure-related physical influences of the tree roots (e.g.

wind sway and main root growth). In reverse, reduced field capacity around the tree stem might enhance soil weathering at depth due to higher drainage. A hint is the correlation of field capacity and soil profile depth (to the bedrock) in the near-stem subsoil.

The soil microsites at tree stems are larger than the average stemflow infiltration area: There are several possible explanations for this, which probably work in concert. Firstly, high water fluxes at large events develop the strongest forces and represent the major part of overall percolation. At large events, during very short time spans, stemflow infiltration rates increase to their maxima. Those events are statistically less important for the average size of stemflow infiltration areas, while they might be the most important drivers for changes in soil properties. Secondly, as proposed above, the tree stem could have a number of physical effects in the soil unrelated to water flow. These effects of trees at their stem foot need further research. Thirdly, changed forcing and properties in tree-close soils might produce feedbacks and responses both physically and biologically, creating a lateral spread of microsites within the soil into neighboring areas, which is also supported by the finding that soil microsites spread out with increasing soil depth.

Soil microsites spread out with soil depth: The critical distance from the stem in which soil properties were significantly different to the bulk area, on average of all soil properties, increases from around 0.5 m in the topsoil (0.05-0.1 m) to around 0.8 m in the subsoil (0.25-0.3 m). The only property which was significantly different tree-close and tree-far in both soil depths, organic carbon content, increased in tree distance from 0.35 m to 0.6 m with soil depth. While the main water movement seems to be vertical at the study site (based on observed patterns), a lateral component of percolation still exists. Lateral flow components are produced due to pressure gradients at high water inputs, and due to tortuosity of flow paths. Pores of all sizes do not lead straight down, but are contorted. While we cannot know whether there is a systematic pattern of directions of preferential flow paths from the stem bases into the deeper soil, water potential and pressure gradients create lateral flow leading from high-input areas as stemflow infiltration areas into drier soil areas further away from tree stems. Thus, water flow as well as root-induced and biologically related impacts on soil properties are likely to spread out laterally with increasing soil depth, depending on flow dynamics and inhibitions by strong vertical pedogenic, geogenic or biological disruptions. Therefore, the depth to which the spread of soil microsites continues,

or the three-dimensional shape of subsurface tree-induced microsites, strongly depends on site and tree characteristics.

In summary, results suggest that soil microsites are formed by a complex interaction of factors, one of which is high water input due to stemflow. Earlier studies viewed near-stem areas as "fertile islands" or, opposingly, areas of depletion concerning water and nutrients (Zinke, 1962; Neite and Runge, 1986; Rampazzo and Blum, 1992; Wilke et al., 1993; Chang and Matzner, 2000; Knoerzer and Gärtner, 2003; Rosier et al., 2016). We are only at the beginning of research on tree-induced soil microsites, and further study is needed to disentangle impacting factors and processes within the soil as well as their ecohydrological and biogeochemical consequences.

4.5 Conclusion

I calculated average stemflow infiltration areas per tree in the course of 24 precipitation events based on field measurements of gross and net precipitation and soil hydraulic properties using a dynamic model (Reynolds and Henderson, 1967). Results show, that stemflow infiltration areas generally are two orders of magnitude smaller than previously estimated, and even one order of magnitude smaller than the tree's basal area. Consequently, stemflow funneling has been underestimated. By accounting for throughfall and stemflow in combination, I can attest that throughfall is negligible in stemflow infiltration areas. Stemflow and throughfall infiltration depths constitute two completely separated regimes, differing by two orders of magnitude. In contrast to their enormous infiltration depth, the area in which stemflow infiltrates is a vanishingly small fraction of the plot. It therefore becomes obvious that stemflow creates special microsites in a forest, with exceptional conditions that differ from the major part of the system.

In a second step, I approached the effect of these extreme flow conditions on the properties of soil microsites at tree stems. Comparing the statistical distribution of soil properties close to trees and far from trees in high numbers, I found significant differences in several variables, that led to two main conclusions: Firstly, the results indicate accelerated soil formation at microsites. The large water fluxes must be driving this pattern, because higher acidification can be excluded. Secondly, I detected changes in soil structure, causing higher conductivities and lower water retention at tree microsites. The different soil structure is caused by the interaction of chemical,

physical and biological processes, which are partly induced directly by the tree and its roots themselves, and partly induced indirectly due to water and nutrient fluxes occurring at the base of the tree. This is shown by a different extent of the impacted soil area at the stem base depending on the soil property. Interestingly, tree-induced soil microsites are much larger than stemflow infiltration areas and increase with soil depth, likely caused by the multitude of processes impacting soil properties around the tree stem, by a lateral component of the enormous percolation rates induced by stemflow, and by positive feedbacks between different observed properties and their related processes.

While the overall amount of stemflow and the area affected by it might be negligible for total sums, the dynamics of stemflow fluxes are enormous and cannot be overseen. They are very likely to activate different flow pathways, and play a different role for subsurface flow and transport than bulk or average infiltration, with a relevant impact on hydrological and biogeochemical processes up to the hillslope and catchment scale. The fate of stemflow in deeper subsurface is hardly accessible and therefore largely unknown. Tree-induced soil microsites highlight the repercussion of extreme water flow conditions induced by stemflow, with a momentum able to change environmental properties within a remarkable radius even for the shallow soils and within the short average life span of a tree on this study plot. The changed soil properties further accelerate stemflow-borne fluxes in the subsurface and might penetrate in deeper areas, as the weathered bedrock, further connecting flow pathways that range outside of the general soil water flow regime sustaining the forest ecosystem.

4.6 Appendix of Chapter 4

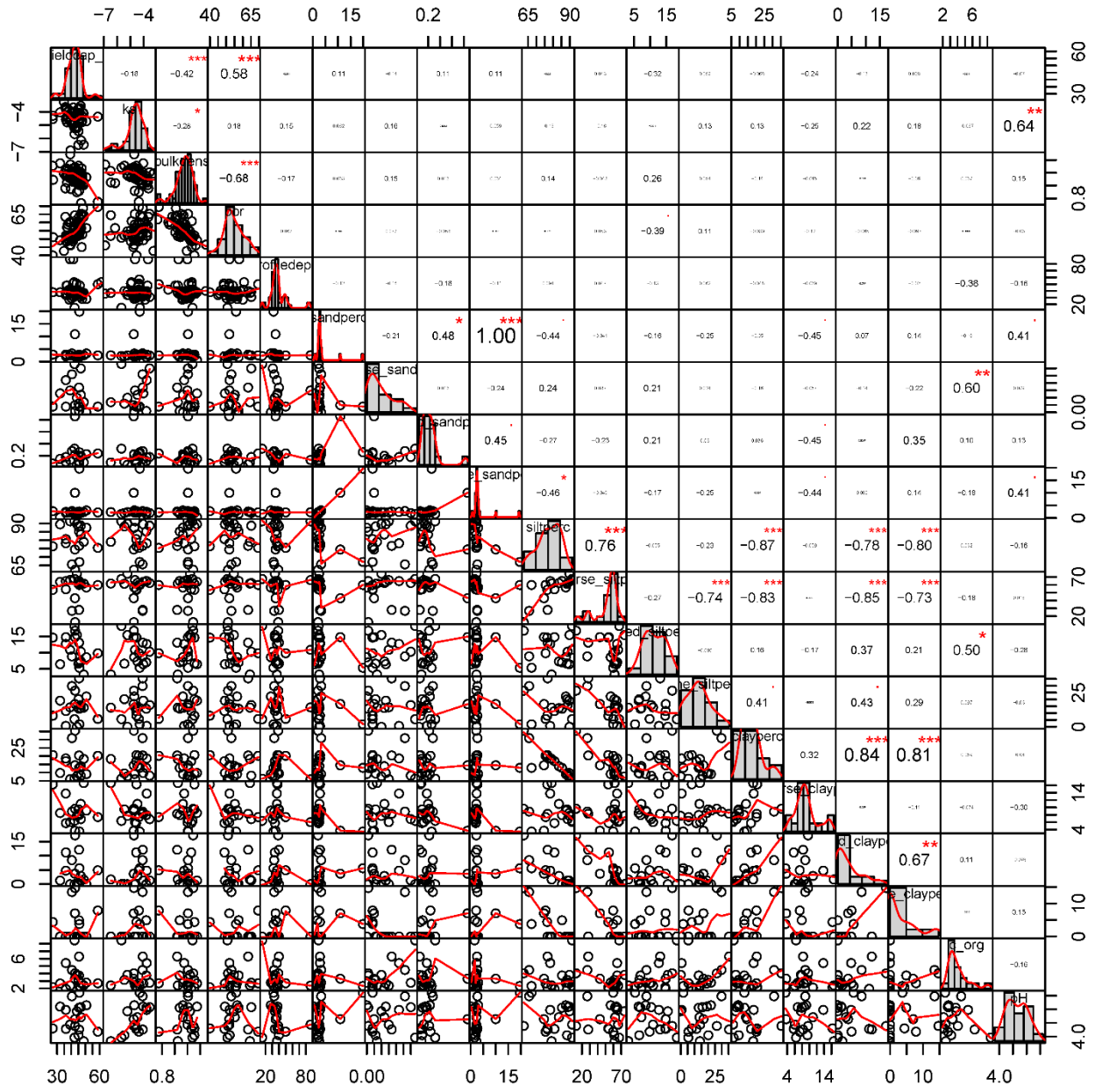

Figure 28: Correlation chart of all tested soil properties in the topsoil (0.05-0.1 m soil depth), tree-close (< 1 m distance from tree center), in order of appearance: Water content at field capacity [vol-%], saturated hydraulic conductivity [m s^{-1}] log-transformed, bulk density [g cm^{-3}], water content at atmospheric pressure [vol-%], profile depth [cm], sand content [%], coarse sand content[%], medium sand content [%], fine sand content [%], silt content [%], coarse silt content [%], medium silt content [%], fine silt content [%], clay content [%], coarse clay content [%], medium clay content [%], fine clay content [%], organic carbon content [%], pH.

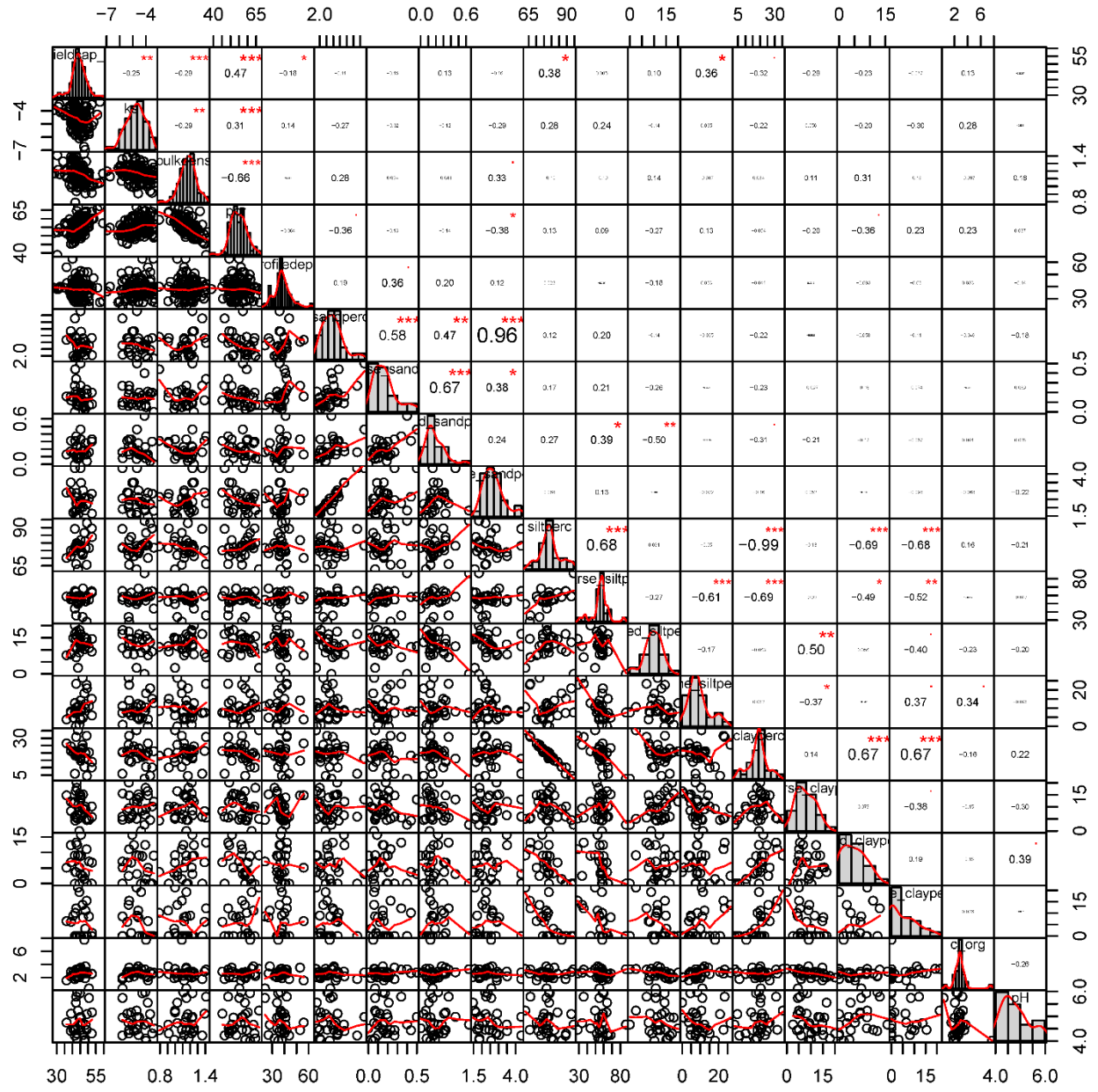

Figure 29: Correlation chart of all tested soil properties in the topsoil (0.05-0.1 m soil depth), tree-far (> 1 m distance from tree center), in order of appearance: Water content at field capacity [vol-%], saturated hydraulic conductivity [m s^{-1}] log-transformed, bulk density [g cm^{-3}], water content at atmospheric pressure [vol-%], profile depth [cm], sand content [%], coarse sand content[%], medium sand content [%], fine sand content [%], silt content [%], coarse silt content [%], medium silt content [%], fine silt content [%], clay content [%], coarse clay content [%], medium clay content [%], fine clay content [%], organic carbon content [%], pH.

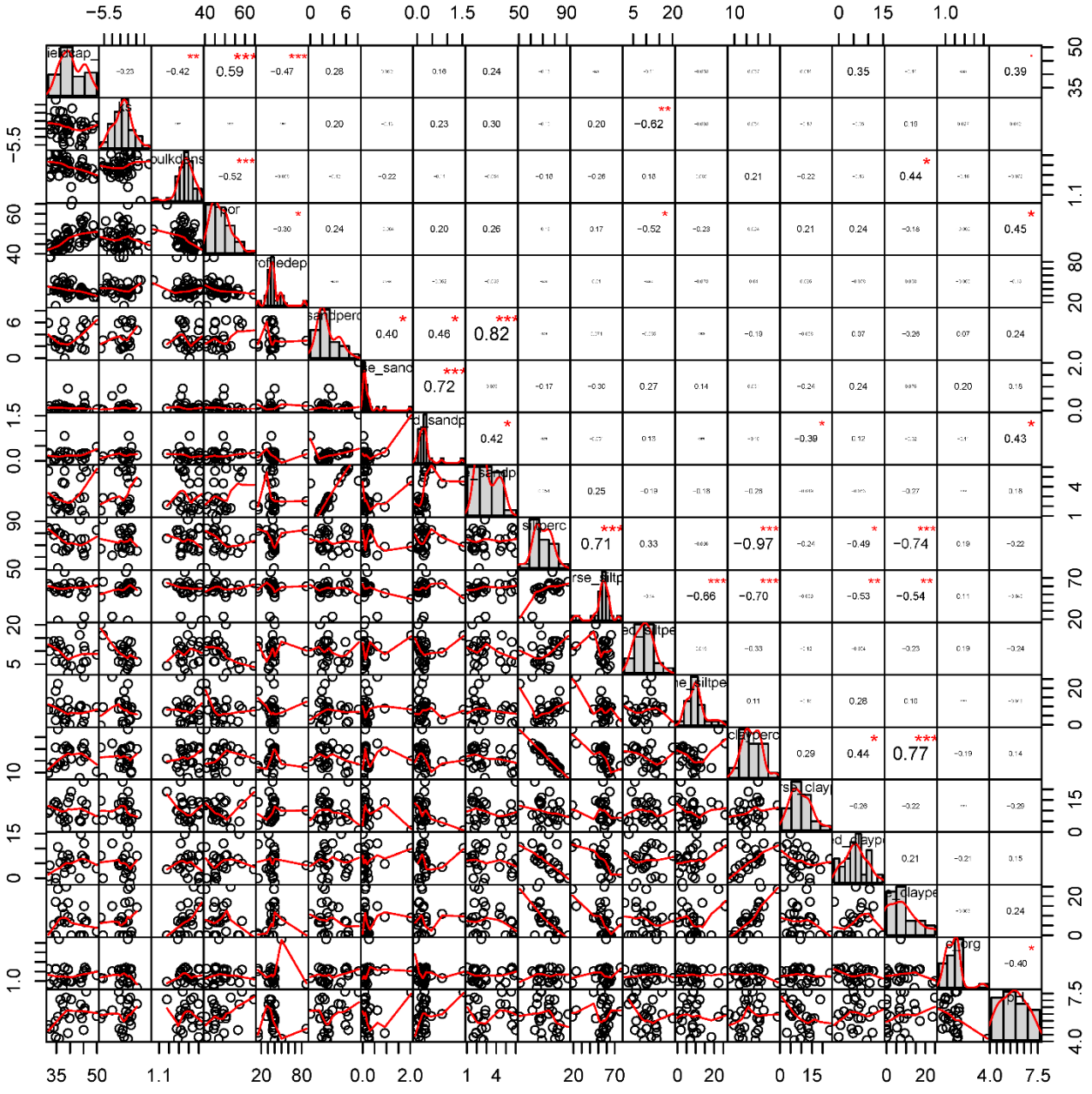

Figure 30: Correlation chart of all tested soil properties in the subsoil (0.25-0.3 m soil depth), tree-close (< 1 m distance from tree center), in order of appearance: Water content at field capacity [vol-%], saturated hydraulic conductivity [m s^{-1}] log-transformed, bulk density [g cm^{-3}], water content at atmospheric pressure [vol-%], profile depth [cm], sand content [%], coarse sand content[%], medium sand content [%], fine sand content [%], silt content [%], coarse silt content [%], medium silt content [%], fine silt content [%], clay content [%], coarse clay content [%], medium clay content [%], fine clay content [%], organic carbon content [%], pH.

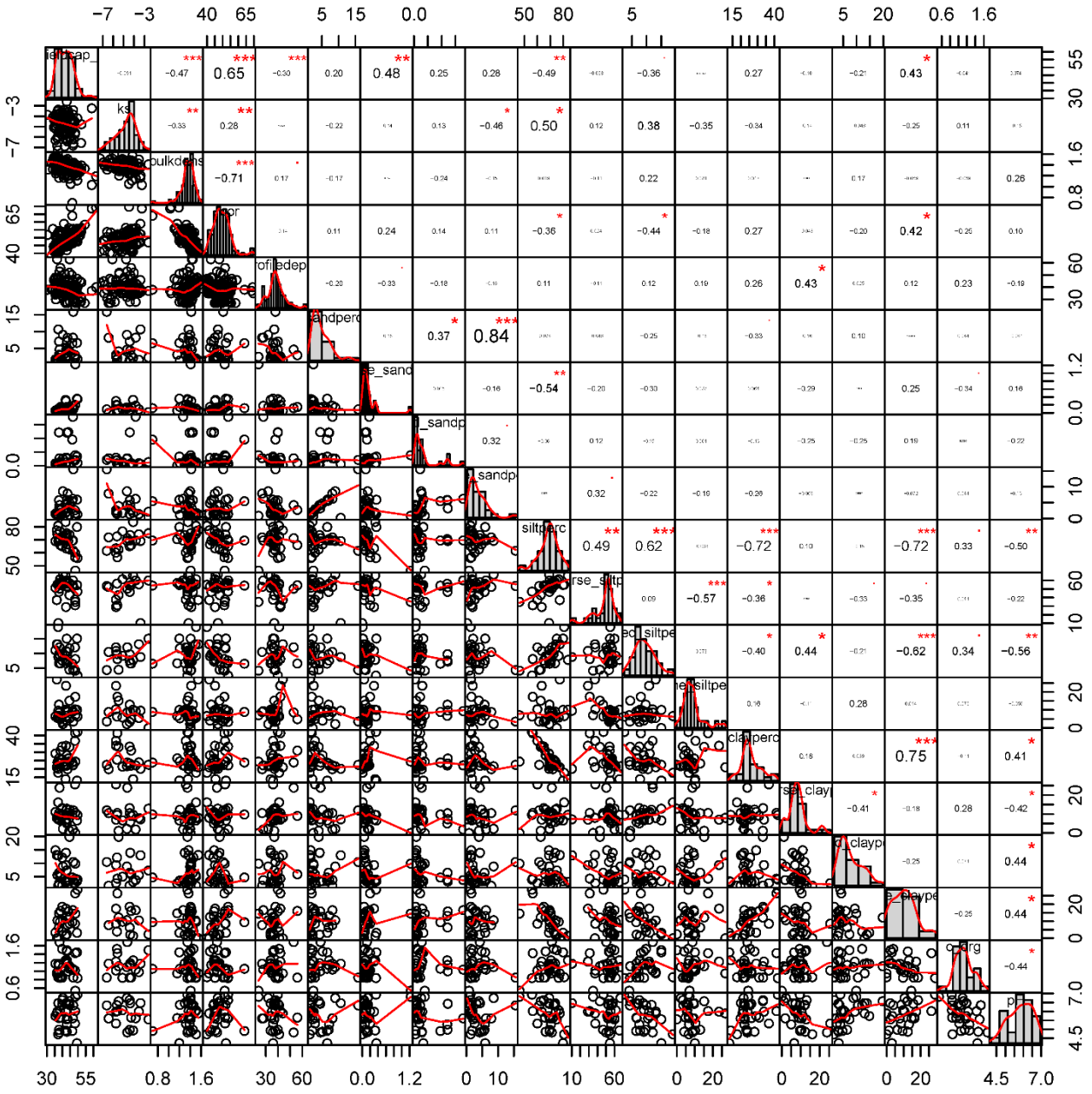

Figure 31: Correlation chart of all tested soil properties in the subsoil (0.25-0.3 m soil depth), tree-far (> 1 m distance from tree center), in order of appearance: Water content at field capacity [vol-%], saturated hydraulic conductivity [m s^{-1}] log-transformed, bulk density [g cm^{-3}], water content at atmospheric pressure [vol-%], profile depth [cm], sand content [%], coarse sand content[%], medium sand content [%], fine sand content [%], silt content [%], coarse silt content [%], medium silt content [%], fine silt content [%], clay content [%], coarse clay content [%], medium clay content [%], fine clay content [%], organic carbon content [%], pH.

5 Synthesis

Vegetation cover is a hub of biological, physical and chemical activity, strongly shaping the processes at the atmosphere-pedosphere interface. Vegetation depends on climate, water resources and soil, but it has shown to also impact on water cycling and soil formation. One of these impacts is the retention and redistribution of downwards-directed water fluxes by the vegetation canopy. The resulting input flux patterning is likely to affect subsequent subsurface processes, but little has been known about which processes are affected and to what degree.

I wanted to learn more about the character of small-scale heterogeneity in net precipitation and its impacts on soil water and soil properties. Most prominently, I aimed to evaluate input hotspots due to stemflow and their fate below the soil surface. Small-scale heterogeneities might shape a site's overall ecohydrological functioning, and hotspots have a high potential of introducing flow mechanisms that play a key role in landscape hydrological responses.

I addressed this goal by the overarching research questions: **(1) By which factors does the vegetation community systematically generate hotspots of net precipitation? (2) How does the high heterogeneity of net precipitation translate to soil water conditions and processes?**

5.1 Review of hypotheses

By approaching stand and soil properties and water fluxes comprehensively and highly resolved in a mixed forest, I was able to draw a picture of the ecohydrological processes driving and driven by downwards-directed water flux patterning. In the following, I will present my major findings, thereby revisiting my hypotheses and rejecting or accepting them.

I found net precipitation to be characterized by a strong variability, which is stable in time. In throughfall, this had been observed before in different ecosystems (Keim et al., 2005; Staelens et al., 2006; Zimmermann et al., 2007), but concerning stemflow, systematic investigations were lacking hitherto (Van Stan et al., 2020). My research could show for the first time that stemflow

fluxes are also temporally stable, and especially so in large precipitation events. At the same time, relative spatial variation is higher in stemflow than in throughfall. This allows a more differentiated view of stemflow character: Knowing that stemflow in general has a hotspot function (details below), I can now add that these hotspots themselves vary substantially in strength. As the variation is temporally stable, this creates long-lasting areas of very large cumulative fluxes at some trees, making them hosts of considerable fractions of larger-scale, long-term inputs. Temporal stability of stemflow increasing with event size additionally shows the important role which connectivity of flow paths in the canopy and down the stems play for the stability of stemflow patterns. Conclusively, flow paths themselves develop in a recurring pattern given a certain wetness level. These results indicate a highly organized heterogeneity due to canopy features for both throughfall and stemflow. Stemflow integrates canopy structure in the crown volume of the respective tree and therefore is strongly dependent on traits and morphology of this tree. My results furthermore show that the neighborhood of the tree drives tree individual stemflow, and that additionally, the neighborhood impacts tree morphological features. This is because neighboring tree's sizes and species shape canopy space occupation. I can therefore accept my first hypothesis: **H1.1:** Neighborhood and stand properties impact tree individual stemflow generation.

The variability of stemflow hotspots is not mitigated on a larger scale, but it persists in forest patches (100 m^2) in the same order of magnitude. Forest patches of this size can be representative for different stages of regeneration after the death of old-growth upper-canopy trees. Competition and shading have most commonly been suspected to be the main neighborhood effects on stemflow production (André et al., 2008; Takahashi et al., 2011; Terra et al., 2018). My results, yet, conclude competition and shading to play only a minor role. In contrast, stand features work in a way that trees concertedly yield more or less stemflow due to their community structure. Tree density was the strongest community effect on individual as well as forest patch stemflow production in my study. Most importantly, woody surface area is increased by tree density, constituting surface to receive and channel rainwater. Further, tree density steepens branching angles, such minimizing drip loss of stemflow. An increased density of mixed forest stands because of more efficient space occupation due to different species' growth strategies (Frech et al., 2003) might additionally explain the observed positive impact of

species diversity on community stemflow yield. This confirms my second hypothesis: **H1.2:** In a natural, diverse forest, different forest patches can strongly vary in stemflow production depending on their community traits. Diverse stands and forest patches increase stemflow variation and therefore hotspot generation.

While my results confirm the hotspot character of stemflow inputs, they moreover show that stemflow funneling at infiltration has been strongly underestimated in previous studies (Voigt, 1960; Reynolds and Henderson, 1967; Návar and Bryan, 1990; Tanaka et al., 1996; Buttle et al., 2014). This finding also contributes to a recent debate on the hotspot character of stemflow based on stemflow infiltration areas (Carlyle-Moses et al., 2018; Van Stan and Gordon, 2018; Van Stan II and Allen, 2020). The hydraulic conductivity of the soil allows for the stemflow to infiltrate within areas smaller than the tree's basal area (which is conventionally used as reference area to express stemflow concentration). Thus, net precipitation hotspots are not weakened in the process of entering the soil, but persist. Stemflow infiltrates almost constantly at soil infiltration capacity, constituting fluxes that are several orders of magnitude larger than throughfall inputs. This results in the acceptance of the next hypothesis: **H2.1:** Stemflow infiltrates into the soil in the direct proximity of the trunk, and has a distinct hotspot character compared to throughfall and throughfall dripping points.

While input hotspots persist entering the soil, net precipitation heterogeneity overall has a minor impact on long-term soil water content patterns. My analyses show additional variance introduced to soil water content patterns by precipitation events. Yet, superimposed patterns of net precipitation in soil water content quickly disappeared again with soil drainage. Predominantly, soil hydraulic properties drove soil water content, creating a stable pattern which quickly reestablished itself after precipitation events. Discussions in literature, as well as the present study, frequently assumed a general, long-lasting effect of net precipitation patterns on soil water content, creating areas of high and low soil water recharge (Alva et al., 1999; Raat et al., 2002; Jost et al., 2004; Teuling and Troch, 2005; Zehe et al., 2010; Rosenbaum et al., 2012; Traff et al., 2015). While the findings may be unexpected, they are logical conclusions upon reconsidering the facts: Additional water input to the soil cannot increase soil water content if the soil is incapable of retaining it. Less water input to the soil, on the other hand, might be quickly countervailed by redistribution due to soil water potential gradients. At the same time, if

precipitation inputs do not imprint on soil water content, this means that they do imprint on soil water fluxes. As water inputs are not retained by the soil, they likely contribute to deep percolation (provided that vertical flow predominates). This mechanism is highlighted by the situation I found at potential hotspot locations – close to tree stems: Surprisingly, near-stem soil was generally drier than further away from trees. This is in opposition to earlier observations (Pressland, 1976; Li et al., 2008; Wang et al., 2011; Jian et al., 2014). Yet, these studies measured soil water content directly after precipitation events, when soil drainage (based on my results) is still ongoing. I found the explanation for low water contents of near-stem soils in soil water retention, which is significantly lower in the vicinity of tree stems. This strongly suggests that water flow hotspots established in the vegetation canopy persist in the soil and induce also hotspots of drainage. In summary, net precipitation patterns are reproduced in soil water content patterns, but only for short periods directly after rainfall. For the most part, soil water content patterns are independent from input patterns, and input hotspots do not result in elevated soil water recharge. I therefore conclude to reject the hypothesis: **H2.2:** Net precipitation patterns imprint on soil water content patterns, and points of high inputs, especially stemflow hotspots, create areas of increased soil water recharge.

As soil water retention is significantly lower around trees, there is a systematic soil pattern due to trees. I identified soil microsites near stems, which differ in several properties from the bulk area. Water retention capacity was lower and hydraulic conductivity was higher due to increased macroporosity, significantly so in the subsoil. Organic carbon content was higher and clay dislocation advanced further, significantly so in the topsoil. These results draw a picture of an accelerated soil formation and a more pronounced soil structure close to trees. Because water fluxes, as a pedogenic factor, are increased near stems, soil formation has further progressed here. Interestingly, this induces a coupling of locations of increased input and locations of increased drainage in the soil. Soil microsite areas at tree stems are larger than mean stemflow infiltration areas and increase in size with soil depth. It can therefore be assumed that stemflow-induced soil water fluxes fan out with increasing depth. Yet, the effect is unlikely to explain the larger extent of soil microsites already in the topsoil. This suggests that stemflow effectively develops soil microsites even at locations of low frequency occurrence of stemflow infiltration further away from the stem, to which stemflow water spreads only during high intensity storms.

Further, soil microsites at trees could be shaped by other factors additional to stemflow, and more research is necessary on this newly emerged topic. My last hypothesis, nevertheless, can be accepted: **H2.3:** Soil properties in the vicinity of tree stems differ distinctly from tree-distant areas, forming microsites, which impact the fate of stemflow fluxes.

5.2 Evaluation of achievements and representativity

My study's results provide new insights to below-canopy precipitation patterns' impacts on subsurface conditions. Vegetation is known to be a key influence on environmental processes at larger scales. My research now shows that vegetation shapes soil and water processes also on small scales. Heterogeneity and diversity of vegetation increase hotspots of downwards-directed water fluxes on the small (< 1 m) and the forest patch (> 10 m) scale. Results strongly suggest that elevated input water fluxes locally enhance soil formation, leading to a coupling of both water input and drainage hotspots at near-stem soil microsites. Thus, vegetation establishes water bypass flow presumably leading from the canopy right into the deeper subsurface. In this way, introduced heterogeneity of downwards-directed water fluxes is likely to impact allover hydrological functioning.

Overall, even though some results were unexpected, the various findings complement each other to form a conclusive picture. Also, my findings match reported observations, and could even help to explain and resolve contradictions. For example, in some studies, soil water content had been found to be impacted by net precipitation inputs, while in other studies, no or no important impact of net precipitation had been found (see Introduction, Section 1.1.3). As my analysis showed net precipitation impacts on soil water content to be short-lived, it became apparent that a lot of measurements confirming the hypotheses were taken in the hours directly after rain events (Pressland, 1976; Li et al., 2008; Wang et al., 2011; Jian et al., 2014), while long-term field and model representations found no, or equally a short-lived, impact (Pressland, 1976; Bouten et al., 1992; Raat et al., 2002; Liang et al., 2007; Coenders-Gerrits et al., 2013). As I noticed, some studies had even found lower water content close to tree stems, but had not further discussed this result (Rutter, 1964; Buttle et al., 2014).

The extensive field sampling provided a comprehensive data set. Its elaborate design results in robust analyses: A stratified random sampling allows for a statistical evaluation that can be considered representative for the population (Campbell, 1989). The combination of independent stratified random sampling designs for different variables on the same plot enabled me to compare the different variables by their statistical properties, without having to measure different variables at the same location, and such, avoiding disturbance. Especially for throughfall, the sample size necessary to cover variance in a stratified random design is well researched (Zimmermann et al., 2010; Zimmermann et al., 2016). For soil properties and soil water, the subject of heterogeneity is a more complex one (Price and Bauer, 1984; Western and Blöschl, 1999; Zehe et al., 2010; Vereecken et al., 2014; Zarlenga et al., 2018). The sampling resolution strongly depends on the scale of interest, which varies largely between studies. I was interested in the spatial scale of throughfall variation to compare throughfall and soil variations, and thus used a similar sampling scheme for soil patterns as for throughfall. Less measurement points could be realized for soil sampling compared to throughfall because of the fixed number of sensors and half of the sampling points being traded off for measuring soil water content in two soil depths instead of only one. The stratified random sampling design for soil measurements was realized in a checkerboard-like arranged subsample of subplots, maintaining a high resolution within the sampled subplots. As significant systematic small-scale patterns were captured in the data, I conclude that the applied sampling was sufficient to approach my research questions, and that the effect of a missing sensor calibration for soil texture was small, owing to the small sampling area extent with similar soil textures (Bogena et al., 2010; Rosenbaum et al., 2012; Jackisch et al., 2020). To be certain that the sampling design was sufficient to capture soil variability, additional sampling and further research would be necessary.

While the results can be considered representative for the study site, the situation is different regarding the representativeness of the study site compared with sites worldwide, and evaluating the findings on ecohydrological processes at this site globally. Heterogeneity of net precipitation has been observed throughout climatological regions and tree and shrub communities (Levia and Germer, 2015). Yet, the role it has ecologically might differ (Guswa and Spence, 2011), depending on the water availability of systems. In the tropics and in humid temperate climates, as in our case, net precipitation distribution has not been reported to affect tree composition,

patterning or productivity (but Neite and Runge (1986) and Wilke et al. (1993) found different herb layer species and moss cover related to stemflow). In contrast, the channeling of intercepted water to the roots is crucial to the survival of vegetation in semiarid shrublands and savannas (Pressland, 1976; Návar and Bryan, 1990; Martinez-Meza and Whitford, 1996; Whitford et al., 1997; Johnson and Lehmann, 2006; Li et al., 2009; Zuo et al., 2009; Wang et al., 2011; Zhang et al., 2013) and cloud forests (Hildebrandt and Eltahir, 2007; Hildebrandt et al., 2007; González-Martínez et al., 2017). As soil water availability and water use efficiency change with different ecosystems, so do precipitation fractions of deep percolation and groundwater recharge (Troch et al., 2009). Especially stemflow hotspots could impact on and feed into different water storage compartments depending on site properties, vegetation and climate.

The impact of vegetation and net precipitation patterns on soil properties can be expected to importantly vary in size and consequence between sites. The effect probably strongly depends on the parent material of the soil, the status of the soil formation process, and vegetation and precipitation chemistry. Different site property combinations could result in different effects. For example, stemflow has been found to create “fertile islands” in some studies (Whitford et al., 1997; Li et al., 2008; Zuo et al., 2009), while it was discussed to produce sites of depletion and structural soil collapse in others (Wilke et al., 1993; Knoerzer and Gärtner, 2003; Van Stan and Gordon, 2018). As a well-drained, relatively young soil on an alkaline bedrock, this site’s soil might have been perfectly suited as a canvas for impacts of input water flux heterogeneity. Older and more strongly weathered soils, as in the tropics, would possibly not reproduce patterns of recent vegetation, because soil formation already is in the final state and cannot be further differentiated by recent processes. Also, very wet soil with a high overall water content due to stagnant water or due to lateral water flow would conceal above-surface signals. Yet, soil microsites can likely manifest in various systems and soils due to high water and element inputs (as induced by stemflow). Such, an increased podsolization has been observed at acidic sites at locations of high water fluxes (Price, 1994; Bogner et al., 2012), and I found a further developed eluvial soil horizon and changed soil hydraulic properties close to trees during field work in Québec, Canada (data not shown).

5.3 Implications

This thesis' results show, how densely intertwined vegetation is with all environmental processes at the earth's surface, and how heterogeneity as a principle of life exists, acts, and organizes also on the small scale.

Vegetation structure has shown to influence the creation of variance, and diversity has shown to enhance hotspot formation of downwards-directed water fluxes in the canopy and soil. Diverse forest stands reach higher tree densities, as trees of different species can move closer together without disturbing each other physically or competing for resources (Frech et al., 2003). This enables a more efficient ecosystem, in respect to the number of individuals and to the biomass per ground area (Frech et al., 2003). Species diversity is generally associated with functional diversity (Chapin et al., 2000; McCann, 2000). My findings confirm this in the sense that forest diversity increased ecohydrological heterogeneity: A diversification of rainwater flow paths as well as below-canopy and subsurface water fluxes creates a spectrum of related biogeochemical and ecohydrological niches (Bundt et al., 2001; Levia and Frost, 2003; Rosier et al., 2016; Van Stan II and Friesen, 2020). Additionally, I found for the example of stemflow, that diversity persists at a patch scale. Horn (1971) argued, that climax forests are unable to regenerate continuously, thus, a stable climax forest ecosystem consists of patches of regeneration in different stages. Only in that fashion, by opening space for competition anew at the fall of trees, can diversity persist and thrive. Continuous niche creation is key to stabilize ecosystems: Diverse ecosystems are more stable and more resistant and resilient against perturbations (McCann, 2000). Diversity-associated niche production in downwards-directed soil water fluxes might help to maintain forest system diversity, health and stability.

While the diversity of soil ecosystem functions is broadly acknowledged, the diversity of soil water flow behavior still widely remains in the dark. Yet, the latter might be key to the segmentation of competing functions and resources of the soil-water system, as feeding the plant-available water pool, streams or groundwater, as well as filtering water in contrast to quick infiltration and drainage to prevent erosion and flooding. Preferential quick flow of water in the soil, be it as finger flow in the matrix, or as macropore and channel flow alongside larger pores, roots or cracks, is long since recognized to be important, but is only marginally understood

(Beven and Germann, 1982, 2013). This concerns triggers of preferential flow as well as its spatial distribution and the drivers thereof (Beven and Germann, 2013; Demand et al., 2019). A number of studies have shown a stronger occurrence of preferential flow in forests (Zhao et al., 2012; Demand et al., 2019) or have observed preferential flow of stemflow inputs underneath tree stems (Martinez-Meza and Whitford, 1996; Taniguchi et al., 1996; Johnson and Lehmann, 2006; Liang et al., 2007; Sansoulet et al., 2008; Li et al., 2009; Schwärzel et al., 2012; Spencer and van Meerveld, 2016). My study delivers hints to how preferential flow could be spatially organized. The higher macroporosity and higher hydraulic conductivity I observed close to trees refer to the soil matrix in relatively small core samples, and thus are not due to large biopores and channels – yet, these structures might coincide: A higher macroporosity and higher conductivity might facilitate the infiltration and collection of water before it is further distributed to macropore flow paths, enhancing the connectivity and accessibility of those preferential pathways. Small-scale accessibility of potential preferential flow paths could enable preferential flow to play a role at the landscape scale, and small-scale variability of soil water fluxes and of soil properties, which form positive feedbacks at tree stems, could produce high preferential flow rates in forests.

Also, stemflow, as input water hotspot (and hot moment), might actively trigger preferential flow in soils: Low intensity input fluxes have a higher probability to infiltrate to the soil matrix, while high intensity fluxes drive macropore flow (Flühler and Roth, 2004). Throughfall, as a "diffuse" input, and stemflow, as a concentrated "point" input (Reynolds and Henderson, 1967; Durocher, 1990; Bialkowski and Buttle, 2015; Liang et al., 2015), have been attributed to driving two distinct flow mechanisms and corresponding hydrological responses by Crabtree and Trudgill (1985) on the hillslope, and by Tang (1996) on the plot scale. Input hotspots would thus activate quick flow in the subsurface, bypassing the soil and eventually contributing to groundwater recharge. Quick and pronounced hydrograph responses towards precipitation signals have been observed in aeration zone groundwater observation wells close to this study's experimental site, which is explained with preferential flow paths at infiltration, within the soil and in the deeper subsurface (Kohlhepp et al., 2017; Lehmann and Totsche, 2020). These findings highlight the role of soil-related preferential flow for groundwater recharge, and give evidence of the relationship in this study's environmental setting. In catchment hydrology, the phenomenon of

the “two water worlds” has been much discussed in recent years (Brooks et al., 2010; Phillips, 2010; Goldsmith et al., 2012; McDonnell, 2014; Berry et al., 2018): As isotope data shows, rivers and plants are fed by two distinct pools of water. In water resources management, the terms “blue” and “green” water have been long used (FAO, 1993), denominating the closed water bodies of surface and groundwater in contrast to water bound in soils and plants. According to the two water worlds hypothesis, the blue and green water pools might be largely separated, meaning that groundwater has not slowly percolated through the soil first, but has bypassed it preferentially and immediately drained into deeper subsurface areas, while more tightly bound water in the soil matrix is used by plants instead of ever percolating into the deeper subsurface. This is because tightly bound soil water is not replaced by new infiltrating precipitation inputs, but remains locked in the pores until high pressure gradients caused by plant roots can extract them (Brooks et al., 2010). As stemflow and throughfall are very likely to supply these two distinct pools, the separation process between plant available soil water and groundwater might thus be decided in the vegetation canopy.

Soil is a heterogeneous medium, and its heterogeneity depends on a whole set of factors. Most soil formation processes are rather slow, such that soil properties are subject to a substantial memory effect (Zimmermann et al., 2006). A soil can be viewed as the cumulative record of impacts during its formation process. Considering that soil formation for the young Holocene soils in most of central Europe has continued for at least 10,000 a, it is no wonder most people find it surprising that I observe differences in soil formation during the lifespan of a tree – maybe not even a very old tree. Changes in soil properties due to vegetation within such short time periods have been observed before, e.g. by Jost et al. (2012) and Fischer et al. (2015), where beech compared to spruce forest and species diversity in a grassland increased soil (macro)porosity and infiltration capacity. There, observed changes were caused by differences in rooting and root decay as well as higher soil organic carbon accumulation and related microbial and faunal activity, enhancing soil structure. These positive relationships are also mirrored in my results. Additionally, my findings now show differences in soil properties not only caused by biological factors, which are in the quick range of soil formation processes, but also by physico-chemical processes. It is usually assumed that soil heterogeneities are random, and that potential drivers cannot be defined because they are complex and lie in the past. My study shows, that

small-scale patterns of soil formation processes and resulting soil properties can be caused by recent environmental factors. The statistical approach of my study allowed to carve out the ongoing impacts from background patterns of past impacts by selecting location groups. Presumably, recent processes of soil formation superimpose on past ones, and even small-scale soil properties heterogeneity follows systematic patterns, which we are only beginning to understand.

5.4 Outlook

The newly acquired state of knowledge opens up a spectrum of research opportunities:

I found that tree morphological features, as influenced by neighbors, as well as stand properties, impact stemflow yields on the tree and on the forest patch scale. These relationships could be further investigated using Lidar data. While Lidar data point clouds are still difficult to process, computational tools already exist that are able to describe variables which now appear promising, due to my findings (Raumonen et al., 2015; Burt et al., 2019; Moorthy et al., 2019). These are woody surface area, tree density, branch density in the canopy, and woody surface density in different heights. Also, the connectivity of flow paths along woody surfaces could be considered. Those data could be evaluated for their impact on stemflow yield and variability on the tree, the patch and the stand scale. Woody surface area and flow path analysis could also be combined with surface roughness and resulting bark water storages to understand the spatial and temporal behavior of stemflow.

Having observed a strong variation of stemflow on the forest patch scale, it would be interesting to learn more about patchy behavior of stands and stand precipitation patterns. Variations and mean values of throughfall could be observed and set in relation to stemflow variations. Characterizing different stage patches by typical stand properties, their heterogeneity could be related to net precipitation heterogeneity, hotspot creation ability and impact on soil property heterogeneity within and between patches.

Using a similar approach to this study with statistical sampling of different properties and comparing their statistical behavior, forests of different diversities, natural forests compared to managed forests, different climate limitations or land uses could be compared. This would enable

us to better understand the role of small-scale heterogeneity of downwards-directed water fluxes in different ecosystems.

In this study, I found that increased soil water fluxes induced by stemflow statistically changed soil properties around tree stems. Going one step further, the amount of stemflow or tree properties could be related to near-stem soil properties or soil water content space-discretely. Making this connection would be feasible by sampling soil properties near trees before starting a stemflow measurement campaign on the same trees, or by extrapolating stemflow data for trees, where soil properties or soil water is observed, with a good stemflow model. In this manner, the effect of stemflow amounts and rates on soil properties and soil water could be more closely examined.

The predominance of preferential soil water flow of stemflow inputs is unambiguous, as evidence has been found in so many studies (Martinez-Meza and Whitford, 1996; Tanaka et al., 1996; Taniguchi et al., 1996; Johnson and Lehmann, 2006; Liang et al., 2007; Sansoulet et al., 2008; Li et al., 2009; Schwärzel et al., 2009; Liang et al., 2011; Schwärzel et al., 2012; Buttle et al., 2014; Bialkowski and Buttle, 2015; Spencer and van Meerveld, 2016). Nevertheless, a comprehensive small-scale observation of preferential flow depending on locations in forests has not yet been accomplished. Identifying preferential flow behavior by time series analysis of soil water content data and relating it to stand and soil properties would address this long-running unanswered question. My results propose, that the distance to the next tree and its species should also be tested, as they have been found to impact soil properties and stemflow. Also, precipitation event properties and soil water content state could be taken into consideration.

The phenomenon of stemflow concentration by the tree stem combined with soil preferential flow along the tree's roots has been described as the "double funneling" effect of trees (Martinez-Meza and Whitford, 1996; Johnson and Lehmann, 2006; Li et al., 2009; Liang et al., 2011; Schwärzel et al., 2012; Spencer and van Meerveld, 2016). My results on soil microsites at tree stems have as well indicated that stemflow fluxes tend to have a lateral flow component in the soil. Other studies found evidence that stemflow impact areas become smaller with soil depth (Tischer et al., 2020). The question arises, how strong stemflow redistributes in the soil: Does the term double funneling apply, or does the vertical flow component dominate, such that preferential soil water fluxes induced by stemflow directly bypass the soil? Event response time

series of soil water content or potential measurements as well as electrical resistivity tomography in high-resolution short transects from trees could give insights to answer this question.

There are a lot of open questions when it comes to stemflow fate in the subsurface, but especially so below the rooting zone. Where do stemflow fluxes go, and what is their role for hydrological processes below the rooting zone? This also leads towards the major question of the ecological meaning of stemflow: Is it a self-watering and self-fertilizing effect? Or are stemflow hotspot fluxes a collateral loss to the ecosystem, yet important for groundwater recharge? It even is conceivable, that both mechanisms exist, and that species, climate or geology decide, which of the effects prevail. Sampling of quality and quantity of seepage water below the rooting zone could be a first approach. This could be achieved by lysimeters, suction cups and/or trenches. Also, high-resolution shallow groundwater sampling would be possible (depending on site properties), as well as groundwater level response, comparing different land uses or, in forests, areas of exclusion and inclusion of stemflow. Different water sampling approaches (of different (eco)hydrological components) could be complemented with the use of tracers or isotope measurements. Yet, methodology to answer the aforementioned questions needs further development and concerted creative efforts.

Comprehension of water balances, water pathways and water-related interactions in the vegetation-soil system becomes increasingly important due to quickly progressing global and climate change, creating water scarcity and threating forest ecosystems due to drought and pests in central Europe as well as due to land use change all over the world (Trumbore et al., 2015; Watson et al., 2018). By studying and drawing attention to the complex interactions of soil, water and ecosystems, environmental sciences can raise a better understanding and appreciation of nature’s life-sustaining services.

6 References

Aboal, J. R., Morales, D., Hernández, M., and Jiménez, M. S.: The measurement and modelling of the variation of stemflow in a laurel forest in Tenerife, Canary Islands, Journal of Hydrology, 221, 161-175, 1999.

Alva, A. K., Prakash, O., Fares, A., and Hornsby, A. G.: Distribution of rainfall and soil moisture content in the soil profile under citrus tree canopy and at the dripline, Irrigation Science, 18, 109-115, 1999.

André, F., Jonard, M., and Ponette, Q.: Influence of species and rain event characteristics on stemflow volume in a temperate mixed oak–beech stand, Hydrological Processes: An International Journal, 22, 4455-4466, 2008.

Aponte, C., García, L. V., and Marañón, T.: Tree species effects on nutrient cycling and soil biota: a feedback mechanism favouring species coexistence, Forest Ecology and Management, 309, 36-46, 2013.

Aubrey, D. P.: Relevance of Precipitation Partitioning to the Tree Water and Nutrient Balance, in: Precipitation Partitioning by Vegetation, Springer, 147-162, 2020.

Augusto, L., Ranger, J., Binkley, D., and Rothe, A.: Impact of several common tree species of European temperate forests on soil fertility, Annals of forest science, 59, 233-253, 2002.

Bachmair, S., Weiler, M., and Troch, P. A.: Intercomparing hillslope hydrological dynamics: Spatio-temporal variability and vegetation cover effects, Water Resources Research, 48, 2012.

Baldrian, P.: Forest microbiome: diversity, complexity and dynamics, FEMS Microbiology reviews, 41, 109-130, 2017.

Baroni, G., Ortuani, B., Facchi, A., and Gandolfi, C.: The role of vegetation and soil properties on the spatio-temporal variability of the surface soil moisture in a maize-cropped field, Journal of Hydrology, 489, 148-159, 2013.

Barton, K.: MuMIn: Multi-Model Inference. R package version 1.42.1., 2018.

Bates, D., Maechler, M., Bolker, M., and Walker, S.: Fitting Linear Mixed-Effects Models using lme4, Journal of Statistical Software, 67, 1-48, 2015.

Bellot, J., and Escarré, A.: Chemical characteristics and temporal variations of nutrients in throughfall and stemflow of three species in Mediterranean holm oak forest, Forest Ecology and Management, 41, 125-135, 1991.

Berger, T. W., Untersteiner, H., Toplitzer, M., and Neubauer, C.: Nutrient fluxes in pure and mixed stands of spruce (Picea abies) and beech (Fagus sylvatica), Plant and Soil, 322, 317-342, 2009.

Berry, Z. C., Evaristo, J., Moore, G., Poca, M., Steppe, K., Verrot, L., Asbjornsen, H., Borma, L. S., Bretfeld, M., and Hervé-Fernández, P.: The two water worlds hypothesis: Addressing multiple working hypotheses and proposing a way forward, Ecohydrology, 11, e1843, 2018.

Bertoldi, G., Della Chiesa, S., Notarnicola, C., Pasolli, L., Niedrist, G., and Tappeiner, U.: Estimation of soil moisture patterns in mountain grasslands by means of SAR RADARSAT2 images and hydrological modeling, Journal of Hydrology, 516, 245-257, 2014.

Beven, K., and Germann, P.: Macropores and water flow in soils, Water resources research, 18, 1311-1325, 1982.

Beven, K., and Germann, P.: Macropores and water flow in soils revisited, Water resources research, 49, 3071-3092, 2013.

Bialkowski, R., and Buttle, J. M.: Stemflow and throughfall contributions to soil water recharge under trees with differing branch architectures, Hydrological Processes, 29, 4068-4082, 2015.

Bischoff, S., Schwarz, M., Siemens, J., Thieme, L., Wilcke, W., and Michalzik, B.: Properties of dissolved and total organic matter in throughfall, stemflow and forest floor leachate of central European forests, Biogeosciences, 12, 2695-2706, 2015.

Blume, H.-P., Brümmer, G. W., Horn, R., Kandeler, E., Kögel-Knabner, I., Kretzschmar, R., Stahr, K., Wilke, B.-M., Thiele-Bruhn, S., and Welp, G.: Scheffer/Schachtschabel, Lehrbuch der Bodenkunde, 16, 2010.

Blume, T., Zehe, E., and Bronstert, A.: Use of soil moisture dynamics and patterns at different spatio-temporal scales for the investigation of subsurface flow processes, Hydrology and Earth System Sciences, 13, 1215, 2009.

Boettcher, S. E., and Kalisz, P. J.: Single-tree influence on soil properties in the mountains of eastern Kentucky, Ecology, 71, 1365-1372, 1990.

Bogena, H. R., Herbst, M., Huisman, J. A., Rosenbaum, U., Weuthen, A., and Vereecken, H.: Potential of wireless sensor networks for measuring soil water content variability, Vadose Zone Journal, 9, 1002-1013, 2010.

Bogner, C., Borken, W., and Huwe, B.: Impact of preferential flow on soil chemistry of a podzol, Geoderma, 175, 37-46, 2012.

Bouten, W., Heimovaara, T. J., and Tiktak, A.: Spatial patterns of throughfall and soil water dynamics in a Douglas fir stand, Water Resources Research, 28, 3227-3233, 1992.

Brocca, L., Melone, F., Moramarco, T., and Morbidelli, R.: Soil moisture temporal stability over experimental areas in Central Italy, Geoderma, 148, 364-374, 2009.

Brocca, L., Zucco, G., Mittelbach, H., Moramarco, T., and Seneviratne, S. I.: Absolute versus temporal anomaly and percent of saturation soil moisture spatial variability for six networks worldwide, Water Resources Research, 50, 5560-5576, 2014.

Brockett, B. F. T., Prescott, C. E., and Grayston, S. J.: Soil moisture is the major factor influencing microbial community structure and enzyme activities across seven biogeoclimatic zones in western Canada, Soil Biology and Biochemistry, 44, 9-20, 2012.

Brooks, J. R., Barnard, H. R., Coulombe, R., and McDonnell, J. J.: Ecohydrologic separation of water between trees and streams in a Mediterranean climate, Nature Geoscience, 3, 100-104, 2010.

Bruelheide, H., Dengler, J., Purschke, O., Lenoir, J., Jiménez-Alfaro, B., Hennekens, S. M., Botta-Dukát, Z., Chytrý, M., Field, R., and Jansen, F.: Global trait–environment relationships of plant communities, Nature Ecology & Evolution, 2, 1906-1917, 2018.

Buckland, S. T., Magurran, A. E., Green, R. E., and Fewster, R. M.: Monitoring change in biodiversity through composite indices, Philosophical Transactions of the Royal Society B: Biological Sciences, 360, 243-254, 2005.

Bui, E. N., and Box Jr, J. E.: Stemflow, rain throughfall, and erosion under canopies of corn and sorghum, Soil Science Society of America Journal, 56, 242-247, 1992.

Bundt, M., Widmer, F., Pesaro, M., Zeyer, J., and Blaser, P.: Preferential flow paths: biological 'hot spots' in soils, Soil Biology and Biochemistry, 33, 729-738, 2001.

Burt, A., Disney, M., and Calders, K.: Extracting individual trees from lidar point clouds using treeseg, Methods in Ecology and Evolution, 10, 438-445, 2019.

Buttle, J. M., Toye, H. J., Greenwood, W. J., and Bialkowski, R.: Stemflow and soil water recharge during rainfall in a red pine chronosequence on the Oak Ridges Moraine, southern Ontario, Canada, Journal of hydrology, 517, 777-790, 2014.

Campbell, R. C.: Statistics for biologists, Cambridge University Press, 1989.

Carlyle-Moses, D. E., Iida, S. i., Germer, S., Llorens, P., Michalzik, B., Nanko, K., Tischer, A., and Levia, D. F.: Expressing stemflow commensurate with its ecohydrological importance, Advances in water resources, 121, 472-479, 2018.

Cattan, P., Ruy, S., Cabidoche, Y.-M., Findeling, A., Desbois, P., and Charlier, J.-B.: Effect on runoff of rainfall redistribution by the impluvium-shaped canopy of banana cultivated on an Andosol with a high infiltration rate, Journal of hydrology, 368, 251-261, 2009.

Cayuela, C., Llorens, P., Sánchez-Costa, E., Levia, D. F., and Latron, J.: Effect of biotic and abiotic factors on inter-and intra-event variability in stemflow rates in oak and pine stands in a Mediterranean mountain area, Journal of hydrology, 560, 396-406, 2018.

Chang, S. C., and Matzner, E.: The effect of beech stemflow on spatial patterns of soil solution chemistry and seepage fluxes in a mixed beech/oak stand, Hydrological Processes, 14, 135-144, 2000.

Chapin, F. S., Zavaleta, E. S., Eviner, V. T., Naylor, R. L., Vitousek, P. M., Reynolds, H. L., Hooper, D. U., Lavorel, S., Sala, O. E., and Hobbie, S. E.: Consequences of changing biodiversity, Nature, 405, 234-242, 2000.

Charlier, J.-B., Moussa, R., Cattan, P., Cabidoche, Y.-M., and Voltz, M.: Modelling runoff at the plot scale taking into account rainfall partitioning by vegetation: application to stemflow of banana (Musa spp.) plant, 2009.

Choi, M., Jacobs, J. M., and Cosh, M. H.: Scaled spatial variability of soil moisture fields, Geophysical Research Letters, 34, 2007.

Chuyong, G. B., Newbery, D. M., and Songwe, N. C.: Rainfall input, throughfall and stemflow of nutrients in a central African rain forest dominated by ectomycorrhizal trees, Biogeochemistry, 67, 73-91, 2004.

Coenders-Gerrits, A. M. J., Hopp, L., Savenije, H. H. G., and Pfister, L.: The effect of spatial throughfall patterns on soil moisture patterns at the hillslope scale, Hydrology and Earth System Sciences, 17, 1749-1763, 2013.

Coenders-Gerrits, M., Schilperoort, B., and Jiménez-Rodríguez, C.: Evaporative Processes on Vegetation: An Inside Look, in: Precipitation Partitioning by Vegetation, Springer, 35-48, 2020.

Crabtree, R. W., and Trudgill, S. T.: Hillslope hydrochemistry and stream response on a wooded, permeable bedrock: the role of stemflow, Journal of Hydrology, 80, 161-178, 1985.

Crockford, R. H., and Richardson, D. P.: Partitioning of rainfall in a eucalypt forest and pine plantation in southeastern Australia: II Stemflow and factors affecting stemflow in a dry sclerophyll eucalypt forest and a Pinus radiata plantation, Hydrological Processes, 4, 145-155, 1990.

Crockford, R. H., Richardson, D. P., and Sageman, R.: Chemistry of rainfall, throughfall and stemflow in a eucalypt forest and a pine plantation in south-eastern Australia: 3. Stemflow and total inputs, Hydrological processes, 10, 25-42, 1996.

Crockford, R. H., and Khanna, P. K.: Chemistry of throughfall, stemfall and litterfall in fertilized and irrigated Pinus radiata, Hydrological Processes, 11, 1493-1507, 1997.

Crockford, R. H., and Richardson, D. P.: Partitioning of rainfall into throughfall, stemflow and interception: effect of forest type, ground cover and climate, Hydrological processes, 14, 2903-2920, 2000.

Dawoe, E. K., Barnes, V. R., and Oppong, S. K.: Spatio-temporal dynamics of gross rainfall partitioning and nutrient fluxes in shaded-cocoa (Theobroma cocoa) systems in a tropical semi-deciduous forest, Agroforestry systems, 92, 397-413, 2018.

Demand, D., Blume, T., and Weiler, M.: Spatio-temporal relevance and controls of preferential flow at the landscape scale, Hydrology and Earth System Sciences, 23, 4869-4889, 2019.

Dezzeo, N., and Chacón, N.: Nutrient fluxes in incident rainfall, throughfall, and stemflow in adjacent primary and secondary forests of the Gran Sabana, southern Venezuela, Forest Ecology and Management, 234, 218-226, 2006.

Drenovsky, R. E., Vo, D., Graham, K. J., and Scow, K. M.: Soil water content and organic carbon availability are major determinants of soil microbial community composition, Microbial ecology, 48, 424-430, 2004.

Durocher, M. G.: Monitoring spatial variability of forest interception, Hydrological Processes, 4, 215-229, 1990.

Eviner, V. T., and Chapin, F. S.: Functional matrix: a conceptual framework for predicting multiple plant effects on ecosystem processes, Annual Review of Ecology, Evolution, and Systematics, 34, 455-485, 2003.

Falkengren-Grerup, U.: Effect of stemflow on beech forest soils and vegetation in southern Sweden, Journal of Applied Ecology, 341-352, 1989.

Famiglietti, J. S., Devereaux, J. A., Laymon, C. A., Tsegaye, T., Houser, P. R., Jackson, T. J., Graham, S. T., Rodell, M., and Van Oevelen, P. J.: Ground-based investigation of soil moisture variability within remote sensing footprints during the Southern Great Plains 1997 (SGP97) Hydrology Experiment, Water Resources Research, 35, 1839-1851, 1999.

Famiglietti, J. S., Ryu, D., Berg, A. A., Rodell, M., and Jackson, T. J.: Field observations of soil moisture variability across scales, Water Resources Research, 44, 2008.

FAO: Land and water integration ad river basin management, FAO informal workshop, Rome, Italy, 1993, 1995.

Fatichi, S., Katul, G. G., Ivanov, V. Y., Pappas, C., Paschalis, A., Consolo, A., Kim, J., and Burlando, P.: Abiotic and biotic controls of soil moisture spatiotemporal variability and the occurrence of hysteresis, Water Resources Research, 51, 3505-3524, 2015.

Fischer, C., Tischer, J., Roscher, C., Eisenhauer, N., Ravenek, J., Gleixner, G., Attinger, S., Jensen, B., de Kroon, H., and Mommer, L.: Plant species diversity affects infiltration capacity in an experimental grassland through changes in soil properties, Plant and Soil, 397, 1-16, 2015.

Flühler, H., and Roth, K.: Physik der ungesättigten Zone, Skript zur Vorlesung Bodenphysik and der ETH Zürich, Version, 2004.

Frech, A., Leuschner, C., Hagemeier, M., and Hölscher, D.: Nachbarschaftsbezogene Analyse der Kronenraumbesetzung von Esche, Hainbuche und Winterlinde in einem artenreichen Laubmischwald (Nationalpark Hainich, Thüringen), Forstwissenschaftliches Centralblatt vereinigt mit Tharandter forstliches Jahrbuch, 122, 22-35, 2003.

Freschet, G. T., Violle, C., Roumet, C., and Garnier, É.: Interactions between soil and vegetation: structure of plant communities and soil functioning, Soils as a Key Component of the Critical Zone 6: Ecology, 6, 83-104, 2018.

Gash, J. H. C.: An analytical model of rainfall interception by forests, Quarterly Journal of the Royal Meteorological Society, 105, 43-55, 1979.

Gedney, N., and Cox, P. M.: The sensitivity of global climate model simulations to the representation of soil moisture heterogeneity, Journal of Hydrometeorology, 4, 1265-1275, 2003.

Germer, S.: Development of near-surface perched water tables during natural and artificial stemflow generation by babassu palms, Journal of hydrology, 507, 262-272, 2013.

Gersper, P. L., and Holowaychuk, N.: Effects of Stemflow Water on a Miami Soil Under a Beech Tree: I. Morphological and Physical Properties 1, Soil Science Society of America Journal, 34, 779-786, 1970.

Gersper, P. L., and Holowaychuk, N.: Some effects of stem flow from forest canopy trees on chemical properties of soils, Ecology, 52, 691-702, 1971.

Ghimire, C. P., Bruijnzeel, L. A., Lubczynski, M. W., Ravelona, M., Zwartendijk, B. W., and van Meerveld, H. I.: Measurement and modeling of rainfall interception by two differently aged secondary forests in upland eastern Madagascar, Journal of hydrology, 545, 212-225, 2017.

Goldsmith, G. R., Muñoz-Villers, L. E., Holwerda, F., McDonnell, J. J., Asbjornsen, H., and Dawson, T. E.: Stable isotopes reveal linkages among ecohydrological processes in a seasonally dry tropical montane cloud forest, Ecohydrology, 5, 779-790, 2012.

Gómez, J. A., Vanderlinden, K., Giráldez, J. V., and Fereres, E.: Rainfall concentration under olive trees, Agricultural water management, 55, 53-70, 2002.

González-Martínez, T. M., Williams-Linera, G., and Holwerda, F.: Understory and small trees contribute importantly to stemflow of a lower montane cloud forest, Hydrological processes, 31, 1174-1183, 2017.

Gould, I. J., Quinton, J. N., Weigelt, A., De Deyn, G. B., and Bardgett, R. D.: Plant diversity and root traits benefit physical properties key to soil function in grasslands, Ecology letters, 19, 1140-1149, 2016.

Guswa, A. J., and Spence, C. M.: Effect of throughfall variability on recharge: application to hemlock and deciduous forests in western Massachusetts, Ecohydrology, 5, 563-574, 2011.

Guswa, A. J.: Canopy vs. roots: Production and destruction of variability in soil moisture and hydrologic fluxes, Vadose Zone Journal, 11, 2012.

Hainich National Park: https://www.nationalpark-hainich.de/en/, access: 7/1/2020, 2020.

Hanchi, A., and Rapp, M.: Stemflow determination in forest stands, Forest Ecology and Management, 97, 231-235, 1997.

Helvey, J.: Interception by eastern white pine, Water Resources Research, 3, 723-729, 1967.

Herwitz, S. R.: Infiltration-excess caused by stemflow in a cyclone-prone tropical rainforest, Earth Surface Processes and Landforms, 11, 401-412, 1986.

Herwitz, S. R.: Raindrop impact and water flow on the vegetative surfaces of trees and the effects on stemflow and throughfall generation, Earth Surface Processes and Landforms, 12, 425-432, 1987.

Hildebrandt, A., Al Aufi, M., Amerjeed, M., Shammas, M., and Eltahir, E. A.: Ecohydrology of a seasonal cloud forest in Dhofar: 1. Field experiment, Water resources research, 43, 2007.

Hildebrandt, A., and Eltahir, E. A. B.: Ecohydrology of a seasonal cloud forest in Dhofar: 2. Role of clouds, soil type, and rooting depth in tree-grass competition, Water Resources Research, 43, 2007.

Hillel, D.: Environmental soil physics considerations, Elsevier Academic Press, San Diego, USA, 1998.

Hofhansl, F., Wanek, W., Drage, S., Huber, W., Weissenhofer, A., and Richter, A.: Controls of hydrochemical fluxes via stemflow in tropical lowland rainforests: Effects of meteorology and vegetation characteristics, Journal of Hydrology, 452, 247-258, 2012.

Holwerda, F., Scatena, F. N., and Bruijnzeel, L. A.: Throughfall in a Puerto Rican lower montane rain forest: A comparison of sampling strategies, Journal of Hydrology, 327, 592-602, 2006.

Horn, H. S.: The adaptive geometry of trees, 3, Princeton University Press, 1971.

Iida, S. i., Kakubari, J. i., and Tanaka, T.: Litter marks indicating infiltration area of stemflow-induced water, Tsukuba geoenvironmental sciences, 1, 27-31, 2005a.

Iida, S. i., Tanaka, T., and Sugita, M.: Change of interception process due to the succession from Japanese red pine to evergreen oak, Journal of Hydrology, 315, 154-166, 2005b.

Iida, S. i., Levia, D. F., Shimizu, A., Shimizu, T., Tamai, K., Nobuhiro, T., Kabeya, N., Noguchi, S., Sawano, S., and Araki, M.: Intrastorm scale rainfall interception dynamics in a mature coniferous forest stand, Journal of Hydrology, 548, 770-783, 2017.

IUSS Working Group WRB: World reference base for soil resources, World soil resources reports, 103, Food and Agriculture Organization of the United Nations, Rome, 2006.

Jackisch, C., Germer, K., Graeff, T., Andrä, I., Schulz, K., Schiedung, M., Haller-Jans, J., Schneider, J., Jaquemotte, J., and Helmer, P.: Soil moisture and matric potential–an open field comparison of sensor systems, Earth System Science Data, 12, 2020.

Jarvis, N., Koestel, J., Messing, I., Moeys, J., and Lindahl, A.: Influence of soil, land use and climatic factors on the hydraulic conductivity of soil, Hydrology & Earth System Sciences Discussions, 10, 2013.

Jian, S. Q., Zhao, C. Y., Fang, S. M., and Yu, K.: Characteristics of Caragana korshinskii and Hippophae rhamnoides stemflow and their significance in soil moisture enhancement in Loess Plateau, China, Journal of Arid Land, 6, 105-116, 2014.

Johnson, M. S., and Lehmann, J.: Double-funneling of trees: Stemflow and root-induced preferential flow, Ecoscience, 13, 324-333, 2006.

Jost, G., Schume, H., and Hager, H.: Factors controlling soil water-recharge in a mixed European beech (Fagus sylvatica L.)–Norway spruce [Picea abies (L.) Karst.] stand, European Journal of Forest Research, 123, 93-104, 2004.

Jost, G., Schume, H., Hager, H., Markart, G., and Kohl, B.: A hillslope scale comparison of tree species influence on soil moisture dynamics and runoff processes during intense rainfall, Journal of Hydrology, 420, 112-124, 2012.

Juchheim, J., Annighöfer, P., Ammer, C., Calders, K., Raumonen, P., and Seidel, D.: How management intensity and neighborhood composition affect the structure of beech (Fagus sylvatica L.) trees, Trees, 31, 1723-1735, 2017.

Jung, K., and Chang, S. X.: Soil and tree chemistry reflected the cumulative impact of acid deposition in Pinus banksiana and Populus tremuloides stands in the Athabasca oil sands region in western Canada, Ecological indicators, 25, 35-44, 2013.

Keim, R. F., Skaugset, A. E., and Weiler, M.: Temporal persistence of spatial patterns in throughfall, Journal of Hydrology, 314, 263-274, 2005.

Keim, R. F., Tromp-van Meerveld, H. J., and McDonnell, J. J.: A virtual experiment on the effects of evaporation and intensity smoothing by canopy interception on subsurface stormflow generation, Journal of Hydrology, 327, 352-364, 2006.

Kellman, M., and Roulet, N.: Stemflow and throughfall in a tropical dry forest, Earth Surface Processes and Landforms, 15, 55-61, 1990.

Kim, G., and Barros, A. P.: Downscaling of remotely sensed soil moisture with a modified fractal interpolation method using contraction mapping and ancillary data, Remote Sensing of Environment, 83, 400-413, 2002.

Klos, P. Z., Chain-Guadarrama, A., Link, T. E., Finegan, B., Vierling, L. A., and Chazdon, R.: Throughfall heterogeneity in tropical forested landscapes as a focal mechanism for deep percolation, Journal of hydrology, 519, 2180-2188, 2014.

Knoerzer, D., and Gärtner, S.: Was umschreibt Verhagerung?, Forstarchiv, 74, 16-25, 2003.

Koch, A. S., and Matzner, E.: Heterogeneity of soil and soil solution chemistry under Norway spruce (Picea abies Karst.) and European beech (Fagus silvatica L.) as influenced by distance from the stem basis, Plant and Soil, 151, 227-237, 1993.

Kohlhepp, B., Lehmann, R., Seeber, P., Küsel, K., Trumbore, S. E., and Totsche, K. U.: Aquifer configuration and geostructural links control the groundwater quality in thin-bedded carbonate-siliciclastic alternations of the Hainich CZE, central Germany, Hydrology and Earth System Sciences, 21, 6091-6116, 2017.

Köppen, W., and Geiger, R.: Handbuch der Klimatologie, Gebrüder Borntraeger, Berlin, 1930.

Krämer, I., and Hölscher, D.: Rainfall partitioning along a tree diversity gradient in a deciduous old-growth forest in Central Germany, Ecohydrology: Ecosystems, Land and Water Process Interactions, Ecohydrogeomorphology, 2, 102-114, 2009.

Krueger, J., Böttcher, J., Schmunk, C., and Bachmann, J.: Soil water repellency and chemical soil properties in a beech forest soil—Spatial variability and interrelations, Geoderma, 271, 50-62, 2016.

Küsel, K., Totsche, K. U., Trumbore, S. E., Lehmann, R., Steinhäuser, C., and Herrmann, M.: How deep can surface signals be traced in the critical zone? Merging biodiversity with biogeochemistry research in a central German Muschelkalk landscape, Frontiers in Earth Science, 4, 32, 10.3389/feart.2016.00032, 2016.

Kuznetsova, A., Bruun Brockhoff, P., and Haubo Bojesen Christensen, R.: lmerTest: Tests in Linear Mixed Effects Models. R package version 2.0-33. 2016.

Lauber, C. L., Hamady, M., Knight, R., and Fierer, N.: Soil pH as a predictor of soil bacterial community structure at the continental scale: a pyrosequencing-based assessment, Applied and Environmental Microbiology, 2009.

Lawrence, J. E., and Hornberger, G. M.: Soil moisture variability across climate zones, Geophysical research letters, 34, 2007.

Legendre, P., and Fortin, M. J.: Spatial pattern and ecological analysis, Vegetatio, 80, 107-138, 1989.

Lehmann, R., and Totsche, K. U.: Multi-directional flow dynamics shape groundwater quality in sloping bedrock strata, Journal of Hydrology, 580, 124291, 2020.

Lenton, T. M.: Environmental tipping points, Annual Review of Environment and Resources, 38, 1-29, 2013.

Leonard, R. E.: Interception of precipitation by northern hardwoods, Station Paper NE-159. Upper Darby, PA: US Department of Agriculture, Forest Service, Northeastern Forest Experiment Station. 16 p., 159, 1961.

Levia, D. F., and Frost, E. E.: A review and evaluation of stemflow literature in the hydrologic and biogeochemical cycles of forested and agricultural ecosystems, Journal of hydrology, 274, 1-29, 2003.

Levia, D. F., Van Stan II, J. T., Mage, S. M., and Kelley-Hauske, P. W.: Temporal variability of stemflow volume in a beech-yellow poplar forest in relation to tree species and size, Journal of Hydrology, 380, 112-120, 2010.

Levia, D. F., Van Stan, J. T., Siegert, C. M., Inamdar, S. P., Mitchell, M. J., Mage, S. M., and McHale, P. J.: Atmospheric deposition and corresponding variability of stemflow chemistry across temporal scales in a mid-Atlantic broadleaved deciduous forest, Atmospheric Environment, 45, 3046-3054, 2011.

Levia, D. F., and Germer, S.: A review of stemflow generation dynamics and stemflow-environment interactions in forests and shrublands, Reviews of Geophysics, 53, 673-714, 2015.

Levia, D. F., Michalzik, B., Näthe, K., Bischoff, S., Richter, S., and Legates, D. R.: Differential stemflow yield from European beech saplings: the role of individual canopy structure metrics, Hydrological processes, 29, 43-51, 2015.

Levia Jr, D. F., and Frost, E. E.: Variability of throughfall volume and solute inputs in wooded ecosystems, Progress in Physical Geography, 30, 605-632, 2006.

Li, X.-Y., Yang, Z.-P., Li, Y.-T., and Lin, H.: Connecting ecohydrology and hydropedology in desert shrubs: stemflow as a source of preferential flow in soils, Hydrology and Earth System Sciences, 13, 1133-1144, 2009.

Li, X.-Y., Lin, H., and Levia, D. F.: Coupling ecohydrology and hydropedology at different spatio-temporal scales in water-limited ecosystems, na, 2012.

Li, X.-Y., Hu, X., Zhang, Z.-H., Peng, H.-Y., Zhang, S.-Y., Li, G.-Y., Li, L., and Ma, Y.-J.: Shrub hydropedology: preferential water availability to deep soil layer, Vadose Zone Journal, 12, 2013.

Li, X. Y., Liu, L. Y., Gao, S. Y., Ma, Y. J., and Yang, Z. P.: Stemflow in three shrubs and its effect on soil water enhancement in semiarid loess region of China, Agricultural and Forest Meteorology, 148, 1501-1507, 2008.

Liang, W.-L., Kosugi, K. i., and Mizuyama, T.: Heterogeneous soil water dynamics around a tree growing on a steep hillslope, Vadose Zone Journal, 6, 879-889, 2007.

Liang, W.-L., Kosugi, K. i., and Mizuyama, T.: A three-dimensional model of the effect of stemflow on soil water dynamics around a tree on a hillslope, Journal of Hydrology, 366, 62-75, 2009.

Liang, W. L., Kosugi, K. i., and Mizuyama, T.: Soil water dynamics around a tree on a hillslope with or without rainwater supplied by stemflow, Water Resources Research, 47, 2011.

Liang, W. L., Kosugi, K. i., and Mizuyama, T.: Soil water redistribution processes around a tree on a hillslope: the effect of stemflow on the drying process, Ecohydrology, 8, 1381-1395, 2015.

Liu, W., Fox, J. E. D., and Xu, Z.: Nutrient budget of a montane evergreen broad-leaved forest at Ailao Mountain National Nature Reserve, Yunnan, southwest China, Hydrological Processes, 17, 1119-1134, 2003.

Llorens, P., and Domingo, F.: Rainfall partitioning by vegetation under Mediterranean conditions. A review of studies in Europe, Journal of hydrology, 335, 37-54, 2007.

Lloyd, C. R., and de O. Marques F., A.: Spatial variability of throughfall and stemflow measurements in Amazonian rainforest, Agricultural and forest meteorology, 42, 63-73, 1988.

Lodhi, M. A. K.: The influence and comparison of individual forest trees on soil properties and possible inhibition of nitrification due to intact vegetation, American Journal of Botany, 64, 260-264, 1977.

Loustau, D., Berbigier, P., Granier, A., and Moussa, F. E. H.: Interception loss, throughfall and stemflow in a maritime pine stand. I. Variability of throughfall and stemflow beneath the pine canopy, Journal of Hydrology, 138, 449-467, 1992.

Lu, J., Zhang, S., Fang, J., Yan, H., and Li, J.: Nutrient Fluxes in Rainfall, Throughfall, and Stemflow in Pinus densata Natural Forest of Tibetan Plateau, CLEAN–Soil, Air, Water, 45, 1600008, 2017.

Lyons, T. W., Reinhard, C. T., and Planavsky, N. J.: The rise of oxygen in Earth's early ocean and atmosphere, Nature, 506, 307-315, 2014.

Magurran, A. E.: Measuring biological diversity, Blackwell Science, Oxford, UK, 105 pp., 2004.

Majima, M., and Tase, N.: Spatial variation of rainfall in a red pine forest, Bull. Environ. Res. Cen. Univ. Tsukuba, 6, 75-82, 1982.

Marin, C. T., Bouten, W., and Sevink, J.: Gross rainfall and its partitioning into throughfall, stemflow and evaporation of intercepted water in four forest ecosystems in western Amazonia, Journal of hydrology, 237, 40-57, 2000.

Martinez-Meza, E., and Whitford, W. G.: Stemflow, throughfall and channelization of stemflow by roots in three Chihuahuan desert shrubs, Journal of Arid Environments, 32, 271-287, 1996.

Martinez, G., Pachepsky, Y. A., Vereecken, H., Hardelauf, H., Herbst, M., and Vanderlinden, K.: Modeling local control effects on the temporal stability of soil water content, Journal of Hydrology, 481, 106-118, 2013.

Martínez García, G., Pachepsky, Y. A., and Vereecken, H.: Effect of soil hydraulic properties on the relationship between the spatial mean and variability of soil moisture, Journal of hydrology, 516, 154-160, 2014.

Masukata, H., Ando, M., and Ogawa, H.: Throughfall, stemflow and interception of rainwater in an evergreen broadleaved forest, Ecological research, 5, 303-316, 1990.

Mauchamp, A., and Janeau, J.-L.: Water funnelling by the crown of Flourensia cernua, a Chihuahuan Desert shrub, Journal of Arid Environments, 25, 299-306, 1993.

McCann, K. S.: The diversity–stability debate, Nature, 405, 228-233, 2000.

McClain, M. E., Boyer, E. W., Dent, C. L., Gergel, S. E., Grimm, N. B., Groffman, P. M., Hart, S. C., Harvey, J. W., Johnston, C. A., and Mayorga, E.: Biogeochemical hot spots and hot moments at the interface of terrestrial and aquatic ecosystems, Ecosystems, 6, 301-312, 2003.

McDonnell, J. J.: The two water worlds hypothesis: Ecohydrological separation of water between streams and trees?, Wiley Interdisciplinary Reviews: Water, 1, 323-329, 2014.

McKee, A. J., and Carlyle-Moses, D. E.: Modelling stemflow production by juvenile lodgepole pine (Pinus contorta var. latifolia) trees, Journal of forestry research, 28, 565-576, 2017.

Metzger, J. C., Landschreiber, L., Gröngröft, A., and Eschenbach, A.: Soil evaporation under different types of land use in southern African savanna ecosystems, Journal of Plant Nutrition and Soil Science, 177, 468-475, 2014.

Metzger, J. C., Wutzler, T., Dalla Valle, N., Filipzik, J., Grauer, C., Lehmann, R., Roggenbuck, M., Schelhorn, D., Weckmüller, J., Küsel, K., Totsche, K. U., and Trumbore, S.: Vegetation impacts soil water content patterns by shaping canopy water fluxes and soil properties, Hydrological processes, 31, 3783-3795, 2017.

Metzger, J. C., Schumacher, J., Lange, M., and Hildebrandt, A.: Neighbourhood and stand structure affect stemflow generation in a heterogeneous deciduous temperate forest, Hydrology and Earth System Sciences, 23, 4433-4452, 2019.

Miralles, D. G., Gash, J. H., Holmes, T. R. H., de Jeu, R. A. M., and Dolman, A. J.: Global canopy interception from satellite observations, Journal of Geophysical Research: Atmospheres, 115, 2010.

Molina, A. J., and del Campo, A. D.: The effects of experimental thinning on throughfall and stemflow: a contribution towards hydrology-oriented silviculture in Aleppo pine plantations, Forest Ecology and Management, 269, 206-213, 2012.

Moorthy, S. M. K., Calders, K., Vicari, M. B., and Verbeeck, H.: Improved Supervised Learning-Based Approach for Leaf and Wood Classification From LiDAR Point Clouds of Forests, IEEE Transactions on Geoscience and Remote Sensing, 2019.

Murakami, S.: Abrupt changes in annual stemflow with growth in a young stand of Japanese cypress, Hydrological Research Letters, 3, 32-35, 2009.

Nacke, H., Goldmann, K., Schöning, I., Pfeiffer, B., Kaiser, K., Castillo-Villamizar, G. A., Schrumpf, M., Buscot, F., Daniel, R., and Wubet, T.: Fine spatial scale variation of soil microbial communities under European beech and Norway spruce, Frontiers in microbiology, 7, 2067, 2016.

Návar, J., and Bryan, R.: Interception loss and rainfall redistribution by three semi-arid growing shrubs in northeastern Mexico, Journal of Hydrology, 115, 51-63, 1990.

Návar, J.: The causes of stemflow variation in three semi-arid growing species of northeastern Mexico, Journal of hydrology, 145, 175-190, 1993.

Návar, J., Charles, F., and Jurado, E.: Spatial variations of interception loss components by Tamaulipan thornscrub in northeastern Mexico, Forest Ecology and Management, 124, 231-239, 1999.

Návar, J.: Stemflow variation in Mexico's northeastern forest communities: Its contribution to soil moisture content and aquifer recharge, Journal of Hydrology, 408, 35-42, 2011.

Neite, H., and Runge, M.: Kleinräumige Differenzierung von Vegetation und Boden durch den Stammablauf in einem Buchenwald auf Kalkgestein, Abhandl. Westfäl. Landesmuseum Naturkunde, 48, 303-316, 1986.

Nuzzo, R.: Statistical errors: P values, the 'gold standard' of statistical validity, are not as reliable as many scientists assume, Nature, 506, 150-153, 2014.

Olson, R. K., Reiners, W. A., Cronan, C. S., and Lang, G. E.: The chemistry and flux of throughfall and stemflow in subalpine balsam fir forests, Ecography, 4, 291-300, 1981.

Opakunle, J. S.: Throughfall, stemflow and rainfall interception in a cacao plantation in south western Nigeria, Trop. Ecol., 30, 244-252, 1989.

Oziegbe, M. B., Muoghalu, J. I., and Oke, S. O.: Litterfall, precipitation and nutrient fluxes in a secondary lowland rain forest in Ile-Ife, Nigeria, Acta Botanica Brasilica, 25, 664-671, 2011.

Parker, G. G.: Throughfall and stemflow in the forest nutrient cycle, in: Advances in ecological research, Elsevier, 57-133, 1983.

Peel, M. C., Finlayson, B. L., and McMahon, T. A.: Updated world map of the Köppen-Geiger climate classification, 2007.

Peng, W., Song, T., Zeng, F., Wang, K., Du, H., and Lu, S.: Spatial distribution of surface soil water content under different vegetation types in northwest Guangxi, China, Environmental earth sciences, 69, 2699-2708, 2013.

Perugini, L., Caporaso, L., Marconi, S., Cescatti, A., Quesada, B., de Noblet-Ducoudre, N., House, J. I., and Arneth, A.: Biophysical effects on temperature and precipitation due to land cover change, Environmental Research Letters, 12, 053002, 2017.

Phillips, F. M.: Soil-water bypass, Nature Geoscience, 3, 77-78, 2010.

Pielke, R. A., Avissar, R., Raupach, M., Dolman, A. J., Zeng, X., and Denning, A. S.: Interactions between the atmosphere and terrestrial ecosystems: influence on weather and climate, Global change biology, 4, 461-475, 1998.

Pilegaard, K., Mikkelsen, T. N., Beier, C., Jensen, N. O., Ambus, P., and Ro-Poulsen, H.: Field measurements of atmosphere-biosphere interactions in a Danish beech forest, Boreal Environment Research, 8, 315-334, 2003.

Pressland, A. J.: Soil moisture redistribution as affected by throughfall and stemflow in an arid zone shrub community, Australian Journal of Botany, 24, 641-649, 1976.

Price, A. G., and Bauer, B. O.: Small-scale heterogeneity and soil-moisture variability in the unsaturated zone, Journal of hydrology, 70, 277-293, 1984.

Price, A. G.: Measurement and variability of physical properties and soil water distribution in a forest podzol, Journal of Hydrology, 161, 347-364, 1994.

Qu, W., Bogena, H. R., Huisman, J. A., Vanderborght, J., Schuh, M., Priesack, E., and Vereecken, H.: Predicting subgrid variability of soil water content from basic soil information, Geophysical research letters, 42, 789-796, 2015.

R Core Team: R: A language and environment for statistical computing. R Foundation for Statistical Computing, Vienna, Austria, 2016.

Raat, K. J., Draaijers, G. P. J., Schaap, M. G., Tietema, A., and Verstraten, J. M.: Spatial variability of throughfall water and chemistry and forest floor water content in a Douglas fir forest stand, 2002.

Rampazzo, N., and Blum, W. E.: Changes in chemistry and mineralogy of forest soils by acid rain, Water, Air, and Soil Pollution, 61, 209-220, 1992.

Rashid, N. S. A., and Askari, M.: Litter marks" around oil palm tree base indicating infiltration area of stemflow-induced water, National seminar on civil engineering research, 2014, 14-15,

Rashid, N. S. A., Askari, M., Tanaka, T., Simunek, J., and van Genuchten, M. T.: Inverse estimation of soil hydraulic properties under oil palm trees, Geoderma, 241, 306-312, 2015.

Raumonen, P., Åkerblom, M., Kaasalainen, M., Casella, E., Calders, K., and Murphy, S.: Massive-scale tree modelling from TLS data, ISPRS Annals of Photogrammetry, Remote Sensing & Spatial Information Sciences, 2, 2015.

Renner, M., Hassler, S. K., Blume, T., Weiler, M., Hildebrandt, A., Guderle, M., Schymanski, S. J., and Kleidon, A.: Dominant controls of transpiration along a hillslope transect inferred from

ecohydrological measurements and thermodynamic limits, Hydrology and Earth System Sciences, 20, 2063-2083, 2016.

Reynolds, E. R. C., and Henderson, C. S.: Rainfall interception by beech, larch and Norway spruce, Forestry: An International Journal of Forest Research, 40, 165-184, 1967.

Rodrigo, A., Avila, A., and Roda, F.: The chemistry of precipitation, throughfall and stemflow in two holm oak (Quercus ilex L.) forests under a contrasted pollution environment in NE Spain, Science of the Total Environment, 305, 195-205, 2003.

Rosenbaum, U., Bogena, H. R., Herbst, M., Huisman, J. A., Peterson, T. J., Weuthen, A., Western, A. W., and Vereecken, H.: Seasonal and event dynamics of spatial soil moisture patterns at the small catchment scale, Water Resources Research, 48, 2012.

Rosier, C. L., Levia, D. F., Van Stan, J. T., Aufdenkampe, A., and Kan, J.: Seasonal dynamics of the soil microbial community structure within the proximal area of tree boles: Possible influence of stemflow, European Journal of Soil Biology, 73, 108-118, 2016.

Rutter, A.: Studies in the water relations of Pinus sylvestris in plantation conditions I. Measurements of rainfall and interception, The Journal of Ecology, 191-203, 1963.

Rutter, A. J.: Studies in the water relations of Pinus sylvestris in plantation conditions. II. The annual cycle of soil moisture change and derived estimates of evaporation, Journal of Applied Ecology, 29-44, 1964.

Rutter, A. J., Kershaw, K. A., Robins, P. C., and Morton, A. J.: A predictive model of rainfall interception in forests, 1. Derivation of the model from observations in a plantation of Corsican pine, Agricultural Meteorology, 9, 367-384, 1971.

Sadeghi, S. M. M., Gordon, D. A., and Van Stan II, J. T.: A Global Synthesis of Throughfall and Stemflow Hydrometeorology, in: Precipitation Partitioning by Vegetation, Springer, 49-70, 2020.

Sansoulet, J., Cabidoche, Y.-M., Cattan, P., Ruy, S., and Šimůnek, J.: Spatially distributed water fluxes in an Andisol under banana plants: Experiments and three-dimensional modeling, Vadose Zone Journal, 7, 819-829, 2008.

Savenije, H. H. G.: The importance of interception and why we should delete the term evapotranspiration from our vocabulary, Hydrological Processes, 18, 1507-1511, 2004.

Schönwiese, C.-D.: Klimatologie, UTB, 2013.

Schröter, M., Härdtle, W., and von Oheimb, G.: Crown plasticity and neighborhood interactions of European beech (Fagus sylvatica L.) in an old-growth forest, European Journal of Forest Research, 131, 787-798, 2012.

Schroth, G., Ferreira Da Silva, L., Wolf, M. A., Geraldes Teixeira, W., and Zech, W.: Distribution of throughfall and stemflow in multi-strata agroforestry, perennial monoculture, fallow and primary forest in central Amazonia, Brazil, Hydrological Processes, 13, 1423-1436, 1999.

Schrumpf, M., Kaiser, K., and Schulze, E.-D.: Soil organic carbon and total nitrogen gains in an old growth deciduous forest in Germany, PloS one, 9, 2014.

Schume, H., Jost, G., and Katzensteiner, K.: Spatio-temporal analysis of the soil water content in a mixed Norway spruce (Picea abies (L.) Karst.)–European beech (Fagus sylvatica L.) stand, Geoderma, 112, 273-287, 2003.

Schwärzel, K., Menzer, A., Clausnitzer, F., Spank, U., Häntzschel, J., Grünwald, T., Köstner, B., Bernhofer, C., and Feger, K.-H.: Soil water content measurements deliver reliable estimates of water fluxes: A comparative study in a beech and a spruce stand in the Tharandt forest (Saxony, Germany), Agricultural and Forest Meteorology, 149, 1994-2006, 2009.

Schwärzel, K., Ebermann, S., and Schalling, N.: Evidence of double-funneling effect of beech trees by visualization of flow pathways using dye tracer, Journal of Hydrology, 470, 184-192, 2012.

Sheil, D.: How plants water our planet: advances and imperatives, Trends in plant science, 19, 209-211, 2014.

Shiklomanov, A. N., and Levia, D. F.: Stemflow acid neutralization capacity in a broadleaved deciduous forest: The role of edge effects, Environmental pollution, 193, 45-53, 2014.

Siegert, C., Levia, D. F., Leathers, D., Van Stan, J. T., and Mitchell, M. J.: Do storm synoptic patterns affect biogeochemical fluxes from temperate deciduous forest canopies?, Biogeochemistry, 132, 273-292, 2017.

Simpson, E. H.: Measurement of diversity, Nature, 163, 688, 1949.

Smuts, J. C.: Holism and evolution, The Macmillan Company, New York, 1926.

Soulsby, C., Braun, H., Sprenger, M., Weiler, M., and Tetzlaff, D.: Influence of forest and shrub canopies on precipitation partitioning and isotopic signatures, Hydrological processes, 31, 4282-4296, 2017.

Spencer, S. A., and van Meerveld, H. J.: Double funnelling in a mature coastal British Columbia forest: spatial patterns of stemflow after infiltration, Hydrological Processes, 30, 4185-4201, 2016.

Staelens, J., De Schrijver, A., Verheyen, K., and Verhoest, N. E.: Spatial variability and temporal stability of throughfall deposition under beech (Fagus sylvatica L.) in relationship to canopy structure, Environmental Pollution, 142, 254-263, 2006.

Staelens, J., De Schrijver, A., Verheyen, K., and Verhoest, N. E.: Rainfall partitioning into throughfall, stemflow, and interception within a single beech (Fagus sylvatica L.) canopy: influence of foliation, rain event characteristics, and meteorology, Hydrological Processes: An International Journal, 22, 33-45, 2008.

Syktus, J. I., and McAlpine, C. A.: More than carbon sequestration: biophysical climate benefits of restored savanna woodlands, Scientific Reports, 6, 1-11, 2016.

Takahashi, K., Uemura, S., and Hara, T.: A forest-structure-based analysis of rain flow into soil in a dense deciduous Betula ermanii forest with understory dwarf bamboo, Landscape and ecological engineering, 7, 101-108, 2011.

Tanaka, T., Tsujimura, M., and Taniguchi, M.: Infiltration area of stemflow-induced water, Annual Report-Institute of Geoscience, University of Tsukuba, 30-32, 1990.

Tanaka, T., Taniguchi, M., and Tsujimura, M.: Significance of stemflow in groundwater recharge. 2: A cylindrical infiltration model for evaluating the stemflow contribution to groundwater recharge, Hydrological processes, 10, 81-88, 1996.

Tang, C.: Interception and recharge processes beneath a Pinus elliotii forest, Hydrological processes, 10, 1427-1434, 1996.

Taniguchi, M., Tsujimura, M., and Tanaka, T.: Significance of stemflow in groundwater recharge. 1: Evaluation of the stemflow contribution to recharge using a mass balance approach, Hydrological Processes, 10, 71-80, 1996.

Terra, M. d. C. N. S., de Mello, C. R., de Mello, J. M., de Oliveira, V. A., Nunes, M. H., Silva, V. O., Rodrigues, A. F., and Alves, G. J.: Stemflow in a neotropical forest remnant: vegetative determinants, spatial distribution and correlation with soil moisture, Trees, 32, 323-335, 2018.

Teuling, A. J., and Troch, P. A.: Improved understanding of soil moisture variability dynamics, Geophysical Research Letters, 32, 2005.

Teuling, A. J., Uijlenhoet, R., and Troch, P. A.: On bimodality in warm season soil moisture observations, Geophysical research letters, 32, 2005.

Thompson, S. E., Harman, C. J., Heine, P., and Katul, G. G.: Vegetation-infiltration relationships across climatic and soil type gradients, Journal of Geophysical Research: Biogeosciences, 115, 2010.

Tischer, A., Michalzik, B., and Lotze, R.: Non-uniform but highly preferential stemflow routing along bark surfaces and actual smaller infiltration areas than previously assumed: A case study on European beech (Fagus sylvatica L.) and sycamore maple (Acer pseudoplatanus L.), Ecohydrology, e2230, in review, 2020.

Traff, D. C., Niemann, J. D., Middlekauff, S. A., and Lehman, B. M.: Effects of woody vegetation on shallow soil moisture at a semiarid montane catchment, Ecohydrology, 8, 935-947, 2015.

Troch, P. A., Martinez, G. F., Pauwels, V. R. N., Durcik, M., Sivapalan, M., Harman, C., Brooks, P. D., Gupta, H., and Huxman, T.: Climate and vegetation water use efficiency at catchment scales, Hydrological Processes: An International Journal, 23, 2409-2414, 2009.

Trumbore, S., Brando, P., and Hartmann, H.: Forest health and global change, Science, 349, 814-818, 2015.

Vachaud, G., Passerat de Silans, A., Balabanis, P., and Vauclin, M.: Temporal Stability of Spatially Measured Soil Water Probability Density Function 1, Soil Science Society of America Journal, 49, 822-828, 1985.

van der Ent, R. J., Coenders-Gerrits, A. M. J., Nikoli, R., and Savenije, H. H. G.: The importance of proper hydrology in the forest cover-water yield debate: commentary on Ellison et al.(2012) Global Change Biology, 18, 806–820, Global Change Biology, 18, 2677-2680, 2012.

Van Genuchten, M. T.: A closed-form equation for predicting the hydraulic conductivity of unsaturated soils 1, Soil science society of America journal, 44, 892-898, 1980.

Van Stan II, J. T., and Allen, S. T.: What We Know About Stemflow's Infiltration Area, Frontiers in Forest and Gobal Change, 3, 61, 2020.

Van Stan II, J. T., and Friesen, J.: Precipitation Partitioning, or to the Surface and Back Again: Historical Overview of the First Process in the Terrestrial Hydrologic Pathway, in: Precipitation Partitioning by Vegetation, Springer, 1-16, 2020.

Van Stan, J. T., and Levia, D. F.: Inter-and intraspecific variation of stemflow production from Fagus grandifolia Ehrh.(American beech) and Liriodendron tulipifera L.(yellow poplar) in relation to bark microrelief in the eastern United States, Ecohydrology: Ecosystems, Land and Water Process Interactions, Ecohydrogeomorphology, 3, 11-19, 2010.

Van Stan, J. T., Lewis, E. S., Hildebrandt, A., Rebmann, C., and Friesen, J.: Impact of interacting bark structure and rainfall conditions on stemflow variability in a temperate beech-oak forest, central Germany, Hydrological Sciences Journal, 61, 2071-2083, 2016.

Van Stan, J. T., and Gordon, D. A.: Mini-review: stemflow as a resource limitation to near-stem soils, Frontiers in plant science, 9, 248, 2018.

Van Stan, J. T., Hildebrandt, A., Friesen, J., Metzger, J. C., and Yankine, S. A.: Spatial Variability and Temporal Stability of Local Net Precipitation Patterns, in: Precipitation Partitioning by Vegetation, Springer, 89-104, 2020.

Vanderlinden, K., Vereecken, H., Hardelauf, H., Herbst, M., Martínez, G., Cosh, M. H., and Pachepsky, Y. A.: Temporal stability of soil water contents: A review of data and analyses, Vadose Zone Journal, 11, 2012.

Veneklaas, E. J., and Van Ek, R.: Rainfall interception in two tropical montane rain forests, Colombia, Hydrological processes, 4, 311-326, 1990.

Vereecken, H., Kamai, T., Harter, T., Kasteel, R., Hopmans, J., and Vanderborght, J.: Explaining soil moisture variability as a function of mean soil moisture: A stochastic unsaturated flow perspective, Geophysical Research Letters, 34, 2007.

Vereecken, H., Huisman, J. A., Pachepsky, Y., Montzka, C., Van Der Kruk, J., Bogena, H., Weihermüller, L., Herbst, M., Martinez, G., and Vanderborght, J.: On the spatio-temporal dynamics of soil moisture at the field scale, Journal of Hydrology, 516, 76-96, 2014.

Vivoni, E. R., Rodríguez, J. C., and Watts, C. J.: On the spatiotemporal variability of soil moisture and evapotranspiration in a mountainous basin within the North American monsoon region, Water Resources Research, 46, 2010.

Voigt, G. K.: Distribution of rainfall under forest stands, Forest Science, 6, 2-10, 1960.

Wang, X. P., Wang, Z. N., Berndtsson, R., Zhang, Y. F., and Pan, Y. X.: Desert shrub stemflow and its significance in soil moisture replenishment, Hydrology and Earth System Sciences, 15, 561, 2011.

Watson, J. E. M., Evans, T., Venter, O., Williams, B., Tulloch, A., Stewart, C., Thompson, I., Ray, J. C., Murray, K., and Salazar, A.: The exceptional value of intact forest ecosystems, Nature ecology & evolution, 2, 599-610, 2018.

Weckmüller, J.: Einfluss kleinräumiger Varianz von Standortfaktoren auf Bodenwasserflüsse und Stofftransport, M.Sc., Institut für Geowissenschaften, Friedrich Schiller Universtiy, Jena, 2017.

Western, A. W., and Blöschl, G.: On the spatial scaling of soil moisture, Journal of hydrology, 217, 203-224, 1999.

Whitford, W. G., Anderson, J., and Rice, P. M.: Stemflow contribution to the 'fertile island'effect in creosotebush, Larrea tridentata, Journal of Arid Environments, 35, 451-457, 1997.

Wilke, B., Bogenrieder, A., and Wilmanns, O.: Differenzierte Streuverteilung im Walde, ihre Ursachen und Folgen, Phytocoenologia, 129-155, 1993.

Zarlenga, A., Fiori, A., and Russo, D.: Spatial variability of soil moisture and the scale issue: a geostatistical approach, Water Resources Research, 54, 1765-1780, 2018.

Zehe, E., Gräff, T., Morgner, M., Bauer, A., and Bronstert, A.: Plot and field scale soil moisture dynamics and subsurface wetness control on runoff generation in a headwater in the Ore Mountains, Hydrology and Earth System Sciences, 14, 873, 2010.

Zhang, Y. F., Wang, X. P., Hu, R., Pan, Y. X., and Zhang, H.: Stemflow in two xerophytic shrubs and its significance to soil water and nutrient enrichment, Ecological research, 28, 567-579, 2013.

Zhao, Y., Tang, J., Graham, C., Zhu, Q., Takagi, K., and Lin, H.: Hydropedology in the ridge and valley: Soil moisture patterns and preferential flow dynamics in two contrasting landscapes, Hydropedology: Synergistic integration of soil science and hydrology. Academic Press, Waltham, MA, 381-411, 2012.

Zimmermann, A., Wilcke, W., and Elsenbeer, H.: Spatial and temporal patterns of throughfall quantity and quality in a tropical montane forest in Ecuador, Journal of Hydrology, 343, 80-96, 2007.

Zimmermann, A., Zimmermann, B., and Elsenbeer, H.: Rainfall redistribution in a tropical forest: Spatial and temporal patterns, Water Resources Research, 45, 2009.

Zimmermann, A., Uber, M., Zimmermann, B., and Levia, D. F.: Predictability of stemflow in a species-rich tropical forest, Hydrological Processes, 29, 4947-4956, 2015.

Zimmermann, A., Voss, S., Metzger, J. C., Hildebrandt, A., and Zimmermann, B.: Capturing heterogeneity: The role of a study area's extent for estimating mean throughfall, Journal of Hydrology, 542, 781-789, 2016.

Zimmermann, B., Elsenbeer, H., and De Moraes, J. M.: The influence of land-use changes on soil hydraulic properties: implications for runoff generation, Forest ecology and management, 222, 29-38, 2006.

Zimmermann, B., Zimmermann, A., Lark, R. M., and Elsenbeer, H.: Sampling procedures for throughfall monitoring: a simulation study, Water Resources Research, 46, 2010.

Zinke, P. J.: The pattern of influence of individual forest trees on soil properties, Ecology, 43, 130-133, 1962.

Zucco, G., Brocca, L., Moramarco, T., and Morbidelli, R.: Influence of land use on soil moisture spatial–temporal variability and monitoring, Journal of hydrology, 516, 193-199, 2014.

Zuo, X., Zhao, X., Zhao, H., Zhang, T., Guo, Y., Li, Y., and Huang, Y.: Spatial heterogeneity of soil properties and vegetation–soil relationships following vegetation restoration of mobile dunes in Horqin Sandy Land, Northern China, Plant and soil, 318, 153-167, 2009.

Publications from this thesis

Chapter 2 / Metzger et al., 2017

Chapter 2 of this thesis is based on the following publication:

Metzger, J. C., Wutzler, T., Dalla Valle, N., Filipzik, J., Grauer, C., Lehmann, R., Roggenbuck, M., Schelhorn, D., Weckmüller, J., Küsel, K., Totsche, K. U., and Trumbore, S.: Vegetation impacts soil water content patterns by shaping canopy water fluxes and soil properties, Hydrological processes, 31, 3783-3795, 2017.

In this publication, the impact of below-canopy precipitation patterns on soil water content patterns was characterized, connecting vegetation-induced heterogeneity of water inputs to their fate in the subsurface. The statistical analysis of extensive field measurements on the 1 ha mixed beech forest plot showed, that soil properties, instead of net precipitation patterns, most prominently shaped spatial patterns of soil water content. Soil properties, yet, showed to be spatially organized due to the position of trees, forming areas of enhanced soil drainage around the trunks. Thus, subsurface fluxes rather than soil water content are driven by water input heterogeneity. Soil water storage, in contrast, depends on soil properties, which show systematic patterns based on tree positions.

Chapter 3 / Metzger et al., 2019

Chapter 3 of this thesis is based on the following publication:

Metzger, J. C., Schumacher, J., Lange, M., and Hildebrandt, A.: Neighbourhood and stand structure affect stemflow generation in a heterogeneous deciduous temperate forest, Hydrology and Earth System Sciences, 23, 4433-4452, 2019.

In this publication, the effects of tree, neighborhood and stand properties on stemflow were identified to assess vegetation controls on precipitation hotspot formation. Stemflow measurements in complete forest patches were linked to vegetation properties on the tree and the patch scale using linear mixed effects models, showing that besides tree size, stand density and species diversity increased stemflow. This could be attributed to a high woody surface area and efficient canopy space occupation. A high spatial variability and a strong temporal stability of stemflow, which increases with event size, indicate that vegetational impacts on flow hotspots are distinct and highly relevant.

Erklärung zu den Eigenanteilen an den Publikationen

Ich erkläre, dass die Eigenanteile an den von mir in dieser Dissertation verwendeten Manuskripte zu deren Verwendung ausreichen (mehr als 50 % betragen).

Ich erkläre außerdem, dass die Koautor*innen der in dieser Dissertation verwendeten Manuskripte mit deren Verwendung einverstanden sind.

Promovendin	Ort	Datum	Unterschrift
Johanna Clara Metzger			

Selbständigkeitserklärung

Ich erkläre, dass ich die vorliegende Arbeit selbständig und unter Verwendung der angegebenen Hilfsmittel, persönlichen Mitteilungen und Quellen angefertigt habe.

Ort, Datum Unterschrift der Verfasserin